ÅBO AKADEMI UNIVERSITY
FACULTY OF SCIENCE AND ENGINEERING

Catalysts for slurry-phase hydrotreating of bio-oil

Master's thesis
by
Emil Högnabba

November 2021

Carried out at VTT Technical Research Centre of Finland and Laboratory of Industrial Chemistry and Reaction Engineering at Åbo Akademi University under the supervision of M.Sc Tyko Viertiö, Research Professor Juha Lehtonen and Professor Dmitry Yu. Murzin.

Abstract

Högnabba, Emil

Catalysts for slurry-phase hydrotreating of bio-oil

Master's thesis

VTT Technical Research Centre of Finland, Laboratory of Industrial Chemistry and Reaction Engineering, Faculty of Science and Engineering, Åbo Akademi University 2021, 82 pages, 31 figures, 13 tables, 4 appendices

Supervisors

M.Sc Tyko Viertiö, VTT Technical Research Centre of Finland
Research Professor Juha Lehtonen, VTT Technical Research Centre of Finland
Professor Dmitry Yu. Murzin, Laboratory of Industrial Chemistry and Reaction Engineering, Åbo Akademi University

Keywords

Bio-oil, isoeugenol, hydrodeoxygenation, slurry-phase, unsupported catalyst, MoS_2, molybdenum, cobalt, sulfide

The European Green Deal, a policy initiative set by the European Commission, aims to reduce greenhouse gas (GhG) emissions, and ultimately achieve an economy with net-zero GhG emissions by 2050. Achieving these targets requires development of new and novel technologies in the field of green chemistry. The focus in this work was evaluating the feasibility of using unsupported catalysts for hydrodeoxygenation (HDO) of lignocellulosic bio-oil. In the literature study, unsupported MoS_2 was identified as a promising catalyst candidate for HDO of lignocellulosic bio-oil. Unsupported (Co)-MoS_2 catalysts were synthesized by hydrothermal synthesis and by thermal synthesis of emulsion liquid precursors. Activated carbon (AC) supported Mo and CoMo catalysts were synthesized as reference catalysts. The catalysts were characterized by numerous methods and their performance was compared to commercial supported hydrotreating catalysts in HDO of isoeugenol. Commercial Ru/C and $NiMo/Al_2O_3$ catalysts yielded high selectivity to propylcyclohexane. Clear differences in performance were observed for the unsupported catalysts, while the performance of both unsupported and carbon supported catalysts was enhanced by the introduction of Co as a promoter, yielding higher selectivity to deoxygenated compounds.

Preface

Funding for this Master's thesis has been provided from Business Finland, VTT, BMH Technology, ESL Shipping, Fortum Recycling & Waste, Neste, Savon Voima, St1, Valmet, and VG Shipping within the CaSH research project (Grant 43385/31/2020).

I would like to thank VTT Technical Research Centre of Finland for providing me the opportunity to write my Master's thesis in the Catalytic Slurry Hydrotreatment (CaSH) project, concerning this challenging yet exciting research area. It has been a great experience to be surrounded by supportive people who have always provided help when it has been needed.

I would like to thank my supervisors M.Sc and doctoral student Tyko Viertiö, Research Professor Juha Lehtonen and Professor Dmitry Yu. Murzin for their support, input, and feedback during the course of the thesis. I would also like to thank the rest of the CaSH project team at VTT including Alexander Reznichenko, Sari Rautiainen, Matti Reinikainen, and Johanna Kihlman for helping with catalyst characterization, analytics, and advice in general. A big thank you also to the rest of the Industrial Synthesis and Catalysis team and laboratory staff at VTT, for helping with equipment and laboratory practices.

Finally, I would like to thank my partner, my family, and my friends for their support during this memorable journey.

Emil Högnabba

Turku, 15th of November 2021

Abbreviations

AHM	Ammonium heptamolybdate
ATTM	Ammonium tetrathiomolybdate
BET	Brunauer-Emmett-Teller
CEL	Colloidal emulsion liquid
CTB	Catalyst-to-bio-oil
CUS	Coordinatively unsaturated sites
DDO	Direct deoxygenation
DOD	Degree of deoxygenation
ELM	Emulsion liquid membrane
HC	Hydrocracking
HDM	Hydrodemetalation
HDN	Hydrodenitrogenation
HDO	Hydrodeoxygenation
HDS	Hydrodesulfurization
HGVO	Heavy gas vacuum oil
HRTEM	High-resolution transmission electron microscopy
HYD	Hydrogenation
H/C	Hydrogen-to-carbon
LHSV	Liquid hourly space velocity
RM	Reverse micelle
TAN	Total acid number
TEM	Transmission electron microscopy
VR	Vacuum residue
XRD	X-ray diffraction
XRF	X-ray fluorescence

Table of Contents

1 Introduction

As the world shifts from the use of fossil resources for chemicals, energy, and fuels, towards renewable resources, new and innovative technologies are important to ensure a smooth transition. Lignocellulosic biomass has been identified as a potential replacement for fossil crude oil in the production of fuels and platform chemicals (Y. Zhang et al., 2020). Lignocellulosic biomasses can be liquefied by different methods to produce bio-oils (Ambursa et al., 2021; Dabros et al., 2018b). However, the resulting brown bio-oil differs greatly from traditional fossil crude oil due to its high acidity and oxygen content and subsequent low heating value (Dabros et al., 2018b). As such, the biocrude can be used as a heating oil; however, in order to be used as a transportation fuel, the oxygen content needs to be reduced significantly (Mortensen et al., 2011).

The oxygen content of the biocrude can be lowered by a catalytic hydrotreatment process called hydrodeoxygenation (HDO) (Mortensen et al., 2011). Unfortunately, the instability of the biocrude along with the impurities it contains can quickly deactivate traditional hydrotreatment catalysts (Mortensen et al., 2016). For this reason, a slurry reactor allowing for the removal of deactivated catalyst and subsequent introduction of fresh catalyst could potentially be a superior option for bio-oil HDO than traditional fixed-bed reactors used in hydrotreating of fossil crude oil (Bergvall et al., 2021). Slurry reactors have mainly been deployed for hydrotreatment of so-called bottom of the barrel fossil-based crudes or residue fractions (Bellussi et al., 2013). These heavy fractions usually contain higher concentrations of heteroatoms such as sulfur and nitrogen as well as metal impurities (Bellussi et al., 2013). The possibility of adapting this kind of reactor setup for hydrotreatment of bio-oil is being considered. Commonly used catalysts in commercial slurry-phase hydrotreatment processes are unsupported transition metal sulfides (Bellussi et al., 2013).

In this work, a literature study was conducted, focusing on the use of unsupported catalysts in HDO of bio-oils and bio-oil model compounds. Catalyst properties, reaction conditions, and additives, among other factors affecting HDO performance, were studied. Based on the findings in the literature part, the catalysts to be prepared and tested in HDO runs were chosen. In the experimental part, unsupported MoS_2 and Co-promoted MoS_2 catalysts were synthesized by different methods, namely a hydrothermal method as well as by thermal synthesis of prepared emulsion catalyst precursors. The performance of the catalysts was evaluated in HDO of isoeugenol, a bio-oil model compound, and was compared to commercially available hydrotreatment catalysts.

2 Literature review

2.1 Catalytic slurry-phase hydrotreatment fundamentals

The catalytic slurry-phase hydrotreatment process involves a catalyst which is dispersed into the liquid phase in the form of fine particles, which are usually submicron in size (Bellussi et al., 2013). Small particles are used to minimize mass transfer effects and to speed up the reaction rate (Al-Attas et al., 2019a). In the slurry hydrotreatment process, gaseous hydrogen is fed into the reactor along with the liquid feedstock containing the catalyst or the catalyst precursor (Bellussi et al., 2013). The catalyst can be prepared either in-situ, through converting of a catalyst precursor which is introduced into the feed or ex-situ, where a catalyst is directly dispersed into the liquid feed (Bellussi et al., 2013). In the reactor, all three phases, i.e., solid, gas, and liquid, are subsequently present. An illustration of a simple slurry-phase hydrotreatment process can be seen in Figure 1. One major advantage of using slurry-phase processes for hydroconversion of heavy oil feeds is the catalysts' ability to limit the formation of coke and other undesirable by-products, such as gas and fuel oil (Bellussi et al., 2013). Catalysts used in slurry-phase reactors typically exhibit high hydrogenation and low cracking activity, with most of the cracking activity being thermal cracking (Bellussi et al., 2013). Formation of coke typically occurs at temperatures above the thermal cracking temperature of ca. 400 °C (Bellussi et al., 2013). Another advantage is a higher stability of the unsupported catalysts typically used in slurry reactors compared to traditional supported hydrocracking catalysts used in fixed-bed reactors, which are more prone to poisoning and deactivation caused by impurities in the feed (Sahu et al., 2015). By using a slurry-phase hydrotreatment process, the frequent shutdowns and pressure drops experienced in other reactor types could possibly be prevented (Zhang et al., 2007). The different catalyst types and combinations used in slurry-phase hydrotreatment processes will be discussed in more detail later. In addition to the robustness of the process, very high conversion of the feedstock can also be achieved using slurry reactors, with many industrial processes used for heavy oil processing reaching over 90% conversion (Bellussi et al., 2013). Slurry reactors can be operated on a once-through basis; however, reaching high conversion rates usually requires recycling of unreacted fractions (Bellussi et al., 2013).

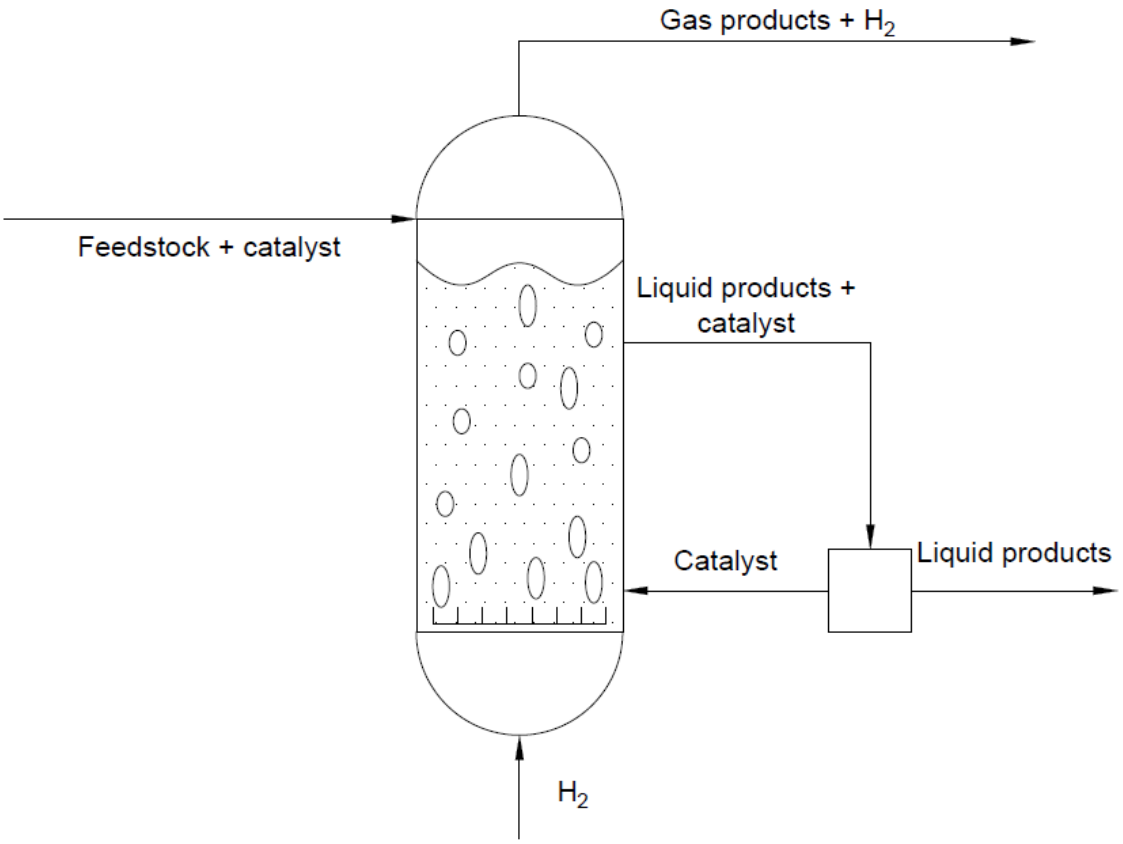

Figure 1. Simple slurry-phase hydrotreatment process. Adapted from Al-Attas et al. (2019a).

2.2 Bio-oil properties and challenges

Bio-oil derived from lignocellulosic biomass is a dark brown, acidic, and oxygen-rich viscous oil that, depending on the liquefaction method and composition of the biomass source, might require mild to more severe hydrotreatment in order to lower its oxygen content and, subsequently, to be used as transportation fuels in vehicles (Venderbosch and Prins, 2010). The most typical liquefaction methods include fast pyrolysis, catalytic pyrolysis, direct liquefaction, and supercritical fluid extraction, with the choice of the liquefaction method affecting such properties as the water content, the oxygen content and the heating value of the crude bio-oil (Ambursa et al., 2021; Dabros et al., 2018b). Typical properties of crude bio-oil are a low heating value, poor volatility, chemical and thermal instability, as well as high polarity, which causes mixing problems with traditional fuels (Liu et al., 2014; Saidi et al., 2014). Crude bio-oils undergo an aging process, where polymerization reactions take place, subsequently increasing the viscosity and molecular weight of the biocrude (Venderbosch and Prins, 2010). This process is further accelerated by high temperatures, oxygen, and UV light exposure (Huber et al., 2006). As mentioned earlier, the oxygen content of bio-oil depends on the liquefaction method, with hydrothermally liquefied bio-oil usually containing ca. 10-20 wt-% oxygen while fast pyrolysis bio-oil usually contains ca. 30-50 wt-% oxygen (Sharma and Kohli, 2020; Yang et al., 2016). Oxygen is bound in the form of many different functional groups which are called oxygenates and include alcohols, aldehydes, esters, carboxylic acids, ketones, phenols etc. (Boldingh & Bauer, 2010; Veses et al., 2016). The crude bio-oil can be separated into two phases, an aqueous phase consisting mainly of monomers and an organic phase composed mainly of oligomers from lignin (Sahebdelfar, 2017). Crude bio-oil contains impurities such as chlorine, sulfur, nitrogen, and alkali metals, which can potentially poison catalysts used in bio-oil HDO (Mortensen et al., 2016). Nevertheless, the main source of catalyst deactivation in HDO of bio-oil is carbon deposition on the catalyst, causing deactivation and reduced catalytic activity (Guo et al., 2018; Wildschut et al., 2009).

2.3 Catalysts for slurry-phase hydrotreating of different feedstocks

2.3.1 Classification of catalysts used in slurry-phase hydrotreatment

Catalysts that are used in slurry-phase hydrocracking can be divided into two major groups, supported and unsupported catalysts (Al-Attas et al., 2019a). The supported catalysts can be defined as systems where at least one metal is impregnated on a support material such as silica (SiO_2) or alumina (Al_2O_3) (Nguyen et al., 2016). Typical supported catalysts used in conventional crude oil hydrotreating are sulfided CoMo, NiMo, and NiW supported catalysts (Wildschut et al., 2009). Noble metal catalysts such as supported Ru and Pd catalysts show high heteroatom hydrogenolysis activity at low temperatures and high hydrogen uptake, while base metal catalysts must be used at higher temperatures to reach adequate activity, which leads to formation of undesirable char or coke (Wildschut et al., 2009). Unfortunately, noble metals are expensive, which makes them economically less feasible (Wildschut et al., 2009). A disadvantage of using supported catalysts is the deposition of heavy hydrocarbons on the active sites of the catalyst leading to blockage of pores, reduced activity, and shorter lifespan of the catalyst (Boldingh and Bauer, 2010; Wildschut et al., 2009). For this reason, support materials with larger pores are used when hydrotreating heavy oil and vacuum residues with supported catalysts (Sahu et al., 2015). This should also be considered when processing bio-oil, where larger pores would allow bulkier molecules easier access to the active sites (Tieuli et al., 2019).

Unsupported catalysts usually contain transition metals, e.g., Mo, Co, Ni, W, Fe, or other group IV-VIII metals, typically present in the form of sulfides or oxides (Boldingh and Bauer, 2010). The major difference between supported and unsupported catalysts is the absence of a support material such as silica or alumina in latter case. One drawback of such catalysts is that the acidity or basicity of support materials cannot be utilized to e.g., influence reaction pathways (Deepa and Dhepe, 2014). However, due to the good availability of active metals in unsupported catalysts, large hydrocarbons reach active sites easier than in porous supported catalysts, where larger molecules might plug the pores (Bellussi et al., 2013). This along with the limited coke formation and being relatively inexpensive makes unsupported slurry catalysts suitable for use in hydrotreating more problematic feedstocks such as heavy fractions and fractions with high concentrations of metals or carbon residues (Bellussi et al., 2013). The coke that is formed in bio-oil HDO when using non-acidic unsupported catalyst can be described as soft coke, as it is oxidized at temperatures below 400 °C, while coke that is deposited on acidic supported catalysts can be described as a hard coke, which must be burned off at temperatures above 400 °C (H. Zhang et al., 2020). The coke on unsupported catalysts can be burned off at

lower temperatures or by washing with a strong solvent (H. Zhang et al., 2020). Unlike supported catalysts, where deactivation of the catalyst is also caused by sintering of the active phases, the mobility or decomposition of active phases plays a minor role in deactivation of unsupported MoS_2 (H. Zhang et al., 2020). Loss of sulfur can cause deactivation in unsupported metal sulfides; however, activity can usually be recovered with a resulfiding process (H. Zhang et al., 2020). Unsupported catalysts can be used under harsher conditions, leading to better heteroatom removal, depolymerization, and conversion of biorenewable feedstock (Boldingh and Bauer, 2010). Unsupported catalysts can be classified into finely powdered, ultradispersed and soluble ones, which can be seen in Figure 2 and will now be discussed in detail (Al-Attas et al., 2019a).

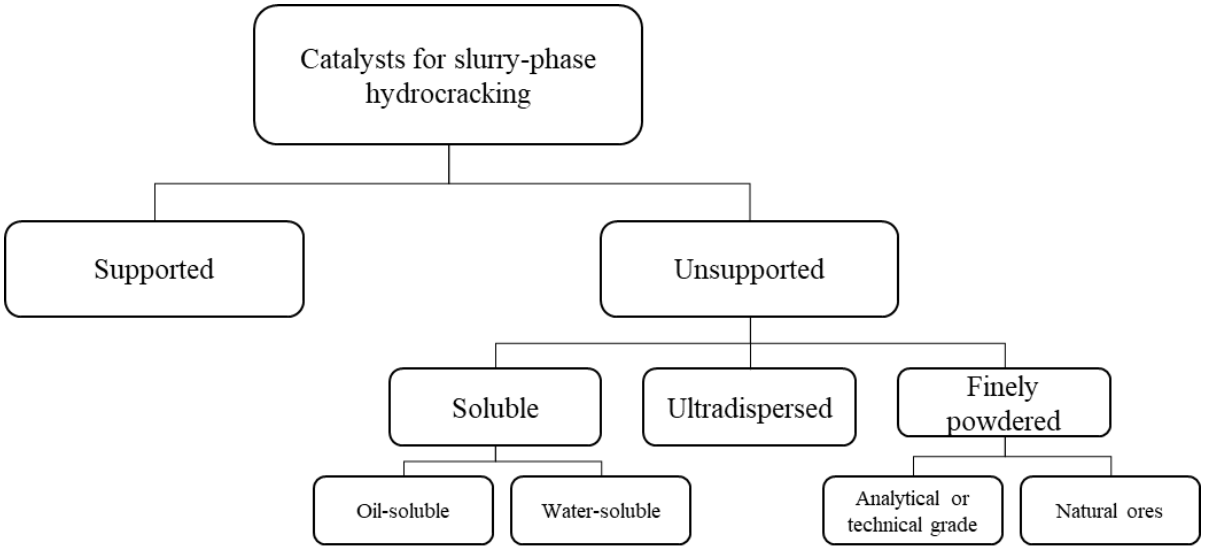

Figure 2. Classification of slurry-phase hydrocracking catalysts. Adapted from Al-Attas et al. (2019a).

2.3.1.1 Finely powdered dispersed catalysts

Finely powdered dispersed catalysts can be classified into analytical/technical grade synthesized catalysts and natural ores (Al-Attas et al., 2019a).

Natural ores

The finely powdered dispersed catalysts of natural ore origin are widely used in industry for slurry-phase hydrocracking purposes due to their availability and low cost (Al-Attas et al., 2019a). Commonly used ores include magnetite, limonite, molybdenite, hematite, ferrite, and laterite (Al-Marshed et al., 2015; Ancheyta, 2013). The ores can be processed by different methods including drying, grinding, milling, and sieving of minerals (Montanari et al., 2017).

A study on hydrocracking of vacuum residue using red mud (containing iron and other metal oxides) as a catalyst was conducted by Nguyen-Huy et al. (2012). Experiments were conducted in a batch reactor at various conditions. A catalyzed and a non-catalyzed run were conducted at 490 °C and 150 bar (90 bar H_2). A catalyst loading of 4.0 wt-% (1.2 g) and a reaction time of 2 hours yielded coke formation of 1.1 and 14 wt-% for catalyzed and non-catalyzed runs, respectively. The gas yield was also lower for the catalytic experiment in comparison to the non-catalyzed run with 9.9 wt-% compared to 15 wt-%. It was determined through characterization of the spent catalyst that the hematite (Fe_2O_3) in red mud, is activated in-situ by sulfur released by thermal cracking to form active pyrrhotite (Fe_xS_y) phases, boosting hydrogenation reactions.

The use of Australian limonite (AL) and Brazilian limonite (BL) for hydrocracking of Brazilian Marlim vacuum residue, with a conventional $NiMo/Al_2O_3$ catalyst used as a reference was investigated by Matsumura et al. (2005). All catalysts were pulverized to a size below 150 μm. At reaction conditions of 440 °C, 100 bar, reaction time of 90 minutes, and a catalyst loading of 3 wt-%, conversions of 88, 64, 77 and 78 wt-% were achieved for non-catalyzed run, $NiMo/Al_2O_3$, BL and AL, respectively. Coke formation was lowest for $NiMo/Al_2O_3$ at 4.1 wt-% followed by BL at 5 wt-% and AL at 8.8 wt-%. All catalysts showed better coke inhibition compared to the blank run, which yielded coke formation of 20 wt-%. In terms of activity, hydrogenation reactions were favored over the $NiMo/Al_2O_3$ catalyst while hydrocracking reactions were favored over the limonite catalysts, yielding higher amounts of lighter compounds. The distribution of products generated using different catalysts can be seen in Figure 3. In general, removal of heteroatoms such as S and V was also better with the conventional $NiMo/Al_2O_3$ catalyst, while Ni removal was higher with the limonite catalysts.

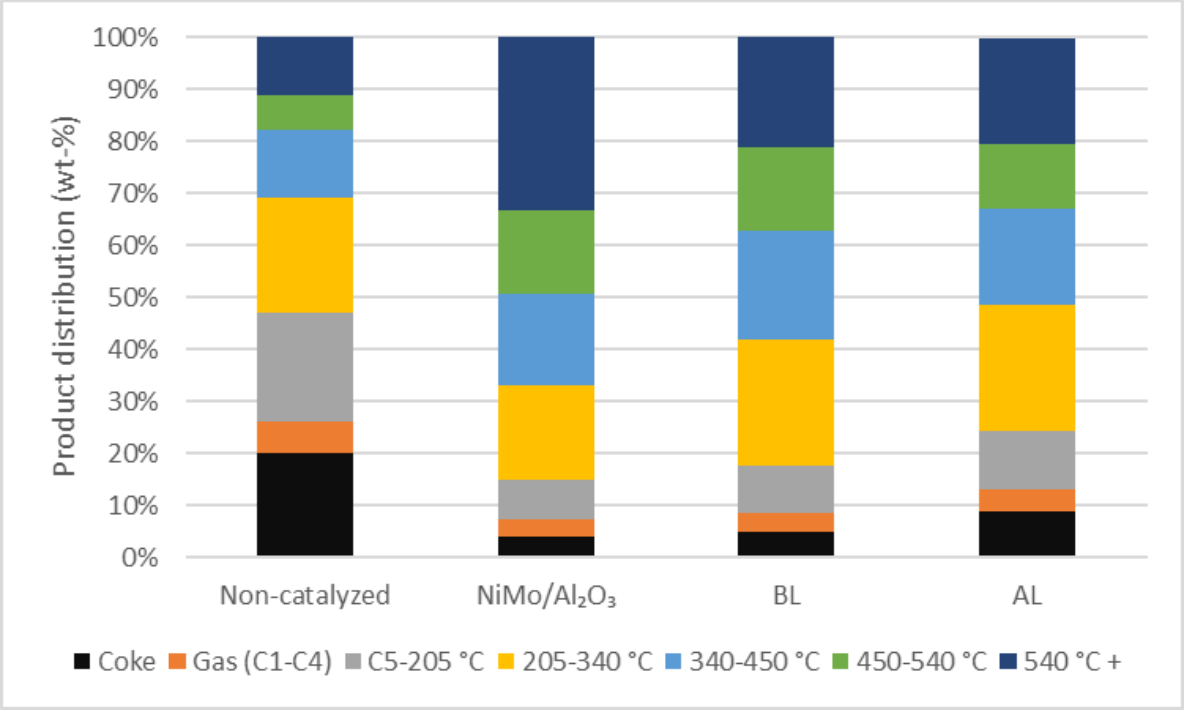

Figure 3. Product distribution in hydrocracking of Brazilian Marlim vacuum residue using limonite ore catalysts at 440 °C, 100 bar H_2, reaction time of 90 minutes and catalyst loading of 3 wt-%. Adapted from Matsumura et al. (2005).

Analytical or technical grade

Finely powdered dispersed catalysts based on synthesized particles usually consist of transition metals including chromium, iron, molybdenum, nickel, and titanium (Al-Attas et al., 2019a). The particles can be oxides, salts, or sulfides and the size order varies between micrometers and nanometers, depending on the preparation method (Montanari et al., 2017). Such preparation methods used include ball milling, hydrothermal synthesis, and precipitation (Ancheyta, 2013; Montanari et al., 2017). Regarding the size of finely powdered dispersed catalysts, Co-doped MoS_2 with particle sizes around 13 nm determined by high-resolution transmission electron microscopy (HRTEM) statistical analysis were reported by Cao et al. (2021). Upgrading of heavy oil utilizing finely powdered catalysts was studied by Al-Marshed et al. (2015). The catalysts were different Fe, Ni, and Mo oxides and sulfides of varying sizes. For Fe, it was expected that the smaller particles would show higher activity due to the higher surface area-to-volume ratio, however variations of the size of Fe_2O_3 particles (≤50 nm and ≤5 µm) did not have a significant effect on the coke formation and product distribution. For the molybdenum-based catalysts MoS_2 (≤2 µm) and MoO_3 (≤100 nm), a better yield of liquid products was achieved with the larger sulfide particles (86 wt-% vs. 84 wt-%) while inhibition

of coke was also better with lower coke yield (4.4 wt-% vs. 5.9 wt-%). It can be concluded that the sulfide form of the catalysts, which is formed in-situ from sulfidation of the metal oxides, helps to enhance hydrogen uptake and hydrogenation due to sulfur-deficient sites in the sulfide catalyst and thus helps prevent condensation and polymerization reactions initiated by free radicals from taking place. The tested Ni-based unsupported catalyst NiO (≤50 nm), also showed good coke suppression and a good product distribution compared to the blank run, with a coke yield of 5.8 wt-% and a liquid product yield of 84.6 wt-% compared to 12 wt-% and 76 wt-% for the blank run, respectively.

NEBULA is a commercialized unsupported hydrotreatment catalyst, produced by Albemarle (former Akzo Nobel Catalysts) and developed in close cooperation with ExxonMobil (Eijsbouts et al., 2007; Gochi et al., 2005). The catalyst is a porous sulfided trimetallic NiMoW sponge catalyst, which has shown better hydrodesulfurization (HDS) and hydrodenitrogenation (HDN) activity than traditional supported $NiMo/Al_2O_3$ and $CoMo/Al_2O_3$ hydrotreating catalysts (Gochi et al., 2005; Plantenga and Leliveld, 2003; Vroman et al., 2001). The use of traditional supported hydrotreating catalysts for hydrodesulfurization of aromatic compounds such as alkyl-substituted dibenzothiophenes involves a two-step mechanism for sulfur-removal, with hydrogenation of the aromatic ring taking place before the actual desulfurization step (Plantenga and Leliveld, 2003). With the NEBULA catalyst, the direct hydrogenolysis pathway is preferred; thus, sulfur can be removed directly without saturation of the aromatic ring (Plantenga and Leliveld, 2003).

2.3.1.2 Ultradispersed nanocatalysts

Ultradispersed nanocatalysts can be achieved through the liquid-phase synthesis of microemulsions containing catalyst precursors (Prajapati et al., 2017). An emulsion can be defined as a colloidal system of non-miscible liquids, e.g., oil and water, where one phase is dispersed and the other one is continuous (Prajapati et al., 2017). A surfactant, which lowers the surface tension between two liquids, is used to stabilize the system (Prajapati et al., 2017). Utilizing this kind of catalyst preparation can provide better dispersion, controlled sizes, and homogeneity of the dispersed catalyst in comparison to finely powdered dispersed catalysts (Son et al., 2008). Another advantage of catalyst preparation using this method is the ability to control nanoparticle size and morphology by adjusting the ratios between oil/surfactant and water/oil (Alkhaldi and Husein, 2014). Usually, the emulsifying procedure involves mixing the organic component containing the feedstock e.g., bitumen and surfactant, with the aqueous solution at a high stirring speed (Galarraga and Pereira-Almao, 2010). There are several

methods that can be used to form microemulsions of different types, with the microemulsion types including emulsion liquid membrane (ELM), colloidal emulsion liquid (CEL) and reverse micelle (RM) (Prajapati et al., 2017). According to a study by Prajapati et al. (2017) focused on comparing different types of microemulsions for obtaining ultradispersed MoS_2, RM proved to be the best option for hydrocracking of vacuum residue (VR), with this type yielding the smallest MoS_2 particles with the average particle size of ca. 120 nm, the narrowest size distribution among the different methods with maximum 65% of particles being in the size order of 120 nm and the least coke formed. Additionally, the catalyst synthesized from the RM-type microemulsion contributed to the highest hydrogenation of the mentioned types, confirmed by the hydrogen-to-carbon (H/C) ratio of the liquid product and the lowest amount of unconsumed hydrogen.

2.3.1.3 Soluble dispersed catalysts

The soluble dispersed catalysts can be classified into two categories, namely oil-soluble and water-soluble (Al-Attas et al., 2019a). These soluble dispersed catalysts are formed from precursors that contain the active metal, usually molybdenum, cobalt, chromium, nickel, or other metals from the groups IVB-VIII, with the metals usually in the form of salts or ligands (Al-Attas et al., 2019a). The catalyst crystals are formed in-situ by sulfidation with H_2S, which is released during HDS reactions or by a feed of a sulfiding agent (Du et al., 2015; Furimsky, 2007). In comparison to finely powdered dispersed catalysts, soluble unsupported catalysts have a higher surface-area-to-volume ratio, leading to higher catalytic activity (Al-Attas et al., 2019a).

Water-soluble dispersed catalysts

Water-soluble dispersed Mo-based catalysts are formed through two major types of water-soluble precursors, namely ammonium molybdates and phosphomolybdic acids (Al-Attas et al., 2019a). Pretreatment such as emulsion, dispersion, and dehydration are needed when preparing water-soluble dispersed catalysts (Al-Attas et al., 2019a). Water-soluble precursors can be prepared by mixing a water solution containing the catalyst precursor with a surfactant (Al-Rashidy et al., 2019). This aqueous phase can then be added dropwise to a heated organic phase such as light vacuum gas oil (LVGO), after which the mixture is stirred and heated (Al-Rashidy et al., 2019). Finally, the mixture is heated and bubbled with nitrogen to remove water (Al-Rashidy et al., 2019). Together with the water-soluble precursor, water or a heteropoly acid can be added to the feedstock, to form organometallic compounds which improve catalyst

activity (Sahu et al., 2015). Advantages of water-soluble dispersed catalysts are the cheap inorganic compounds from which the precursors are synthesized such as for example ammonium tetrathiomolybdate (ATTM) and ammonium heptamolybdate (AHM) (Al-Attas et al., 2019a). Unfortunately, in comparison to oil-soluble dispersed catalysts, water-soluble dispersed catalysts exhibit lower catalytic activity due to evaporation of water and sintering of the formed active sites causing generation of large particles, which reduces the capability of dispersing into the tiny particles (Al-Attas et al., 2019a). Examples of catalysts are molybdates, MoS_2, NiMo and CoMo complexes as well as ferrous salts (Quitian and Ancheyta, 2016).

Oil-soluble dispersed catalyst

Oil-soluble dispersed catalysts are more commonly used than water-soluble ones, due to their higher activity and better dispersion in heavy oil (Al-Attas et al., 2019a). These catalysts have a unique ability to disperse well in the heavy fraction, with a high surface area-to-volume ratio, a property which is useful from the standpoint of catalytic activity (Sahu et al., 2015). Compounds used to form oil-soluble precursors include organic amine metal salts, organic acids, and quaternary ammonium compounds containing metals (Al-Attas et al., 2019b; Furimsky, 2007). Examples of oil-soluble MoS_2 precursors are molybdenum dithiophosphate (Mo-DTP) and molybdenum dithiocarbamate (Mo-DTC) (Watanabe et al., 2002). Compared to the water-soluble equivalents, oil-soluble precursors are more expensive to synthesize (Sahu et al., 2015). Molybdenum is the preferred choice when it comes to active metals used in oil-soluble dispersed catalysts, due to its high hydrogenation activity and limited coke formation (Du et al., 2015; Nguyen et al., 2016). Hydrocracking of Liaohe vacuum residue was investigated by Chenguang et al. (1998), using different oil-soluble metal precursors. The best catalytic performance was again achieved with Mo followed by Ni, Ru, Co, V, and Fe.

2.3.2 Catalyst combinations and synergies

2.3.2.1 Supported and dispersed dual catalyst system

As mentioned previously, the main properties of unsupported catalysts are related to their strong hydrogenation characteristics and anti-coking properties, while their influence on cracking is low. By introducing a second catalyst, for example a supported acidic catalyst with cracking activity, a good combination of properties could be achieved (Al-Attas et al., 2019a). In these catalysts, the support provides the acidity for cracking while the active metal is responsible for hydrogenation (Al-Attas et al., 2019a). However, supported acidic cracking

catalysts are susceptible to deactivation, due to the presence of metals in the feed and coke formation, when used on their own (Al-Attas et al., 2019a). The anti-coking properties of the unsupported MoS_2 catalyst could prevent this from happening (Al-Attas et al., 2019a). The synergies of the catalyst combination could ultimately lead to a higher conversion of the feed and better selectivity to the desired products (Al-Attas et al., 2019c; Chianelli et al., 2006).

In a study by Al-Attas et al. (2019c), the synergies of a commercial supported hydrocracking catalyst (Ni-W/SiO_2-Al_2O_3-(Y-zeolite)) and a metallocalixarene-based dispersed catalyst (Ni-p-tert-butylcalix[4]arene) for the hydrocracking of heavy gas vacuum oil (HGVO) was investigated and compared to the standalone cracking catalyst. The combination of the two catalysts resulted in lower coke and gas formation by 35.9% and 13.9%, respectively, while the yield of distillate and naphtha increased only slightly (ca. 1%). The coke yield was low for both cases, with 1.5 wt-% and 0.9 wt-%, for the standalone commercial catalyst and a combination of the catalysts, respectively. Conversion remained unchanged for both cases at ca. 83% and generally, the yields of the different fractions were quite similar for both cases. The quality of the liquid product was improved with the dual catalyst combination, with a higher H/C ratio and a lower sulfur content achieved, proving the synergy of the combined catalyst system.

2.4 Factors affecting catalyst performance in hydrotreatment of bio-oil and its model compounds

In this section, factors affecting the performance of the catalyst in hydrodeoxygenation (HDO) and other hydrotreatment processes will be discussed. Different properties of the catalyst, such as the active phase, support, promoter, shape, and dispersion, affect the performance of the catalyst. Other factors such as process conditions and additives will also be discussed, as they have an impact on the catalyst and process performance. The catalyst performance can be judged based on several metrics such as activity, coke formation, selectivity, and stability. The efficiency, quality, and performance of a bio-oil HDO process can be expressed with the yield of organic fraction ($Y_{organic}$) and the degree of deoxygenation (DOD) as follows:

$$Y_{organic} = \frac{m_{organic}}{m_{feed}} \times 100\% \quad (1)$$

$$DOD = \left(1 - \frac{O_{organic}}{O_{feed}}\right) \times 100\% \quad (2)$$

In equation (1), $m_{organic}$ and m_{feed} are the masses of the resulting organic fraction and the crude bio-oil feed respectively, while in equation (2), $O_{organic}$ and O_{feed} are the concentration of oxygen in the organic product and the feed (Dabros et al., 2018b). The expressions for the yield and DOD can be defined differently in different papers, depending on for example, whether the aqueous phase of the biocrude is included in the experiments and calculations. It might be good to keep in mind that 100% deoxygenation is not always the goal, with oxygen-containing compounds such as methanol, ethanol, and dimethyl ether (DME) being also considered as good fuel components. Furthermore, there is a trade-off between the oil yield and DOD, with high DOD correlating with a lower oil yield, since other compounds such as water and gases are formed (Dabros et al., 2018b). Conversion and selectivity can also be used to compare different catalysts and their performance as well as product distribution. The equations for conversion and selectivity are:

$$Conversion = \left(1 - \frac{n_{residual\ reactant}}{n_{initial\ reactant}}\right) \times 100\% \quad (3)$$

$$Selectivity = \frac{n_{Product}}{n_{reacted\ reactant}} \times 100\% \quad (4)$$

In equation (3), the moles of the residual reactant or the unreacted reactant is compared to the initial moles of the reactant (Wang et al., 2015). In equation (4) the moles of a certain product are compared to the total moles of reacted substrate, i.e., the total moles of products (Wang et al., 2015).

2.4.1 Active component

The active species used in HDO include sulfides, oxides, carbides, and phosphides of transition metals as well as reduced transition metals (including noble and non-noble metals) (Dabros et al., 2018b). Commonly used metals in HDO catalysts are Co, Fe, Ni, Mo, Pt, Pd, Ru, and W (Dabros et al., 2018b). These different types of active species will now be discussed in more detail.

Sulfides

Sulfides are a good choice for bio-oil HDO due to their activity and being tolerant to sulfur, which is also present in bio-oil, albeit in lower concentrations compared to fossil crude oil (Dabros et al., 2018b). A common sulfided catalyst is MoS_2, which is widely used in oil refineries in hydrodesulfurization (HDS) processes (Y. Zhang et al., 2020). MoS_2 can be both unpromoted and promoted (Dabros et al., 2018b), and the roles of promoters will be discussed later. The active sites in HDO using MoS_2 catalysts are widely accepted to be the coordinatively unsaturated sites (CUS) on the edges of MoS_2, where sulfur or oxygen from the oxygenated compound can adsorb in a way that C-O cleavage can take place and the deoxygenated compound and water can be formed (Dabros et al., 2018b). The coordinatively unsaturated sites are converted into sulfur-saturated sites by the adsorption of H_2S (Şenol et al., 2007). The exact mechanism taking place during HDO is still debated thus it will not be discussed in further detail (Dabros et al., 2018b). The use of sulfides as catalysts requires feeding of H_2S, using different sulfiding agents if there is not enough sulfur available in the liquid feedstock, in order to enhance/maintain activity of the catalyst and prevent oxidation and subsequent deactivation (Furimsky, 2000). One disadvantage is that the excessive use of sulfiding agent can contaminate the product with sulfur (Furimsky, 2000; Popov et al., 2010).

Oxides

Oxides of Mo, Ni, W, V, or other metals can be applied as the active phase in HDO. When using oxides, a lower H_2 pressure should be used to prevent the oxide from reduction and thus making it inactive (Prasomsri et al., 2013). A lower H_2 pressure might be considered economically favorable but might lead to a larger amount of coke, as higher H_2 pressures usually help in mitigating coke formation (Dabros et al., 2018b). Sulfur is also potentially detrimental to activity of the oxide catalyst, due to its strong adsorption (Rodriguez and Hrbek, 1999). For these reasons, reaction conditions should be optimized to keep the oxide in its active form. Oxide HDO activity correlates with the presence and strength of acid sites, with Lewis acidity affecting the initial chemisorption step while Brønsted acidity affects availability of hydrogen at the surface of the catalyst in form of hydroxyl groups (Dabros et al., 2018b).

The HDO of phenol using partially reduced W and Ni-W oxides on an active carbon (AC) support was studied by Echeandia et al. (2010). The conditions in the fixed bed reactor were 150-300 °C and 15 bar. All catalysts exhibited activity, however the bi-metallic Ni-W(P) and Ni-W(Si) catalysts using different precursors during synthesis containing P and Si, respectively, showed significantly higher conversion than the other catalysts with almost 100% conversion to oxygen-free compounds at 300 °C.

Reduced transition metals

Using reduced transition metals (e.g., Ni, Pt, Pd, Ru, Rh) as an active phase in HDO catalysts is possible, since they show activity in hydrogenation (HYD) and HDO reactions (Dabros et al., 2018b). Reduced transition metal catalysts do not require a feed of H_2S to maintain catalytic activity such as sulfides but on the contrary, they are susceptible to sulfur poisoning; thus, sulfur present in bio-oil could potentially poison the catalyst during HDO (Mortensen et al., 2016). In reduced transition metal catalysts, the interaction between the active phase and the support is important, with adsorption of oxygenates happening on the metal-support interface and hydrogen donation promoted by the active metal (Mortensen et al., 2016). Reduced transition metals can further be divided into noble (e.g., Pd, Pt, Ru) and non-noble metals (e.g., Ni). The use of noble metals for HDO of beech wood bio-oil in a batch reactor was studied by Wildschut et al. (2009) at both mild and severe conditions of 250 °C, 100 bar and 350 °C, 200 bar, respectively. Of the catalysts tested, Ru/C and Pd/C yielded good results in severe conditions, with a DOD over 85% and the oil yield over 53%. One drawback of the noble metal catalysts is their relatively high price in comparison to other types (Ambursa et al., 2021). Non-noble metals such as Ni, Co, and Fe are attractive due to their low price and high activity in

HDO (Čelič et al., 2015; Olcese et al., 2012). Čelič et al. (2015) studied the use of Ni nanoparticles from a metal-organic framework (MOF) precursor (MIL-77(Ni)) for HDO of glycerol-solvolyzed lignocellulosic biomass. The experiments were conducted in a slurry reactor at 300 °C and 8 MPa H_2. Ni nanoparticles were formed in-situ as the precursor decomposed and formed particles with the final size of 100 nm. The Ni nanoparticles showed high activity at relatively mild conditions and exhibited more than 10 times higher mass activity in terms of mass Ni metal for hydrogenolysis than commercially available Ni nanoparticles (10 nm) supported on SiO_2-Al_2O_3. This was explained by the high purity and crystallinity of the MOF, leading to a better control over the size, shape, and homogeneous distribution of the formed particles.

Phosphides

Different metal phosphides can be used as the active phase in HDO catalysts (Whiffen and Smith, 2010). Ni and Co phosphides on activated carbon (AC) support were studied in the HDO of fast pyrolysis oil from hardwood sawdust by Guo et al. (2018). A commercial Ru/C catalyst with 5 wt-% Ru was used as a benchmark. The experiments were performed in a batch reactor at 300 °C and 50 bar H_2, with the total pressure varying between 110-170 bar depending on the catalyst used, for 3 hours. 40 g of pyrolysis oil and 2 g of catalyst were added to the reactor, translating into a catalyst loading of 5 wt-%. Of the phosphide catalysts, the best results were achieved with catalysts with a metal-to-phosphorous (M/P) ratio of 3:2 for both Ni and Co. With the NiP/AC catalyst with a M/P ratio of 3:2 a 66 wt-% oil yield was achieved, while a slightly under 60 wt-% yield was achieved with the corresponding CoP catalyst. Varying the M/P ratio was detrimental for the oil-yield, which might be explained by formation of new active species on the surface or due to changes in acidity of the catalyst. In comparison to the Ru/C reference catalyst, the results of the NiP/AC with M/P ratio of 3:2 were comparable in terms of the fraction yields, with a slightly higher coke formation with the NiP catalyst. However, the properties of the oil fraction from the NiP catalyst were better than for Ru/C, with a higher DOD of 65 wt-% compared to 42 wt-% and as a result better higher heating value (HHV) at 37.2 vs. 32.5 MJ/kg based on the Dulong formula (Guo et al., 2018). The Dulong formula for HHV is defined as:

$$HHV\ \left(\frac{MJ}{kg}\right) = 0{,}3383 \times C + 1{,}422 \times \left(H - \frac{O}{8}\right) \quad (5)$$

where C, H and O are the amounts of carbon, hydrogen, and oxygen in terms of weight-% (Guo et al., 2018). The DOD and HHV for the Co-based catalyst with the same M/P ratio were 62 wt-% and 36.2 MJ/kg, respectively. Catalyst characterization of the fresh and spent catalysts showed lower Brunauer-Emmett-Teller (BET) specific surface areas and larger average pore sizes for all catalysts, which is likely explained by coke and solids formation leading to the plugging of micropores. The commercial Ru/C catalyst showed least reduction of the surface area of all tested catalysts.

Oxidation and deactivation of a Ni_2P/SiO_2 catalyst in HDO of guaiacol (2-methoxyphenol) was noticed when a low pressure of 1 bar was used, while this was not the case at 8 bar (Moon et al., 2014). Water was also found to contribute to the oxidation of NiP to less active species such as oxides and phosphates (Li et al., 2011).

Carbides

Carbides were studied by Sharma and Kohli (2020) for HDO of bio-oil from fast pyrolysis of pine sawdust in a batch reactor at 350 °C and 45 bar for 2 hours. The unsupported carbide slurry catalysts used in the experiments were NiC, MoC and NiMoC and the catalyst loading in the reactor during experiments was 0.57, 0.57 and 0.09 wt-%, respectively. It was determined that the use of the catalysts yielded somewhat higher liquid product yield than the blank run, however the large difference was in the amount of solids formed, with the blank run yielding over 55% solids and all catalyzed runs all yielding under 40% solids. However, the performance of the carbides was not as good as the sulfide slurry-catalysts tested in the same study. In addition, carbides have been shown to be susceptible to oxidation caused by water, which is inevitable in bio-oil HDO (Engelhardt et al., 2017; Mortensen et al., 2015).

2.4.2 Catalyst support

The role of the support in HDO is dependent on the active species in the catalyst system and on the oxygen compounds to be hydrotreated (Dabros et al., 2018b). The effect of different supports using the same active phase was investigated by Phan et al. (2015) in HDO of the bio-oil model compound guaiacol. The active phase of NiMo was impregnated on to γ-Al_2O_3, CeO_2, and SBA-15 (mesoporous silica) support materials. Experiments were conducted in an autoclave at 250 °C and 50 bar H_2 for 3 hours. The BET surface area of the SBA-15 support material was clearly the highest at 853 m^2/g, compared to 132 m^2/g and 83 m^2/g for γ-Al_2O_3 and CeO_2, respectively. Consequently, the surface area for the NiMo impregnated on SBA-15 support was also the highest at 270 m^2/g while on γ-Al_2O_3 and CeO_2, the specific areas were

86 m^2/g and 27 m^2/g. In the experiments, 40 g of 3 wt-% guaiacol in n-hexadecane solution and 2 g of catalyst was loaded into the reactor. The chemical composition of the catalysts was the same in terms of the amount of active phase and support. The metal loading of the catalysts was 30 wt-% MoO_3 and 6 wt-% NiO. The SBA-15 supported catalyst yielded the best results with a conversion of 90% and a DOD of 67.5%. However, the coke deposition was also the highest for this support at 2.6 wt-%. Conversion and DOD for CeO_2 support were 23% and 20% respectively, while for Al_2O_3 the corresponding values were 15% and 18.5%. Coke deposition for CeO_2 and Al_2O_3 was 0.7 wt-% and 2.3 wt-%, respectively. Clearly the performance of the SBA-15 support was the best in terms of activity and conversion, which can be explained by the good dispersion of NiMo on the SBA-15 supports, while the deposition of coke was slightly higher than with the other two support materials. The results are summarized in Figure 4.

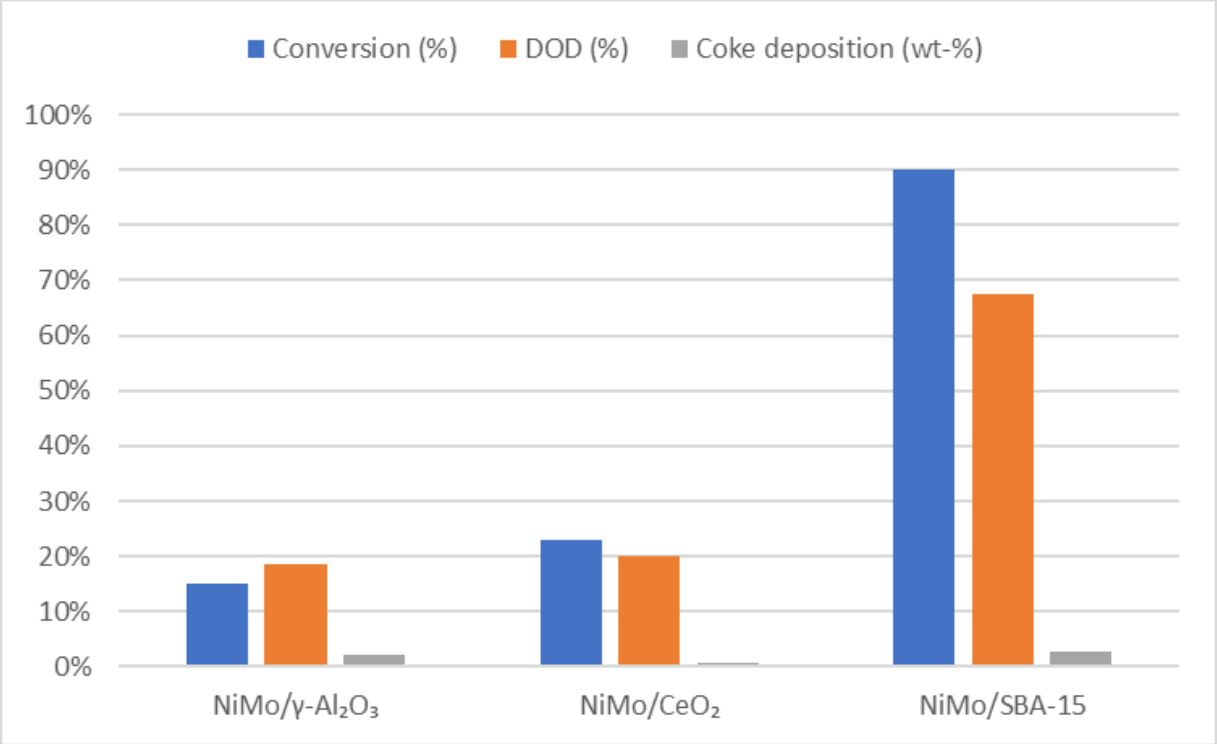

Figure 4. Effect of support on conversion, degree of deoxygenation (DOD) and coke deposition in HDO of guaiacol at 250 °C and 50 bar H_2 for 3 hours. Adapted from Phan et al. (2015).

A major difference when comparing supported and unsupported HDO catalysts is cracking activity. The low acidity of unsupported catalysts such as MoS_2 and MoO_2 leads to a low promotion of C-C bond cleavage in comparison to a catalyst with an acidic support such as

alumina (Grilc et al., 2015). In a study by Grilc et al. (2015), hydrodeoxygenation of lignocellulosic biomass with different unsupported Mo and W catalysts was compared. All unsupported MoS_2 catalysts led to high selectivity of hydroxyl group (-OH) HDO with selectivity in the range 93-97% relative to decarbonylation and decarboxylation, which is beneficial from the standpoint of carbon retention and the liquid product yield. It can be concluded that there was limited catalyst activity towards hydrocracking, decarbonylation and decarboxylation reactions when using the unsupported MoS_2. It should however be kept in mind that high acidity of support materials correlates with coke formation (Grilc et al., 2015). For example, γ-Al_2O_3 support, which is commonly used in conventional hydrotreating, has a high acidity which translates into high coke formation on the catalyst surface, consequently leading to deactivation (Popov et al., 2010). High coke formation is particularly problematic when using porous support materials, since solids and coke plug the pores and thus reduce catalyst activity (Nimmanwudipong et al., 2011).

One often overlooked property of suitable support materials for bio-oil HDO is water stability (Dabros et al., 2018b). The water content in bio-oil and the water that is formed during HDO can in the case of γ-Al_2O_3, convert it into boehmite (AlOOH), decreasing activity since active species can get trapped in the support lattice (Laurent and Delmon, 1994; Venderbosch et al., 2010).

2.4.3 Promoter

Both in the case of supported and unsupported MoS_2 based catalysts, Ni and Co are often used as promoters to enhance catalytic performance by improving hydrogenation activity as well as stability against deactivation (Dabros et al., 2018b). The increased activity can be linked to the formation of highly active NiMoS and CoMoS phases (Zhu et al., 2016). It has also been suggested that different types of active sites or phases are more suited to hydrotreat different types of oxygenated functional groups (Dabros et al., 2018a). The reaction pathways in bio-oil HDO can also be influenced by the promoter (Guo et al., 2019).

A study by Ruinart de Brimont et al. (2012) on HDO of ethyl heptanoate (at 250 °C and 15 bar) with an unsupported Ni-promoted MoS_2 catalyst, showed an increase in selectivity towards decarboxylation (DCO) in relation to HDO with an increase in the amount of Ni-promotion.

As already mentioned, the role of promoters in supported hydrotreatment catalysts is to improve catalyst activity, stability, and to influence reaction pathways. The effect of Ce and Cu promoters on a NiMo/γ-Al_2O_3 supported catalyst in HDO of bio-oil from fast pyrolysis of

cassava rhizome was studied by Sangnikul et al. (2019). The effect of 4% Ce or Cu promotion resulted in ca. 66% lower oxygen content in comparison to the untreated bio-oil. The corresponding number for the unpromoted NiMo/γ-Al_2O_3 catalyst was 52.5%. The increase in HDO can be linked to the ability of Cu to promote hydrogenation (Khromova et al., 2014) and Ce to promote hydrodecarboxylation (HDC) (Liu et al., 2012) reactions.

Water stability of MoS_2/Al_2O_3 and Co-promoted Co-MoS_2/Al_2O_3 supported catalysts was compared by Badawi et al. (2011). A decrease of H_2S/H_2O ratio (addition of water) led to deactivation in both catalysts, however deactivation could be reversed in the Co-promoted catalyst by decreasing the feed of water and returning to the initial water-free conditions. Subsequently, 90% of the initial catalyst activity could be recovered. In comparison, deactivation of the non-promoted catalyst could only be partly reversed and is likely explained by a combination of the following phenomena: the formation of oxidic phase, sintering of the sulfide phase, active site poisoning by water and exchange of S-O of the outer layer of sulfide slabs.

Different promoters for unsupported MoS_2, namely Co, Fe, and Ni, in HDO of p-cresol (4-methylphenol), a phenolic model compound for lignin-derived bio-oil, were studied by Guo et al. (2019). In general, the use of phenols as model compounds for HDO of bio-oil has to do with the high bond energy of the $C_{aromatic}$-O bond in comparison to other C-O bonds in bio-oil, making HDO of this bond more difficult. In the study, the activity of the catalysts as well as the effects of Fe/Mo molar ratio and hydrogen pressure on DOD and selectivity were investigated. Optimal results were achieved with the Fe/Mo molar ratio of 0.7 resulting in conversion of 96.3% and DOD of 95.7% at 250 °C and 4 MPa H_2 after 3 hours. In comparison, the mono-metallic sulfides MoS_2 and FeS showed conversion of 32.5% and 1.6% respectively, proving the low activity of FeS as a standalone catalyst. The improved activity could be explained by the synergy of Fe sulfides and MoS_2, with the former acting as a donor phase to supply activated hydrogen and in this way enhancing conversion. The Fe-promoted MoS_2 was also compared with Ni- and Co-promoted MoS_2, prepared according to the same principle and with the same ratio of promoter-to-Mo of 0.7. The conversions at 250 °C, 40 bar H_2 and 1.5 h of reaction time for Ni-MoS_2, Co-MoS_2 and Fe-MoS_2 were 28.1%, 73.5% and 78.6% respectively. Differences in selectivity of toluene could also be noticed between the catalysts giving 39.5% for Ni and 98.1% for Co. The toluene selectivity value for Fe was ca. 95%. For Ni-promoted MoS_2, higher selectivity towards methylcyclohexane and 4-methylcyclohexene was observed, indicating that more saturation of the aromatic ring was achieved with the Ni-promoted MoS_2 as opposed to Co- and Fe-promoted MoS_2. It can be added that the Fe-

promoted MoS_2 had the largest specific area at 81.3 m^2/g compared to 29.5 m^2/g and 25.3 m^2/g for Co and Ni.

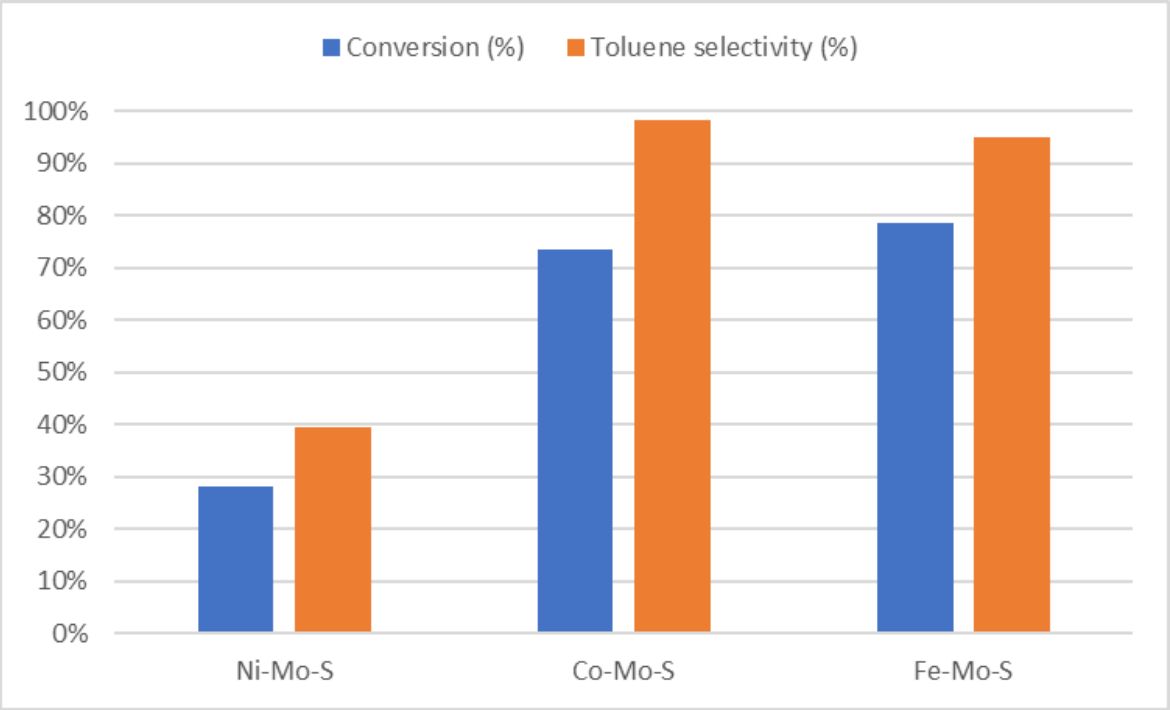

Figure 5. Conversion and selectivity to toluene in HDO of p-cresol at 250 °C and 40 bar H_2 for 1.5 hours of reaction time with Ni-, Co- and Fe-promoted MoS catalysts. Adapted from Guo et al. (2019).

A similar study was conducted by Cao et al. (2021), also on HDO of p-cresol using Co-promoted nano-MoS_2 catalyst in a fixed-bed reactor. A non-promoted MoS_2 catalyst resulted in 17% conversion at process conditions of 220 °C and 3 MPa. Already small amounts of Co-promotion at Co/(Co+Mo) ratio of 0.1 resulted in conversion of 85.6%. An optimal promotion was reached at Co/(Co+Mo) ratio of 0.3, which led to conversion of ca. 99%. Higher ratios than this led to excessive Co and subsequently the catalytic activity decreased.

2.4.4 Process conditions

2.4.4.1 Temperature

As it has been mentioned already earlier, cracking reactions in slurry reactors with unsupported catalysts are mainly of thermal nature. Typically, bio-oil HDO is performed in the temperature range of 250-400 °C (Mortensen et al., 2011). At higher temperatures more cracking reactions take place, leading to a higher coke formation and gas yield while decreasing the oil yield

(Elliott et al., 2009). The temperature has also an effect on reaction pathways of bio-oil components, with different reactions dominating at certain temperatures (Dabros et al., 2018b). For example, certain undesirable reactions take place at higher temperatures while reaction pathways can also become inhibited. One such example is the hydrogenation of aromatics becoming unfavorable at elevated temperatures due to chemical equilibrium of hydrogenation reactions (Ternan et al., 1979).

In a study by Elliott et al. (2009), HDO of bio-oil in a fixed-bed reactor was investigated at 140 bar. An increase in temperature from 310 °C to 340 °C led to an increase in the DOD from 65% to 70% while at temperatures above 340 °C, cracking started to take place. An increase in temperature from 310 °C to 360 °C was detrimental to the oil yield, as it decreased from 75% to 56% while the gas-yield increased threefold. Simultaneously DOD decreased from 65% to 52%. Clearly there is an optimal temperature for HDO reactions, with too high temperatures having a negative effect on the desired products and performance.

Temperature also influences the catalyst stability, with a lower reaction temperature being beneficial for catalyst stability (Liu et al., 2017). In a study by Liu et al. (2017), it was reported that a Co-promoted MoS_2 could be reused 7 cycles (8 hours per cycle) without a loss of activity when the reaction temperature was lowered to 180 °C from 300 °C (3 MPa H_2). Conversion for the Co-promoted single layer MoS_2 at 180 °C and 30 bar H_2, was 98% after 8 hours while the conversion was 84% after 1 hour when the temperature was set to 300 °C. A Co-promoted few layer MoS_2 yielded a conversion of 21% after 2 hours at 180 °C. Typical sulfided Mo catalysts suffer from deactivation caused by sulfur loss at higher temperatures, which was in this case prevented by the lower reaction temperature (Saidi et al., 2014). However, performance was clearly sacrificed for stability in this case.

2.4.4.2 Hydrogen pressure

A high hydrogen pressure in HDO is beneficial for saturation of unstable species, limiting coke formation and ensuring good solubility of hydrogen in bio-oil (Kwon et al., 2011; Venderbosch et al., 2010). In a study by Mortensen et al. (2011), the hydrogen consumption and DOD correlation was investigated. Hydrogen consumption increased as a function of DOD and when reaching higher DOD, the slope became steeper. This was explained by the difference in hydrogen consumption between bio-oil compounds and the different reactivity of different compounds, including the least reactive phenolic ones.

The effect of hydrogen pressure in HDO of p-cresol using a Fe promoted MoS_2 catalyst with the Fe/Mo molar ratio of 0.7 was investigated by Guo et al. (2019). It was noticed that a

higher pressure and thus a more severe hydrotreatment resulted in significantly higher conversion of p-cresol. At 1 and 4 MPa H_2, the Fe-Mo-0.7 catalyst yielded conversions of 28% and 95%, respectively.

As mentioned earlier, a high hydrogen pressure can diminish coke formation by saturating unstable species and coke precursors. Low atmospheric hydrogen pressure was investigated for HDO of acetone with a MoO_3 catalyst by Prasomsri et al. (2013). There was a significant drop in conversion at lower hydrogen pressures as a function of time-on-stream (TOS), while the drop in conversion decreased as the hydrogen pressure was increased. It was determined that the H_2 partial pressure had a significant effect on the performance and deactivation of the catalyst, with a higher hydrogen pressure contributing to regeneration of active sites and preventing coke from blocking active sites.

Similar observations were made in HDO of fast pyrolysis oil from rice husk using ethanol as a solvent and a $Pt/SO_4^{2-}/ZrO_2$/SBA-15 catalyst (Dang et al., 2013). The initial hydrogen pressure was varied between 5 bar and 20 bar at different temperatures and ethanol-to-bio-oil ratios. At comparable conditions, coke formation was lower when a higher initial hydrogen pressure (20 bar) was applied, indicating that formation of coke was better suppressed at higher hydrogen pressure. Slightly better selectivity to the desired saturated products was also achieved at higher hydrogen pressures.

2.4.4.3 Catalyst loading

The catalyst loading can have a significant impact on the catalytic performance in HDO of bio-oil. The loading of an unsupported catalyst is typically much lower than for supported catalysts, with unsupported catalyst loading usually being in the 500-2000 ppm range (Liu, 2016; Prajapati et al., 2017). The effect of catalyst loading on product properties, yields, oxygen removal, and coke formation was studied by Y. Zhang et al. (2020), where an aqueous solution of the catalyst precursor, ammonium paramolybdate tetrahydrate ($(NH_4)_6Mo_7O_{24} \cdot 4H_2O$), was emulsified in light cycle oil (LCO) with the help of a surfactant. LCO was chosen as the reaction medium and continuous phase in which the bio-oil was emulsified. The dispersed unsupported MoS_2 catalyst was formed in-situ as the precursor decomposed and a sulfiding agent was fed to the reactor. By varying the feed of the catalyst precursor, the catalyst concentration could be controlled. Experiments were conducted at 360 °C and 79 bar with a hydrogen feed of 1000 L H_2/L bio-oil feed and a liquid hourly space velocity (LHSV) of 0.60 h^{-1}. By analyzing the results of different runs, it could be determined that the product quality improved with increasing catalyst loading (g Mo/g bio-oil), as both degree of deoxygenation

(DOD) and hydrogen consumption increased. Catalyst loading values of 0.003 and 0.008 corresponded to DOD values of 72% and 91%, respectively. The values for hydrogen consumption were 316 and 723 L H_2/L bio-oil for the respective catalyst loading values. The results are illustrated in Figure 6. Other affected properties in the bio-oil were decreased density and acidity in terms of the total acid number (TAN). Higher catalyst loadings led to a slight decrease in CO_2 formation, while an increase in CO formation could be noticed, indicating less decarboxylation and an increase in decarbonylation reactions. The amount of formed coke was relatively small, ranging from 0.8 to 1.8 g/100 g bio-oil and a value of 1.0 g/100 g bio-oil obtained for the catalyst loading of 0.006. Coke formation did not decrease beyond this by increasing the catalyst loading. Finally, the retention of carbon in the oil-phase was estimated to be around 64% to 71% depending on the formation of CO and CO_2.

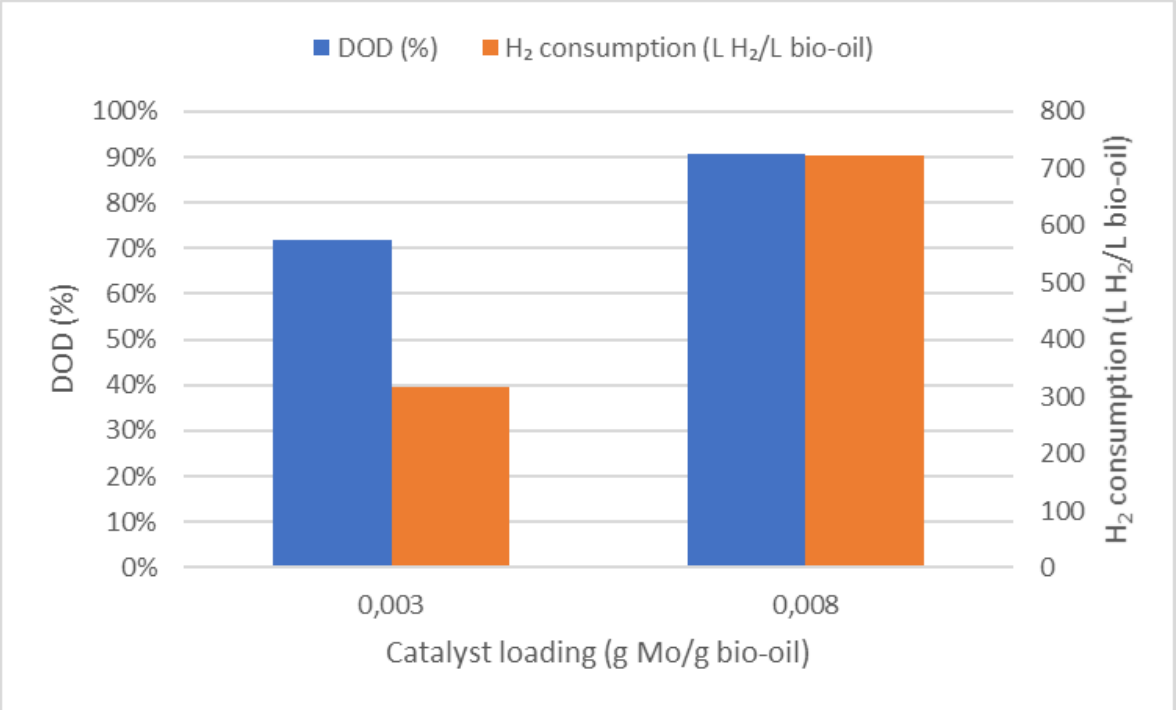

Figure 6. The effect of catalyst-to-bio-oil (CTB) ratio on DOD (left) and hydrogen consumption (right). Adapted from Y. Zhang et al. (2020).

The impact of catalyst concentration on HDO of hydrothermally liquified bio-oil from food processing waste was studied by Sharma and Kohli (2020). An oil-soluble precursor for formation of a MoS_2 catalyst was used in a batch reactor at 350 °C and 45 bar for 2 hours. The catalyst concentration was varied between 500 and 1700 ppm and a blank run without the catalyst was used as a reference. All catalytic experiments showed higher activity than the

blank one in terms of the liquid product yield, conversion, and coke suppression. The highest liquid yield and the lowest solids formation was achieved with a catalyst loading of 1100 ppm Mo. The highest HDO activity or DOD was achieved with a catalyst loading of 1500 ppm Mo, however the formation of solids was also higher. With the catalyst loadings of 1100 and 1500 ppm Mo, the DOD were 58% and 69% respectively. An increase in the catalyst concentration beyond 1500 ppm Mo, led to a decrease in DOD.

A similar finding was made by Bergvall et al. (2021), investigating co-refining of pyrolysis oil with vacuum gas oil (VGO) in a slurry reactor, using in-situ formed MoS_2 particles. At reaction conditions of 435 °C and residence time of 1 hour, the catalyst loading was reduced from 900 to 180 ppm Mo between two runs. This led to lower DOD, decreasing from 94% to 85%. The total gas yield was also the highest of all runs when the catalyst loading was 180 ppm Mo, which could indicate that the low catalyst concentration could not provide sufficient hydrogenation and thus suppress CO and CO_2 formation.

2.4.5 Structure and morphology

The structure of the catalyst can play a large role in the activity (Yang et al., 2008). As discussed in the previous chapter, unsupported catalysts can be prepared by different methods, which in turn influences the formation and structure of the particles and subsequently such properties as the specific surface, the pore volume, and the pore size. The morphology and structure thus play an important role in HDO performance and selectivity of products (Yang et al., 2008). The effect of different solvents used during catalyst synthesis on Co-MoS_2 particle morphologies and their performance in HDO of p-cresol were studied by Song et al. (2018). The different morphologies could be analyzed using field emission scanning electron microscope (FESEM) images. MoO_3 was used as a precursor in the synthesis of MoS_2 with different morphologies. The use of ethanol as a solvent yielded MoS_2 in the form of nanorods, while ethanol as solvent along with urea additive resulted in MoS_2 nanotubes with a stripe-like feature on the surface. The use of hydrazine in conjunction with ethanol gave MoS_2 with nanoparticle morphology while hydrazine as an additive and water as a solvent formed MoS_2 nanoflowers. In terms of HDO performance, all morphologies yielded a similar product distribution with a high selectivity towards toluene (>90%). However, in terms of conversion there were noticeable differences between the morphologies, with 99% conversion achieved with the nanoflower morphology, 78% with nanotubes, 53% with nanoparticles while conversion with nanorods was clearly the worst at slightly over 30%.

Similarly, the structure-activity relationship of unsupported catalysts was tested and discussed by Grilc et al. (2015). Different MoS_2 catalysts were compared in HDO of liquefied lignocellulosic biomass, giving similar selectivity for HDO reactions in all cases, with differences in the yield of organic and tar phases. There was also a difference in the time needed for reaching the same hydroxyl group conversion for different shapes and morphologies of MoS_2. An urchin-like unsupported MoS_2 catalyst exhibited higher HDO activity in comparison to a MoS_2(IF)/C catalyst, a type of inorganic fullerene interconnected by carbon. However, both catalysts yielded a similar product composition under the same reaction conditions, which might point to the existence of fewer active sites in the MoS_2(IF)/C catalyst, which had a higher specific surface are than the urchin-like MoS_2. The urchin-like MoS_2 with its high concentration of active sites on the needles of the catalyst, will not suffer the same mass-transfer limitations that the MoS_2(IF)/C catalyst or traditional porous catalysts might have, since it does not contain small tubular pores that might get blocked and thus result in deactivation. In addition to the different MoS_2 shapes compared, commercially available MoO_2, Mo_2C and nanotubes of WS_2 were tested as received. These catalysts exhibited lower HDO activity than both the urchin-like MoS_2 and the MoS_2(IF)/C catalyst. The characteristics of the tested catalysts are summarized in Table 1.

Table 1. Characteristics of tested catalysts in HDO of solvolyzed lignocellulosic biomass. Adapted from Grilc et al. (2015).

Catalyst	Particle size (µm)	Surface area (m^2/g)	Pore size (nm)	Pore volume (cm^3/g)
MoS_2 (urchin-like)	1	26	27	0.17
MoS_2 (IF)/C	50-100	303	1.9	0.15
MoS_2 (commercial)	3-7	5	22	0.03
MoO_2 (commercial)	0.2-1	5	14	0.01
Mo_2C (commercial)	1-5	3	12	0.01
WS_2 (commercial)	0.1-0.3	6	19	0.03

2.4.6 Additives

2.4.6.1 Surfactant

Surfactants can be used to lower surface tension between polar and non-polar liquids, as is the case when using solvents in conjunction with bio-oil to enhance mixing (Y. Zhang et al., 2020). An emulsion of bio-oil and LCO was prepared by Y. Zhang et al. (2020), for HDO of bio-oil using a MoS_2 catalyst. The non-miscible phases (polar bio-oil and non-polar LCO) were successfully mixed by preparing a bio-oil-in-LCO microemulsion using a surfactant solution with a Hypermer B246SF-to-methanol ratio of 2.5:1. It was noticed that no pressure build-up took place, indicating that polymerization reactions of the bio-oil were well suppressed at the reactor inlet. The effect of the surfactant concentration on solid formation was subsequently investigated. With no surfactant the solids yield was 12.8 g/100 g bio-oil, while the formation of solids dropped to 3.1 and 0.5 g/100 g bio-oil for 0.6 and 1.3 wt-% of the surfactant,

respectively. A further increase of the surfactant concentration did not lead to lower amounts of solids. Clearly, the use of the surfactant distributed the polar bio-oil effectively into the non-polar continuous LCO and had a positive effect on the suppression of coke and solids formation.

Surfactants can be used to modify the morphology of the formed particles in hydrothermal synthesis of MoS_2 (Wang et al., 2014b). The use of surfactants and their effect on the morphology and surface area of the particles in the synthesis of MoS_2 catalysts for HDO of p-cresol was studied by Wang et al. (2014b). The MoS_2 catalysts were prepared by a hydrothermal method with such surfactants as hexadecyltrimethylammonium bromide (CTAB), polyvinylpyrrolidone (PVP), and sodium lauryl benzenesulfate (DBS). The catalysts were prepared using 2.3 g of ammonium heptamolybdate, 3 g of thiourea and 0.3 g of a surfactant in 250 ml of ultrapure water with subsequent synthesis taking place afterwards. Catalyst characterization results can be seen in Table 2. The results show that the catalysts prepared using surfactants have much higher specific surface areas than the catalyst prepared without any surfactant. MoS-CT exhibited the highest surface area followed by MoS-DB and MoS-PV. In comparison, MoS_2 prepared without surfactant had a much smaller specific surface area. The same trend could be seen for the pore volume also. The amount of stack layers in the Rim-Edge model was also affected by the surfactants. HDO experiments were conducted in batch autoclave reactor at 300 °C, 40 bar H_2 and a stirring speed of 900 rpm for 3 h. The amount of catalyst loaded into the reactor was 0.6 g while 13.5 g of p-cresol and 86.2 g of dodecane were added, resulting in a catalyst loading of ca. 4.4 wt-% relative to p-cresol. A correlation between the specific surface areas of the catalysts and the conversions could be noted, with MoS-CT having the highest surface area and yielding the highest conversion. The catalysts prepared with a surfactant clearly performed better than the catalyst prepared without one. There were also clear differences in the reaction pathways and product distributions for the different catalysts with varying hydrogenation-dehydration-to-direct deoxygenation (HYD/DDO) ratios. This can be explained by the different structures of the catalysts, with a lower stacking degree of 3.7 stacks for MoS-DB corresponding to higher HYD selectivity while the higher stacking degree of 4.9 stacks for the MoS-PV catalyst corresponds to a higher DDO selectivity. The DDO and HYD selectivity correlate with the number of layers in the catalyst, which can be explained by the Rim-Edge model of MoS_2. An improvement in HDO activity and different product selectivity could be achieved by using surfactants in the synthesis of the catalysts, influencing such properties as the surface area and morphology.

Table 2. Summary on effects of surfactants on the catalytic properties and performance in HDO of p-cresol at 300 °C and 40 bar H_2 for 3 hours. Adapted from Wang et al. (2014b).

Catalyst	Surfactant	Surface area (m^2/g)	Stack layers	Conversion (%)	HYD/DDO ratio
MoS	-	80	4.6	40	0.34
MoS-CT	hexadecyltrimethylammonium bromide (CTAB)	158	4.3	99	0.31
MoS-DB	sodium lauryl benzenesulfate (DBS)	145	3.7	98	0.77
MoS-PV	polyvinylpyrrolidone (PVP)	131	4.9	91	0.08

2.4.6.2 Solvent

Solvents or liquid hydrogen donors have been proposed as a potential solution to combat coke formation during hydrocracking of heavy oil, by preventing condensation of large aromatic radicals (Kim et al., 2017). Hydrogen donors can be classified into three different types depending on their nature, namely radical hydrogen, anionic hydrogen, and molecular hydrogen donors (Shi and Que, 2003). In a study by Kim et al. (2017), the roles of hydrogen donors in upgrading vacuum residue (VR) were studied at 400 °C and 10 MPa H_2. An unsupported MoS_2 catalyst with the size of 4-8 nm formed from a molybdenum hexacarbonyl precursor was used. When used only with molecular hydrogen and without a hydrogen donor solvent, the MoS_2 catalyst yielded coke formation of 7.2 wt-%. The hydrogen donors used were tetralin, naphthalene, decalin and 1-methylnapthalene giving coke formation of 1.2, 2.9, 4.6 and 5.0 wt-% respectively, which is significantly better than the run without a solvent. A higher yield of the liquid products was also achieved when using hydrogen donor solvents.

Solvents/reaction media such as methanol, ethanol, butanol, dodecane etc. can also be used to improve viscosity and flow properties of bio-oil (Xu et al., 2014). The role of 1-butanol solvent in the HDO of bio-oil from pyrolysis of pine sawdust using a commercial Ru/C catalyst in a batch operating autoclave was studied by Xu et al. (2014). 1-butanol as solvent was investigated in both subcritical and supercritical conditions, with the latter achieved at 287 °C

and 49 bar. Bio-oil and 1-butanol were mixed at 1:1 ratio with 50 g of each component together with 5 g catalyst. The reaction conditions were varied between 250-300 °C and the corresponding pressure was 88-115 bar (20 bar H_2) with a reaction time of 3 h, with runs performed both with and without solvents. Solvent addition had a significant effect on many parameters. At 250 °C the viscosity decreased from 254 to 7 cSt with addition of a solvent. Comparison of the upgraded bio-oils showed an increased carbon and hydrogen content when the solvent was used, with the corresponding number increasing from 62% to 64% and 7.3% to 10.5%, while the oxygen content decreased from 31% to 25%. Formation of solids was also lower with a decrease from 2.5% to 0.3% in the presence of the solvent. At supercritical conditions (300 °C), further improvement of parameters was achieved with even lower viscosity and the oxygen content dropping to 14.5%. The role of 1-butanol in this experiment was determined to serve 5 different functions, namely, to serve as a reaction medium, take part in the reactions (esterification of carboxylic groups), enhance hydrogen dissolution, protect the catalyst, and improve product properties. In the presence of the solvent, polymerization reactions are limited due to a lower reactant concentration of oxygenated groups and thus a lower chance of polymerization reactions. As 1-butanol takes part in reactions with carboxylic acids, the acidity and corrosiveness of the bio-oil is reduced. The solubility of H_2 can also be improved with the presence of 1-butanol, promoting hydrogenation and hydrodeoxygenation reactions. Characterization of the catalyst was performed after runs with and without the solvent as well as for the fresh catalyst. Using XRD and the Sherrer equation, it was noticed that the Ru crystallites in the catalyst without the solvent protection were larger than in the case with the solvent protection. It was determined by transmission electron microscopy (TEM) that the crystallites increased in size as a result of the experiment. For the catalyst in the presence of solvent, the crystallites had grown slightly in comparison to the fresh catalyst. However, the particles were distributed quite homogenously. The spent catalyst in the case without solvent had significantly larger particles sizes than the spent catalyst used in the presence of a solvent, likely due to carbon deposition. Increase of particle sizes was caused by metal particle migration and sintering under high temperatures. The characteristics of fresh and spent catalysts can be found in Table 3. BET specific surface area was 808 m^2/g for the fresh catalyst with 82% and 42% reduction for the spent catalysts used without and with the solvent (1:1 bio-oil-to-1-butanol) at 300 °C and 11.5 MPa for 3 h, respectively. A pore size reduction was also noticed, following the same pattern. It can be concluded that the use of 1-butanol had a positive effect on both the upgraded bio-oil and on catalyst performance. However, the use of large amounts of solvents might not be feasible on a large industrial scale (Lee et al., 2016).

Table 3. Characteristics of fresh and spent Ru/C catalyst used with and without solvent in HDO of bio-oil at conditions of 300 °C and 11,5 MPa for 3 hours. The 1-butanol-to-bio-oil ratio was 1:1 in the run with solvent. Adapted from Xu et al. (2014).

Catalyst	BET surface area (m^2/g)	Total pore volume (cm^3/g)
Fresh	808	0.6
With solvent	467	0.4
Without solvent	148	0.2

2.4.6.3 Sulfiding agent

Sulfiding agents are mainly used to form the active species in sulfided catalysts, by e.g., sulfidation of a metal oxide to a sulfide such as MoS_2 (Al-Attas et al., 2019a). Sulfiding agents are also used to improve catalyst stability during operation by stabilizing active centers (Horáček and Kubička, 2017). Commonly used compounds include dimethyl disulfide (DMDS), thiols or H_2S (Horáček and Kubička, 2017). H_2S is formed once the compounds break down (Rana et al., 2007; Viljava et al., 2000). In a study by Horáček and Kubička (2017), the effect of sulfiding agent flow was investigated in HDO of bio-oil from pyrolysis of spruce with commercial CoMoS and NiMoS hydrotreatment catalysts supported on alumina. In this study dimethyl disulfide (DMDS) was used, which in reaction conditions decomposed to form H_2S. DMDS was applied for both ex-situ catalyst activation as well as for stabilizing the active sites during HDO operation. At a 0.01 wt-% DMDS feed (relative to the bio-oil feed) catalyst deactivation and destruction of active sites was noticed with the CoMoS catalyst, with increasing amounts of heteroatoms including nitrogen and sulfur in the products as a function of time on stream. Nitrogen was said to originate from the bio-oil, which indicates a reduction in HDN activity due to inhibition or destruction of active sites. Sulfur found in the products was reported to have been caused by destruction of active sites in the catalyst, thus leading to lower HDS activity. Sulfur leaching from the catalyst to the organic phase was also reported to contribute to a higher sulfur content in the products. This was confirmed by elemental analysis, with 122 ppm of sulfur present in the pyrolysis bio-oil and an increasing amount of sulfur present in the products as a function of time on stream (TOS). Over 150 ppm sulfur was present in the products after 40 hours on stream. An increase in DMDS dosing from 0.01 to 0.2 wt-%

along with a switch to the NiMoS catalyst was said to counter a rapid decline in the catalyst activity. The contamination of products with sulfur and subsequent removal should be kept in mind when using sulfided catalysts for HDO.

2.5 Industrial processes utilizing slurry-phase catalytic hydrotreatment

Industrial processes utilizing slurry-phase catalytic hydrotreatment have mainly been developed for hydroprocessing heavy oil fractions of fossil origin, with quite a limited number of commercialized processes (Bellussi et al., 2013). Turning heavier fractions such as bitumens and asphaltenes into lighter fractions that can be used as transportation fuels is often the goal, thus utilizing the entire crude oil makeup and improving process efficiency and economics (Montanari et al., 2017). The progressive depletion of light crudes has also led to an increased interest in residue upgradation (Montanari et al., 2017).

2.5.1 The Eni Slurry Technology (EST) process

The Eni Slurry Technology (EST) process developed by the Italian company Eni, is a hydrocracking process for conversion of heavy oil feeds such as asphaltenes to lighter distillates that can be used as transportation fuels (Bellussi et al., 2013). The EST process is operated in a temperature range of 400-450 °C and a pressure of 15 MPa (Bellussi et al., 2013). One problem with the modern slurry technologies is achieving high conversion of the feedstock. In order to reach a high conversion, unreacted heavy fractions need to be recirculated back into the reactor and this has proved to be a problem in many slurry technologies, as it has caused performance and operational issues (Bellussi et al., 2013). A huge advantage of the EST process is that nearly complete conversion can be achieved, with the EST process said to have a conversion rate of 98-99%, high hydrodesulfurization (HDS) over 80% and hydrodemetalation (HDM) over 99% yields (Ancheyta, 2013). This is achieved by recirculating the unreacted heavy fractions back into the slurry reactor after fractionation. A small amount of the unreacted heavy fraction is purged to remove coke precursors and different metallic sulfides (Ni, V) from the recirculated heavy product (Bellussi et al., 2013). When removing the purge, a small amount of catalyst is also removed which is then replaced by introducing new catalyst precursor to the feed (Bellussi et al., 2013). However, the amount of catalyst that is removed is small, since the amount of purge removed is about 1-3 wt-% of the fresh feed (Bellussi et al., 2013). The components in the purge that are removed can be separated through a decanter centrifuge to recover the solid fraction or cake, containing the heavy fractions, coke, and metal sulfides and the liquid fraction which is recirculated back into the slurry reactor (Bellussi et al., 2013). The components of the solid fraction can be further separated to recover such metals as Mo, V, and Ni (Bellussi et al., 2013).

The catalyst used in the EST process is an unsupported molybdenum sulfide (MoS_2) with the shape of nanosized nanolamellae, which is sulfided in-situ from an oil-soluble

molybdenum naphthenate precursor. In the EST process, hydrogen is activated on the edges of a monodispersed (MoS_2) layer (Montanari et al., 2017). This allows for quick addition of hydrogen atoms to the free radicals which have formed as a result of thermal cracking, limiting aromatic condensation reactions and minimizing the formation of coke (Montanari et al., 2017). Different types of catalyst systems were studied by Eni during the development of the technology (Bellussi et al., 2013). Dispersed catalysts based on metals such as Fe, Co, Ni, and V were tested; however, Mo was chosen due to it exhibiting the highest catalytic activity from the hydrogenation standpoint (Bellussi et al., 2013). The use of metal promoters such as nickel to improve catalytic activity of the dispersed MoS_2 particles was studied, with both in-situ and ex-situ introduction of the promoter (Bellussi et al., 2013). The interactions of the catalyst and the promoter were studied; however, only slight increases in hydrodesulfurization (HDS) and hydrodenitrogenation (HDN) could be observed during ex-situ preparation of the catalyst and the promoter (Bellussi et al., 2013).

2.5.2 HCAT/HC

The HCAT/HC technology also known as High Conversion Hydrocracking Homogeneous Catalyst $(HC)_3$ technology has been developed by Alberta Research Council for the upgrading of heavy oil fractions such as crude oils and bitumens (Al-Attas et al., 2019a). The technology is nowadays licensed by Headwater Technology Innovation (HTI) (Al-Attas et al., 2019a). The process utilizes in-situ formation of the dispersed catalyst from oleo-soluble organometallic precursors such as iron pentacarbonyl or molybdenum 2-ethylhexanoate, with the catalyst being formed once the feed is heated up to the reaction conditions coupled with in-situ sulfidation to form MoS_2 or FeS_x (Bellussi et al., 2013). The technology provides high conversion (up to 95%) of the feedstock and excellent anti-coking properties by enhancing hydrogenation reactions (Castañeda et al., 2012). The size of the catalyst particles was determined to be close to the size of the asphaltenes in the heavy oil fraction (Zhang et al., 2007). The technology has been implemented commercially at Neste's refinery in Porvoo, Finland in a Chevron Lummus Global LC-FINING ebullated bed reactor operating on a once-through basis (Bellussi et al., 2013; Chevron Lummus Global, 2007). The MoS_2 catalyst acts as a co-catalyst together with a supported hydrotreatment catalyst, complementing the hydrocracking function of the supported catalyst with a high hydrogenation activity (Kunnas and Smith, 2011).

2.5.3 Veba Combi Cracker (VCC)

The Veba Combi Cracker (VCC) process has been developed from the Bergius process, which is used for liquefaction of coal (Bellussi et al., 2013). In the VCC process, the heavy oil residue is slurried with a Bovey coal powder and red mud (bauxite residue from alumina production by Bayer process) catalyst containing iron and other metals, with an iron concentration of ca. 5.0 wt-% (Al-Attas et al., 2019a). The role of the additive and the catalyst is mainly to prevent the formation of coke. The VCC process is claimed to have conversion over 90% (Sahu et al., 2015). Operating conditions of the process are usually in the temperature range of 440-485 °C and the pressure range of 220-250 bar (Bellussi et al., 2013; Zhang et al., 2007). The VCC process typically operates on a once-through basis (Ziegelaar and Schleiffer, 2016).

2.5.4 UOP Uniflex process

The UOP Uniflex process has been developed from the CANMET Hydrocracking Process and UOP Unicracking and Unionfining Process Technologies (Gillis et al., 2010). The UOP Uniflex process is flexible with respect to the feedstock and can process feeds such as vacuum residues and heavy crudes (Gillis et al., 2010). The process utilizes a nanoscale catalyst based on molybdenum, which main functions are promoting hydrogenation of cracked products, limiting saturation of aromatic rings, and limiting coke formation (Kapustin et al., 2021). In the UOP Uniflex process, an upflow of hydrogen is bubbled through the liquid-filled reactor, leading to back-mixing and near-isothermal conditions (Gillis et al., 2010). This allows the process to be operated at a higher temperature and together with a partial recycling of the unreacted heavy fraction, a high conversion exceeding 90% can be reached (Gillis et al., 2010). Typical process conditions in the upflow reactor of the UOP Uniflex technology are in the temperature range of 435-470 °C and a pressure of 13.8 MPa (Gillis et al., 2010).

2.5.5 PDVSA HDH-Plus process

The PDVSA HDH-Plus technology for upgrading of Orinoco Belt heavy crudes utilizes a catalyst based on different compounds containing iron or molybdenum, which is dispersed in the feed with the help of a catalytic emulsion (Bellussi et al., 2013). Typical operating conditions in PDVSA HDH-Plus process are temperatures of 430-460 °C, total pressure of 170-210 bar (H_2 partial pressure of 125-150 bar) with conversion reported to be above 85% (Bellussi et al., 2013).

Table 4. Summary of industrial slurry-phase catalytic processes and properties.

Process	Pressure (bar)	Temperature (°C)	Catalyst	Conversion (%)	References
Eni Slurry Technology (EST)	150	450	MoS_2	≥98%	(Ancheyta, 2013) (Bellussi et al., 2013) (Montanari et al., 2017)
HCAT/HC	-	-	FeS_x, MoS_2	≤95%	(Al-Attas, Ali, et al., 2019a) (Bellussi et al., 2013) (Castañeda et al., 2012) (Kunnas & Smith, 2011) (S. Zhang et al., 2007)
Veba Combi Cracker (VCC)	220-250	440-485	Fe and other metals	≥90%	(Al-Attas, Ali, et al., 2019a)
UOP Uniflex process	138	435-470	Mo	≥90%	(Gillis et al., 2010) (Kapustin et al., 2021)
PDVSA HDH-Plus	170-210	430-460	Fe, Mo	≥85%	(Bellussi et al., 2013)

2.6 Suitable catalysts for slurry-phase hydrotreatment of bio-oil

2.6.1 Recent bio-oil HDO experiments

This section aims to compare real bio-oil HDO experiments with both unsupported and supported catalysts, by highlighting catalytic performance of different catalyst systems in terms of DOD and formation of coke/solids. All reviewed experiments were conducted in batch autoclaves using real bio-oil feeds, while most experiments also utilized a solvent. A summary of experiments and corresponding catalysts, conditions, and results can be seen in Table 5.

2.6.1.1 Unsupported catalysts

Research papers on the use of unsupported catalysts for real lignocellulosic bio-oil feeds are quite limited, while papers on model compound HDO are more readily available (Cao et al., 2021; Song et al., 2018; Whiffen and Smith, 2010). Studies utilizing unsupported MoS_2 catalysts for palm oil (Burimsitthigul et al., 2021) and bio-oil from liquefied food processing waste (Sharma and Kohli, 2020) also exist; however, the composition of these oils, which are rich in fatty acid derivatives and straight-chain oxygenated hydrocarbons, differ largely from the compounds in lignocellulosic bio-oil, which include phenols, aldehydes, ketones etc. (Burimsitthigul et al., 2021; Sharma and Kohli, 2020). Nevertheless, some promising results have also been achieved in HDO of lignocellulosic bio-oil using Mo-based unsupported catalysts, which can be seen in Table 5. A high degree of deoxygenation and relatively low coke formation has been achieved with different Mo-based catalysts (Grilc et al., 2015; Liu, 2016; Yang et al., 2016).

2.6.1.2 Supported catalysts

The use of noble metal catalysts such as Ru/C (Xu et al., 2014) and Pt/C (Oh et al., 2017), have been proven efficient in bio-oil HDO with high HDO activity and a relatively low coke formation. Using supercritical 1-butanol as a solvent together with the Ru/C catalyst contributed to a minimal coke formation (0.2 wt-%). A relatively low coke formation was also achieved with Fe, Co, and Fe-Co on SiO_2 support; however, HDO activity was lower than for the previously mentioned noble metal catalysts even though the reaction time was longer (Cheng et al., 2017). HDO experiments with NiMo and Cu or Ce-promoted NiMo on γ-Al_2O_3 yielded high formation of coke (over 40 wt-%) and can be linked to a high acidity of γ-Al_2O_3 but also to a relatively low hydrogen pressure (Sangnikul et al., 2019). Different Ni-based catalysts on SBA-15 support were tested by (Oh et al., 2020). The tested active phases were

NiCu, NiMn, and NiZn, with all active phases yielding similar DOD (44.5-55.6 %) and coke formation (9.3-12.8 wt-%).

Table 5. Summary of recent bio-oil HDO experiments with unsupported and supported catalysts.

Feedstock	Bio-oil source	Liquefaction method	Process type	Catalyst	Conditions				Catalytic performance		References
					Temperature (°C)	Pressure (bar)	Time (h)	Catalyst loading (wt-%) [a]	DOD (%)	Solids (wt-%)	
Unsupported catalysts											
Bio-oil/Tetralin (75/25 wt-%)	Dry sawdust	Solvolysis in glycerol/diethylene glycol	Batch	MoS_2 (Commercial)	300	80	1	1.5	81.5	≈31[b]	M. Grilc et al., 2015
Bio-oil/Tetralin (75/25 wt-%)	Dry sawdust	Solvolysis in glycerol/diethylene glycol	Batch	MoO_2 (Commercial)	300	80	1	1.5	74.8	≈34[b]	M. Grilc et al., 2015
Bio-oil/Tetralin (75/25 wt-%)	Dry sawdust	Solvolysis in glycerol/diethylene glycol	Batch	Mo_2C	300	80	1	1.5	82.2	≈54[b]	M. Grilc et al., 2015
Bio-oil/Tetralin (75/25 wt-%)	Dry sawdust	Solvolysis in glycerol/diethylene glycol	Batch	MoS_2 (Urchin-like)	300	80	1	1.5	80.4	≈15[b]	M. Grilc et al., 2015
Bio-oil/Tetralin (75/25 wt-%)	Dry sawdust	Solvolysis in glycerol/diethylene glycol	Batch	MoS_2(IF)/C	300	80	1	1.5	82.9	≈32.5[b]	M. Grilc et al., 2015
Bio-oil/Ethanol (33/67 wt-%)	Dried cornstalk	Hydrothermal liquefaction	Batch	NiMoS	370	40 (H_2)	1	0.3	74.24	≈4[c]	T. Yang et al., 2016
Bio-oil/Ethanol (33/67 wt-%)	Dried cornstalk	Hydrothermal liquefaction	Batch	NiMoS	310	40 (H_2)	1	0.3	53.6	≈2[c]	T. Yang et al., 2016
Bio-oil/Tetralin (33/67 wt-%)	Norweigan spruce	Fast pyrolysis	Batch	NiMoS	250	50 (H_2)	3	0.249[i]	83.6[h]	7.9[g]	K. Liu, 2016
Bio-oil/Tetralin (33/67 wt-%)	Norweigan spruce	Fast pyrolysis	Batch	NiMoS	200	50 (H_2)	3	0.249[i]	75.5[h]	10.2[g]	K. Liu, 2016
Supported catalysts											
Bio-oil	Pine sawdust	Fast pyrolysis	Batch	Ru/C	300	20	3	10	48	9.9[b]	X. Xu et al., 2014
Bio-oil/1-butanol (50/50 wt-%)	Pine sawdust	Fast pyrolysis	Batch	Ru/C	300	20	3	10	68	0.2[b]	X. Xu et al., 2014
Bio-oil	Pine sawdust	Fast pyrolysis	Batch	Mo_2C/CNF	350	40	1	25	72.8	24.66[d]	J. Remón et al. 2021
Bio-oil/Methanol (50/50 wt-%)	Pine sawdust	Fast pyrolysis	Batch	Fe-Co/SiO_2	300	34.5 (H_2)	5	10	40.6	3.30[e]	S. Cheng et al., 2017
Bio-oil/Methanol (50/50 wt-%)	Pine sawdust	Fast pyrolysis	Batch	Co/SiO_2	300	34.5 (H_2)	5	10	29	6.04[e]	S. Cheng et al., 2017
Bio-oil/Methanol (50/50 wt-%)	Pine sawdust	Fast pyrolysis	Batch	Fe/SiO_2	300	34.5 (H_2)	5	10	34.8	6.89[e]	S. Cheng et al., 2017
Bio-oil/Ethanol (80/20 wt-%)	Yellow poplar	Fast pyrolysis	Batch	Ni/AC	300	30 (H_2)	1	5	49.2	9.1[f]	S. Oh et al., 2017
Bio-oil/Ethanol (80/20 wt-%)	Yellow poplar	Fast pyrolysis	Batch	Ni/SBA-15	300	30 (H_2)	1	5	54.9	16.8[f]	S. Oh et al., 2017
Bio-oil/Ethanol (80/20 wt-%)	Yellow poplar	Fast pyrolysis	Batch	Ni/Al-SBA-15	300	30 (H_2)	1	5	49.2	18.6[f]	S. Oh et al., 2017
Bio-oil/Ethanol (80/20 wt-%)	Yellow poplar	Fast pyrolysis	Batch	Pt/C (Commercial)	300	30 (H_2)	1	5	73.7	7.7[f]	S. Oh et al., 2017
Bio-oil/Ethanol (80/20 wt-%)	n/a	Fast pyrolysis	Batch	NiCu/SBA-15	300	30 (H_2)	0.75	4	44.5	10[f]	S. Oh et al., 2020
Bio-oil/Ethanol (80/20 wt-%)	n/a	Fast pyrolysis	Batch	NiMn/SBA-15	300	30 (H_2)	0.75	4	49.1	9.3[f]	S. Oh et al., 2020
Bio-oil/Ethanol (80/20 wt-%)	n/a	Fast pyrolysis	Batch	NiZn/SBA-15	300	30 (H_2)	0.75	4	55.6	12.8[f]	S. Oh et al., 2020
Bio-oil	Cassava rhizome	Fast pyrolysis	Batch	NiMo/γ-Al_2O_3	300	10 (H_2)	1	15	52.5	40.9[e]	P. Sangnikul et al., 2020
Bio-oil	Cassava rhizome	Fast pyrolysis	Batch	Cu-NiMo/γ-Al_2O_3	300	10 (H_2)	1	15	66.2	51.1[e]	P. Sangnikul et al., 2020
Bio-oil	Cassava rhizome	Fast pyrolysis	Batch	Ce-NiMo/γ-Al_2O_3	300	10 (H_2)	1	15	66.3	54.3[e]	P. Sangnikul et al., 2020

[a] Catalyst loading is expressed in proportion to bio-oil content.

[b] Tar formation was expressed as Y_{tar} (wt-%) = ($m_{tar} - m_{cat}$)/$m_{biocrude}$ × 100%.

[c] Solids formation was expressed as Y_{solids} (wt-%) = m_{solids} (g) / $m_{biocrude + solvent}$ (g) x 100 %.

[d] Solids formation was expressed as Y_{solids} (wt-%) = m_{solids} (g) / $m_{biocrude}$ (g) x 100 %. Mass of solids was determined with gravimetric analysis.

[e] Coke formation was determined based on weight difference between fresh and spent catalyst using thermogravimetric analysis (TGA) and expressed as wt-% of total products.

[f] Char formation expressed as Y_{char} (wt-%) = (m_{solids} (g) - m_{cat} (g)) / ($m_{bio-oil}$ (g) + $m_{ethanol}$ (g)) x 100 %.

[g] Solids formation was expressed as Y_{solids} (wt-%) = m_{solids} (g) / $m_{products}$ (g) x 100 %. Catalyst was not separated from solids.

[h] Degree of deoxygenation has been calculated based on organo-oxygen in biocrude and deoxygenated bio-oil. Oxygen in both aqueous and organic phase have been included in calculations.

[i] 2000 ppm Mo and 490 ppm Ni were added to reactor for in-situ sulfidation.

2.6.2 Suitable catalyst candidates for slurry-phase hydrotreatment of bio-oil and corresponding properties

Catalyst properties and their effects on bio-oil HDO performance were discussed earlier. Classification of the catalyst types, depending on their preparation methods, were discussed in the beginning. Depending on the preparation method and additives used, different sizes, specific surface areas, and morphologies of the formed particles can be achieved, having a direct effect on the HDO activity and performance of the catalyst. The advantages and disadvantages of different active species were covered, with high HDO activity obviously already mentioned as one criterion. In addition, the active phase should result in low coke formation and be resistant to deactivation caused by for example water, oxidation, or feed impurities such as sulfur. The active phase should preferably also be readily available and cheap, which makes the use of noble metal catalysts such as Ru/C less attractive. When using supported catalysts, the support should preferably have low acidity, as acidic supports tend to form more coke and lead to more cracking reactions. The low acidity of unsupported catalysts is positive in terms of limited coke formation, low activity towards cracking reactions, and a high liquid product yield. The lack of the support means that it cannot be used to influence reaction pathways and selectivity; however, this can to some degree be achieved by modifying the morphology of the dispersed catalyst or by promoting the catalyst with a suitable promoter. The activity of the active phase can also be enhanced with the use of a promoter. External factors such as reaction conditions should be optimized, considering the inverse relationship between the performance and the catalyst stability, with harsher conditions leading to lower stability. Based on the literature review, sulfided catalysts such as the unsupported MoS_2 have been identified as promising candidates for the HDO of bio-oil, since these catalysts have many of the required features and properties. Low acidity of unsupported catalysts is beneficial for low coke formation in HDO of bio-oil. For this reason, unsupported catalysts do not suffer from plugging of the pores in the same way as supported counterparts. MoS_2 catalyst has been frequently used also in the recent research, yielding good results in terms of conversion and deoxygenation while at the same time limiting coke formation (Grilc et al., 2015; Y. Zhang et al., 2020). Coupling this catalyst with an appropriate promoter to further improve activity has also been studied and has been shown to improve catalyst performance (Cao et al., 2021; Wang et al., 2014a). Finding and developing suitable and efficient catalysts for bio-oil HDO is of paramount importance for the feasibility of the technology.

3 Experimental

Unsupported MoS_2 and Co-promoted MoS_2 catalysts were synthesized by a hydrothermal method as well as by preparing liquid catalyst precursors by an emulsion method. Cobalt was chosen as the promoter in unsupported MoS_2 as it favors the direct deoxygenation (DDO) reaction pathway in HDO of p-cresol, removing the -OH group directly from the aromatic ring (Wang et al., 2014a). In the case of nickel, the reaction pathway usually involves hydrogenation of the aromatic ring before oxygen is removed (Wang et al., 2015). To compare supported vs. unsupported catalysts, Mo and Co-promoted Mo catalysts on activated carbon support were synthesized. Activated carbon was chosen as the support due to its low acidity, which is favorable for mitigating coke formation (Grilc et al., 2015).

3.1 Chemicals

Chemicals utilized in this work are presented in Table 6 and were used without further purification.

Table 6. Chemicals utilized in this work along with their purity and supplier.

Entry	Chemical	Purity (%)	Supplier
1	Norit® SA2 Activated Charcoal	>95	ACROS Organics
2	Ammonium heptamolybdate tetrahydrate	≥99	Merck
3	Cobalt (II) nitrate hexahydrate	99	ACROS Organics
4	Kerosene	≥95	Sigma-Aldrich
5	n-Dodecane	≥99	Merck
6	n-Dodecane	≥99	VWR Chemicals
7	n-Dodecane	≥99	Sigma-Aldrich
8	Span® 80 (Sorbitan oleate)	N/A	Fluka
9	Tween® 80 (POE (20) sorbitan monooleate)	N/A	VWR Chemicals
10	HDK® H18 Pyrogenic Silica	>99.8	Wacker
11	HDK® H20 Pyrogenic Silica	>99.8	Wacker
12	Dimethyl sulfoxide	≥99.9	Riedel-de Haën
13	Thiourea	≥99	Merck
14	Hydrochloric acid AnalaR® NORMAPUR® 37%	35-38	VWR Chemicals
15	Ethanol Etax Aa	99.5	Altia Industrial
16	Dimethyl disulfide	≥99	Sigma-Aldrich
17	Isoeugenol (cis + trans)	98	Sigma-Aldrich
18	Molybdenum (IV) sulfide	N/A	Fluka

3.2 Catalyst synthesis

3.2.1 Synthesis of Mo/AC and CoMo/AC supported catalysts

The designed loading of molybdenum on the activated carbon support, i.e., Norit SA2 activated charcoal was 11.2 wt-% and the catalyst synthesis was conducted using the incipient wetness impregnation (IWI) method. In the CoMo on activated carbon (AC) catalyst, the planned Co/Mo molar ratio was 0.5. Typically, synthesis was carried out by weighing 9.5 g of Norit SA2 activated carbon support material into a double neck round bottom flask. The activated carbon was then dried for 2 hours by heating the flask to 120 °C. After 2 hours, the flask was vacuumed, and drying was continued overnight. Heating was turned off the next morning. The impregnation solution was prepared by weighing 2.20 g of ammonium heptamolybdate tetrahydrate (AHM) ($(NH_4)_6Mo_7O_{24} \cdot 4\ H_2O$). AHM was dissolved in MilliQ water by magnetic stirring and MilliQ water was added until the total volume of the solution was 8.5 ml, as this was the total pore volume of the dried support material. The same procedure was used for the CoMo/AC catalyst, with the difference that 1.81 g of cobalt (II) nitrate hexahydrate ($Co(NO_3)_2 \cdot 6\ H_2O$) was dissolved in MilliQ water in a separate measuring cylinder before mixing with AHM. MilliQ water was then added until the total volume was 8.5 ml. The impregnation solution, which can be seen in Figure 7, was added to the dropping funnel attached to the flask.

Figure 7. CoMo impregnation solution for dry impregnation of activated carbon.

The vacuum tap was closed, and the dropping funnel tap was opened, allowing the solution to enter the cylinder, and subsequently the pores of the support material. The flask was then ‘’clapped’’ in order to distribute the solution evenly and break down bigger pieces of the support material that had lumped together. The impregnation solution was then allowed to absorb into the pores overnight. The catalyst was thereafter dried at 80 °C under vacuum for 5 hours using a Buchi rotavapor. After drying was completed, calcination of the catalyst in nitrogen was performed in a rotating calcination oven, shown in Figure 8, at 250 °C for 2 hours with a temperature ramp of 5 °C/min and a nitrogen flow of 0.3 l/min. Both Mo/AC and CoMo/AC catalysts were pre-sulfided using excess dimethyl disulfide (DMDS) prior to HDO runs. Sulfidation was conducted at conditions of 30 bar H_2 of initial pressure and 350 °C for 1 hour.

Figure 8. Rotating calcination oven used for calcination of prepared activated carbon catalysts.

3.2.2 Synthesis of MoS_2 and Co-MoS_2 by hydrothermal method

Unsupported MoS_2 and Co-MoS_2 synthesis by hydrothermal method was conducted with a one-step procedure based on literature from Wang et al. (2014a, 2016, 2017). The chemistry, including the decomposition of compounds and formation of MoS_2 in hydrothermal synthesis, is described by equations (6)-(9) (Waskito et al., 2019).

$$SC(NH_2)_2 + 2H_2O \rightarrow 2NH_3 + CO_2 + H_2S \quad (6)$$

$$(NH_4)_6Mo_7O_{24} \rightarrow 6NH_3 + 7MoO_3 + 3H_2O \quad (7)$$

$$MoO_3 + 3H_2S + H_2O \rightarrow MoO_2 + SO_4^{2-} + 2H^+ \quad (8)$$

$$MoO_2 + 2H_2S \rightarrow MoS_2 + 2H_2O \quad (9)$$

At first, 0.61 g of ammonium heptamolybdate tetrahydrate (AHM) ($(NH_4)_6Mo_7O_{24} \cdot 4\ H_2O$) and 0.8 g of thiourea ($SC(NH_2)_2$) were dissolved in 20 ml of MilliQ water. For the Co-promoted MoS_2, 0.50 g of cobalt (II) nitrate hexahydrate ($Co(NO_3)_2 \cdot 6\ H_2O$) was also added to the same solution, yielding a Co/Mo molar ratio of 0.5. The pH of this solution was then adjusted to 0.8 with 37% HCl and was monitored using a Mettler Toledo SevenGo pH meter. Adjusting the pH caused the solution to turn black. A lower pH is said to enhance the nucleation rate during hydrothermal synthesis, producing MoS_2 with smaller crystallites (Zhang et al., 2018). The solution and a magnetic stirring bar were then added to a 40 ml in-house built autoclave equipped with a Teflon cup. The autoclave and the heating setup can be seen in Figure 9.

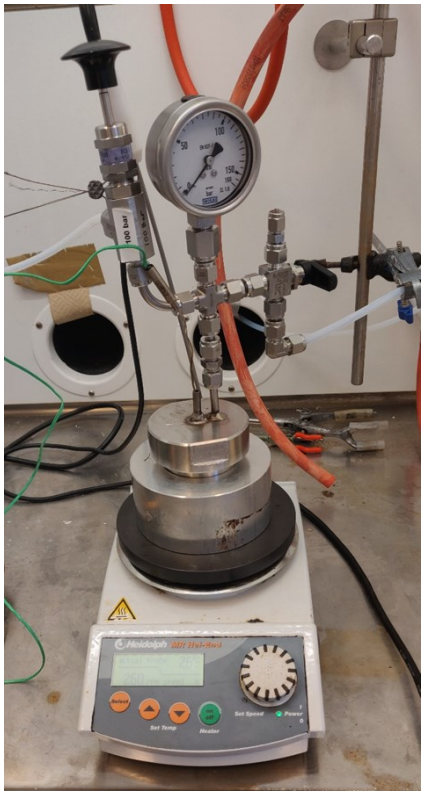

Figure 9. Autoclave for hydrothermal synthesis of (Co)-MoS_2. During synthesis the autoclave was thermally insulated using insulation bandage.

The autoclave was then sealed and flushed with nitrogen three times while a pressure test at 30 bar was also conducted prior to synthesis. Synthesis was performed by heating the autoclave to 200 °C and keeping it at this temperature for 20 h. Magnetic stirring during synthesis was set to 260 rpm. During synthesis, the total pressure increased up to 25 bar. After 20 hours the reactor was cooled, depressurized into the fume hood exit, and flushed with nitrogen to remove excess gases such as H_2S. The autoclave was then opened and the solution containing the black catalyst was poured into a beaker, which can be seen in Figure 10.

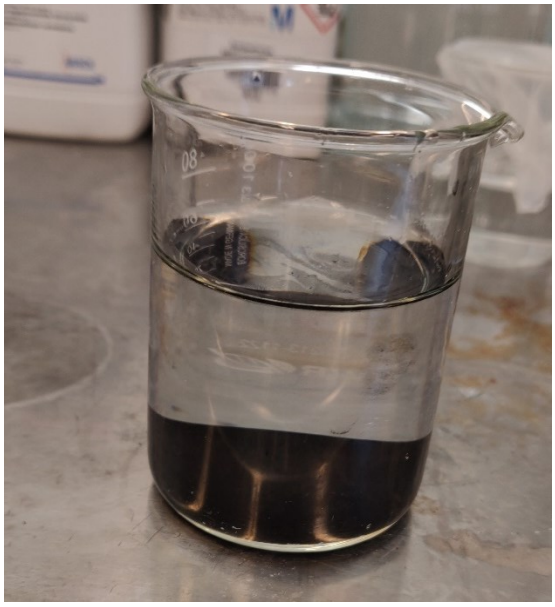

Figure 10. Solution containing (Co)-MoS_2 catalyst particles.

The solution was filtered using a funnel and a filter paper and was subsequently washed three times using Etax Aa 99.5% ethanol to remove residual water and water-soluble impurities. The wet catalyst was weighed and then dried in vacuum at 50 °C for 5 hours using a rotavapor, as can be seen in Figure 11.

Figure 11. Vacuum drying of (Co)-MoS_2 catalyst particles at 50 °C using a Buchi Rotavapor.

The dry catalyst was weighed, after which the flask was flushed with nitrogen. The catalyst was stored under nitrogen.

3.2.3 Synthesis of MoS_2 and Co-MoS_2 by emulsion method

Liquid catalyst precursors were prepared by an emulsion approach, whereby metal salts and optionally a sulfiding agent were dissolved in an aqueous phase. The aqueous phase was mixed with the organic phase, consisting of an organic solvent and a surfactant or stabilizing particles. Finally, high-shear mixing was used to mix the two phases. Thermal synthesis of the catalyst from the prepared emulsion catalyst precursors can then be performed to form the catalyst particles either in-situ or ex-situ.

Prior to preparing the final catalyst emulsions, a screening process was conducted (see Appendix A). Screening included the testing of different compositions, surfactants, and agitation methods. Tested surfactants and stabilizing particles included Span 80, Tween 80, Wacker HDK H18 silica nanoparticles, and Wacker HDK H20 silica nanoparticles. The hydrophilic-lipophilic balance (HLB) is a measure for the degree to which a surfactant is hydrophilic or lipophilic (Kassem et al., 2019). A typical HLB value for water-in-oil (w/o) emulsifiers is in the range of 4-6 while the typical value for oil-in-water (o/w) emulsifiers is 8-18 (Kassem et al., 2019). The HLB values of Span 80 and Tween 80 are 4.3 and 15, respectively (Kassem et al., 2019). Emulsions prepared with Tween 80 were not very stable, which can in part be explained by its HLB value, and consequently Span 80 was more suitable for use in stabilizing the w/o emulsions. Of the tested Wacker HDK silica nanoparticles (SiO_2), HDK H18 provided more stable emulsions than HDK H20. The particles have similar surface area (170-230 m^2/g); however, differ in their hydrophobicity (Hohl et al., 2016). The amount of silanol groups (Si-OH) attached to the particle surface affects hydrophobicity of the particles, with low amounts of silanol leading to more hydrophobic particles (Hohl et al., 2016). The residual silanol content can be defined as relative silanol content in relation to the hydrophilic silica and the corresponding values for HDK H18 and HDK H20 are 25% and 50%, respectively (Hohl et al., 2016). The viscosity of emulsions stabilized with HDK H20 particles quickly increased as the concentration of nanoparticles was increased, which led to the formation of thick slurries, whereas this did not happen with HDK H18 stabilized emulsions. The emulsions were confirmed to be of w/o type by conducting dilution tests, in which n-dodecane and water were used as the diluents. Dilution with water led to the formation of two distinct phases while dilution with n-dodecane yielded a single phase.

The final liquid emulsion catalyst precursors were prepared with n-dodecane (C12) as the organic phase instead of kerosene, with the latter used during screening. By using a pure hydrocarbon such as n-dodecane instead of kerosene, a crude oil middle distillate containing

different types of hydrocarbons including paraffins, naphthenes, and aromatics, analyzing product samples from HDO runs is easier, since the emulsion is added to the reactant solution. Recipe development was partly based on the patent by Stanciulescu et al. (1996). Emulsion preparation was conducted by first preparing an aqueous solution containing 10 w/v-% ammonium heptamolybdate tetrahydrate. In Co-promoted emulsions, cobalt (II) nitrate hexahydrate was added in an amount corresponding to a Co/Mo molar ratio of 0.5. Dimethyl sulfoxide (DMSO) (C_2H_6OS) was added as a sulfiding agent to the aqueous solution in stoichiometric amount. A Co-MoS_2 emulsion containing no DMSO was also prepared in the same manner. In this case dimethyl disulfide (DMDS) was used as a sulfiding agent and added separately in a pre-sulfiding step prior to HDO of isoeugenol. The organic phase in the emulsions was prepared by mixing either Span 80, a non-ionic surfactant, or Wacker HDK H18 pyrogenic silica nanoparticles, with n-dodecane. Span 80 was directly dissolved in n-dodecane, while HDK H18 silica nanoparticles were added slowly to stirred n-dodecane. The water/oil (w/o) emulsions were then prepared by dropwise addition of the aqueous phase to the organic phase while being agitated by a IKA T18 Ultra-Turrax Homogenizer. After the aqueous phase was added, the emulsions were agitated at 6500 rpm and 9500 rpm for 5 minutes at each rpm speed. The emulsion compositions were chosen based on the most stable compositions during the emulsion screening process. With Span 80 it was a composition containing 5 vol-% Span 80 in the oil phase and a w/o ratio of 50/50 vol-%. Using HDK H18 silica nanoparticles it was a composition containing 5 w/v-% HDK H18 silica nanoparticles in the organic phase and with a w/o ratio of 25/75 vol-%. Emulsions containing DMSO as the sulfiding agent can be seen in Figure 12, while the emulsion pre-sulfided with DMDS prior to HDO run is displayed in Figure 13.

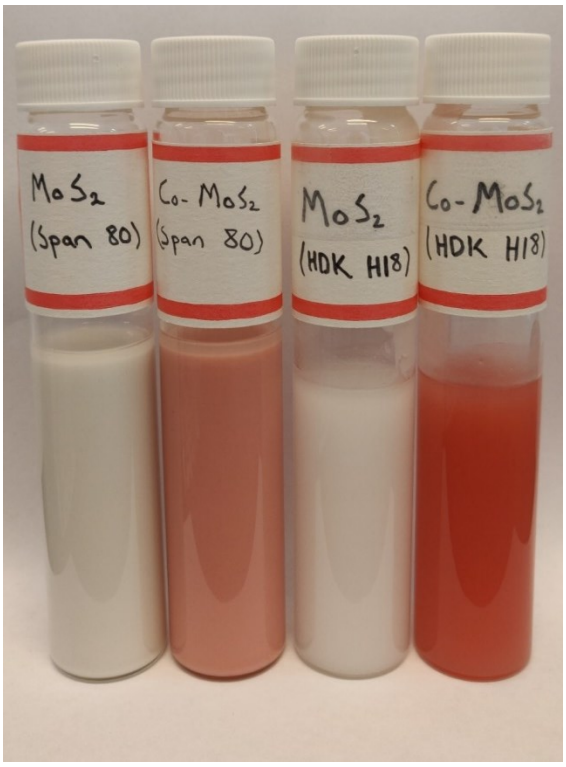

Figure 12. Side-by-side picture of prepared MoS_2 and Co-MoS_2 emulsion catalyst precursors using both Span 80 and HDK H18 surfactants.

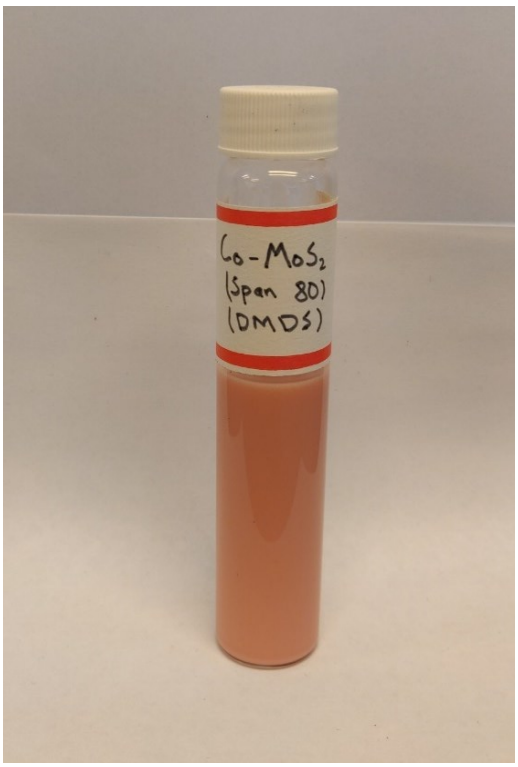

Figure 13. Prepared Co-MoS_2 emulsion catalyst precursor using Span 80. The emulsion catalyst precursor was sulfided using DMDS prior to HDO run.

3.3 Catalyst characterization

3.3.1 Characterization of Mo/AC and CoMo/AC catalysts

Nitrogen physisorption with a Micromeritics 3Flex 3500 N_2 physisorption instrument was used to study the porosity of the synthesized catalysts by physisorption of nitrogen at -196 °C. The samples were degassed at 200 °C using vacuum degassing for 18 h before experiments. The morphology, the dispersion of metal on the support material, and the elemental composition was characterized using a Carl Zeiss Merlin field emission scanning electron microscope (FESEM) with energy dispersive spectroscopy (EDS). The elemental composition was also studied using a PANalytical Axios mAX wavelength dispersive X-ray fluorescence (WDXRF) spectrometer. Inductively coupled plasma optical emission spectrometry (ICP-OES) was utilized for determining the metal content using an Agilent Technologies synchronous vertical dual view (SVDV) 5110 ICP-OES. The operating procedure used in ICP analysis of all analyzed samples is documented in Appendix D.

3.3.2 Characterization of (Co)-MoS_2 by emulsion method

A Nikon Ci-L fluorescence microscope was used initially to study emulsion droplet size, providing information on the size of in-situ formed particles. The particle size distribution (PSD) and the droplet size were determined using LD with a Beckman Coulter LS230 MW Particle size analyzer using the Micro Liquid Module after dispersing it in dodecane. The metal content of emulsion samples was determined using an Agilent Technologies synchronous vertical dual view (SVDV) 5110 ICP-OES.

3.3.3 Characterization of (Co)-MoS_2 by hydrothermal method

The morphology and structure of hydrothermally synthesized MoS_2 and Co-MoS_2 was characterized using a Carl Zeiss Merlin field emission scanning electron microscope (FESEM) with energy dispersive spectroscopy (EDS). Nitrogen physisorption was used to study the porosity of the synthesized catalysts using a Micromeritics 3Flex 3500 N_2 physisorption instrument by physisorption of nitrogen at -196 °C. The samples were degassed at 200 °C using vacuum degassing for 20 h before experiments. X-ray diffraction (XRD) was conducted to study crystallinity of the synthesized catalysts while also providing information about the existing metal phases. XRD measurements were performed on a PANalytical X'Pert Pro MPD rotating anode X-ray diffractometer with monochromatic Cu Kα radiation (λ = 1.54060 Å) at a voltage and current of 45 kV and 40 mA, respectively. The 2θ was scanned over the range of

10−90°. ICP-OES was utilized for determining the metal content of samples using an Agilent Technologies synchronous vertical dual view (SVDV) 5110 ICP-OES.

3.4 Hydrodeoxygenation (HDO) experiments of isoeugenol

Performance of the prepared catalysts was tested in a batch reactor in HDO of a model compound. Isoeugenol was used as a model compound for lignocellulosic bio-oil in the HDO runs. Isoeugenol is an aromatic compound containing three different functional groups including allyl, hydroxy, and methoxy groups, therefore making it a quite representative model compound for lignin-derived bio-oils (Gao et al., 2015). The proposed reaction pathway for HDO of isoeugenol can be seen in Figure 14, where U represents unknown compounds which are possibly oligomers or other compounds strongly adsorbed on the catalyst surface (Tieuli et al., 2019).

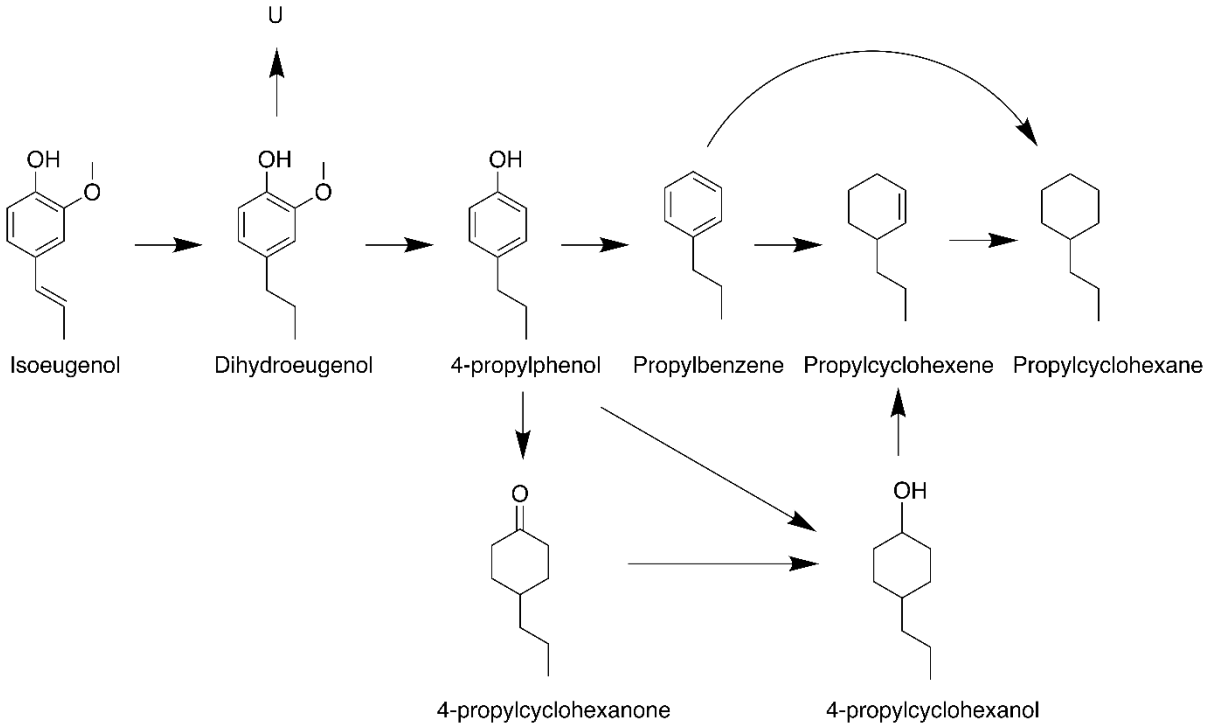

Figure 14. Proposed reaction pathway in HDO of isoeugenol. Adapted from Tieuli et al. (2019).

HDO experiments were conducted in a 200 ml Büchi stainless steel autoclave equipped with a stirrer. The reactor setup can be seen in Figure 15 while a piping and instrumentation diagram (PI&D) is given in Appendix C. For the HDO experiments, the reactor was typically loaded with 100 ml of n-dodecane and 0.2 g of isoeugenol. The catalyst loading of the active phase (MoS_2, CoS_2 and NiS) was typically 0.1 g (50 wt-%) except for Ru/C, in which case 0.005 g Ru (2.5 wt-%) was loaded into the reactor. Catalyst loading and preparation procedures prior to HDO runs for the tested catalysts are discussed in Sections 3.4.2–3.4.5. The initial hydrogen

pressure was set to 30 bar H_2 and the stirring was set to 900 rpm to minimize mass transfer limitations. The reactor was then heated to 300 °C, which increased the total pressure to approximately 50 bar. Experiments were conducted for 3 h once the target temperature was reached. The liquid samples were taken at the beginning of the experiment once the target temperature was reached and with intervals of 1 hour thereafter. Two samples were taken every hour, yielding a total of eight samples per HDO experiment.

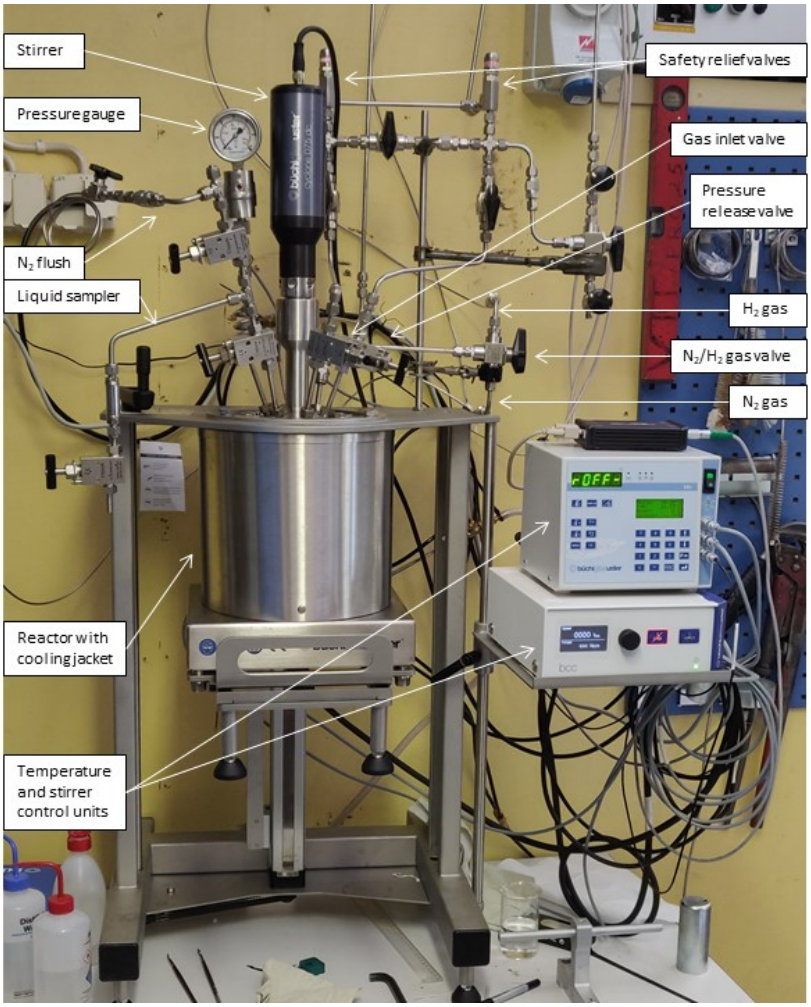

Figure 15. The batch reactor setup used for HDO experiments.

3.4.1 GC analysis of liquid samples

The liquid samples were analyzed using a gas chromatograph equipped with a flame ionization detector (GC-FID). An Agilent ULTRA 1 19091A-115 capillary column (50 m x 320 µm x 0.52 µm) was used for GC analysis. The following settings were used in the GC runs: injector temperature of 320°C, detector temperature of 320°C, helium as the carrier gas, pressure of 82 kPa, total flow of 49.5 ml/min, column flow of 1.5 ml/min, linear velocity of 24 cm/s, purge

flow of 3 ml/min, injection volume of 1.0 µl, and a split ratio of 30. The temperature program used in the GC method for the liquid sample analysis can be seen in Table 7.

Table 7. Temperature program in the GC method for analysis of liquid phase samples.

Ramp (°C/min)	Temperature (°C)	Hold (min)
	60	2
10	250	0
10	300	0

Retention times of compounds identified using gas chromatography-mass spectrometry (GC-MS) are shown in Table 8.

Table 8. Compounds present in the liquid phase in HDO of isoeugenol and their respective retention times.

Compound	Retention time (min)
Heptane (C7)	3.9
Propylcyclohexane	9.6
Propylbenzene	9.8
Undecane (C11)	12.2
Dodecane (C12)	14.1
Tridecane (C13)	14.2
4-propylphenol	14.3
Tetradecane (C14)	14.5
Pentadecane (C15)	15.2
2-methoxy-4-propylphenol*	15.9
Isoeugenol (cis + trans)	16.3, 16.8

*Dihydroeugenol

An example of a chromatogram displaying peaks at these different retention times can be seen in Figure 16.

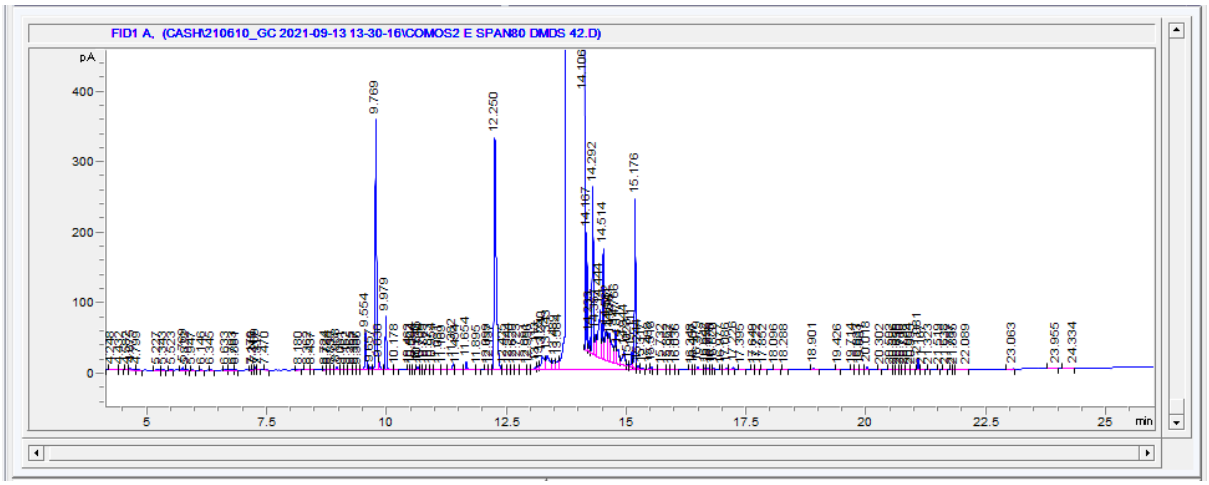

Figure 16. Chromatogram image from GC analysis of sample 4.2 in HDO of isoeugenol over Co-MoS_2-E-Span 80 DMDS catalyst.

The concentrations of the products were calculated by correcting the peak area with a mass-based response factor f_i which is given in equation (10).

$$f_i = \frac{A_i}{A_{st}} \times f_{st} \tag{10}$$

where A_i is the signal (peak area) of the compound i, A_{st} is the signal of the standard (solvent) and f_{st} is the response factor of the standard. The corrected peak area was thus calculated as follows:

$$A_{corr,i} = f_i \times A_i \tag{11}$$

The mass-% of the compound i at time t in a sample was expressed as:

$$x_{i,t} = \frac{A_{corr,i}}{A_{corr,total}} \times 100\% \tag{12}$$

Conversion of the reactant at time t was calculated using the following equations:

$$X_t(\%) = \frac{C_0 - C_t}{C_0} \times 100\% = 100\% - x_{isoeugenol,t} \quad (13)$$

where C_0 is the initial concentration (mol/l) of isoeugenol and C_t is the concentration of isoeugenol at time t. The relative amount of total carbon in each compound was calculated as:

$$S_{C,i} = \frac{x_{i,t} \times w_{C,i}}{X_t \times w_{C,t}} \times 100\% \quad (14)$$

where $x_{i,t}$ is the mass-% of compound i at time t, X_t is the conversion of the reactant at time t while $w_{C,i}$ and $w_{C,t}$ are the carbon content in the compound i and reactant, respectively. The amounts were then scaled to percentages of the total amount. Products not recognized to originate from isoeugenol were omitted. The selectivity of compound i was then calculated as follows:

$$S_a(\%) = \frac{C_{a,t}}{\sum C_{a+b+c+d\ldots+w,t}} \quad (15)$$

where $C_{a,t}$ is the concentration of compound a at time t and $\sum C_{a+b+c+d\ldots+w,t}$ is the concentration sum of all products at time t determined to originate from isoeugenol.

3.4.2 HDO with Ru/C catalyst

A commercial Ru/C catalyst with 5% Ru was tested. The catalyst was crushed and sieved to a particle size under 400 µm and was used without further treatment. 0.1 g of the catalyst was loaded into reactor for the HDO run, yielding 0.005 g Ru and a catalyst loading of 2.5 wt-% relative to isoeugenol.

3.4.3 HDO with NiMo/Al_2O_3 catalyst

A commercial NiMo/Al_2O_3 catalyst supplied by Ranido was used as a reference catalyst. The metal loading on the catalyst was 23 wt-% MoO_3 and 4 wt-% NiO. 0.33 g of the catalyst was loaded into the reactor, with the assumption that all MoO_3 and NiO reacted to MoS_2 and NiS during pre-sulfidation with DMDS, with this amount yielding 0.1 g of MoS_2 and NiS in total. Prior to the HDO run, the catalyst extrudates were crushed and sieved to obtain particles with a size below 100 µm. The crushed catalyst was added to 50 ml of n-dodecane and sulfided using 0.2 ml DMDS (excess S). Sulfidation was conducted under 30 bar H_2 for 1 hour once the target temperature of 350 °C was reached. The rest of n-dodecane (50 ml) containing isoeugenol (0.2 g) was added to the reactor after sulfidation.

3.4.4 HDO with Mo/AC and CoMo/AC catalysts

Activated carbon supported Mo and CoMo catalysts were used in amounts corresponding to 0.1 g of sulfides in total. The catalysts were sulfided at 350 °C under 30 bar H_2 for 1 hour with excess DMDS in 50 ml n-dodecane prior to use. Isoeugenol (0.2 g) was then dissolved in the rest of n-dodecane (50 ml) and added to the reactor after sulfidation.

3.4.5 HDO with MoS_2 and Co-MoS_2 synthesized from emulsion precursors

MoS_2 and Co-MoS_2 precursor emulsions were used in HDO runs by diluting the amount of emulsion needed to form 0.1 g of MoS_2 and CoS_2. The organic content of emulsions was accounted for when preparing the reagent solution containing isoeugenol. MoS_2 (Span 80), Co-MoS_2 (Span 80) and MoS_2 (HDK H18) were sulfided in-situ simultaneously during isoeugenol HDO. The Co-MoS_2 (Span 80) emulsion prepared without DMSO was pre-sulfided under 30 bar H_2 using excess DMDS (0.2 ml) for 1.5 hours prior to isoeugenol HDO run.

3.4.6 HDO with hydrothermally synthesized MoS_2 and Co-MoS_2

Hydrothermally synthesized MoS_2 and Co-MoS_2 were used without further pretreatment. 0.1 g of catalyst was loaded into the reactor.

4 Results and discussion

4.1 Catalyst characterization results

4.1.1 Characterization results of Mo/AC and CoMo/AC catalysts

SEM-EDS results from analysis of the supported activated carbon catalysts indicate a particle size of approximately 50 µm, which can be seen in Figure 17.

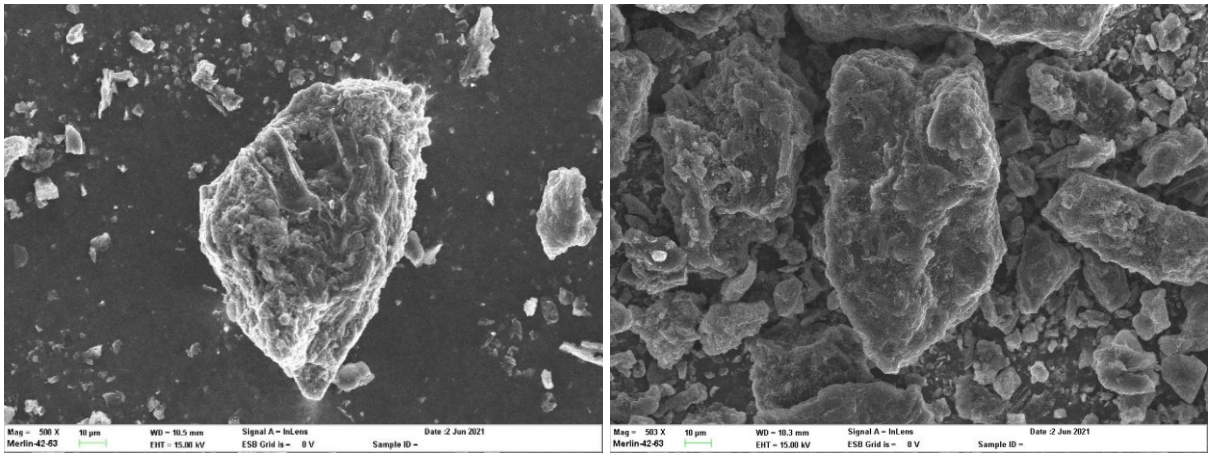

Figure 17. SEM-EDS images of Mo/AC (left) and CoMo/AC (right) catalysts.

The dispersion of Mo on activated carbons support in the Mo/AC catalyst can be seen in Figure 18. Evidently, Mo is quite evenly dispersed on the support material, although a slightly higher Mo concentration can be observed on the edges of the support material. Quantifiying the elemental composition of carbon catalysts with EDS is difficult, due to the light nature of the carbon element. In addition, the use of carbon tape for preparation of the sample may also skew the results. Nevertheless, the Co/Mo atomic ratio given by EDS has been included in Table 9 and is relatively close to the targeted ratio of 0.5. The sample size in this case is only 3 EDS points and should, therefore, be viewed with caution.

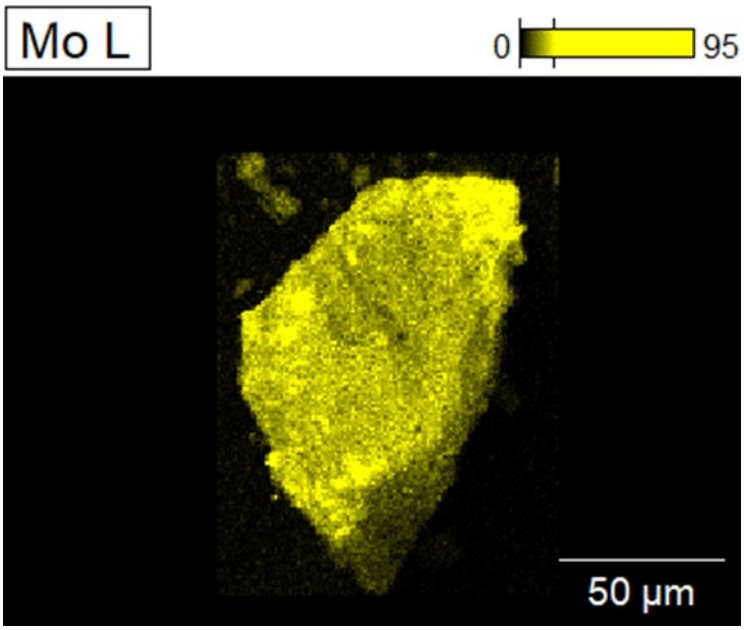

Figure 18. SEM-EDS image displaying the dispersion of molybdenum on activated carbon support in Mo/AC catalyst.

Physisorption results of activated carbon catalysts are summarized in Table 9. Similar results are seen for both Mo/AC and CoMo/AC catalysts, with a similar decrease of the BET surface area for both catalysts compared to the activated carbon support material. Naturally, the average pore diameter and pore volume are also similar for both catalysts. The activated carbon catalysts were also characterized using XRF, however, due to carbon being too light an element for XRF, the metal loading on carbon could not be quantified with XRF. The Co/Mo atomic ratio from XRF measurements has been included in Table 9. The metals present were also analyzed with ICP; however, as carbon is also too light an element for ICP, only the Co/Mo atomic ratio has been included in Table 9. The Co/Mo atomic ratio given by XRF is quite close to the planned ratio of 0.5, while a slightly larger deviation from this value is seen for the ratio given by ICP.

Table 9. Characteristics of prepared supported catalysts.

	AC	Mo/AC	CoMo/AC
Specific surface area (m^2/g)[a]	699	461	466
Average pore diameter (nm)[b]	3.3	3.7	3.7
Pore volume (cm^3/g)[c, d]	0.58	0.43	0.43
Co/Mo atomic ratio (SEM)	-	-	0.4, 0.4, 0.9 (0.57)[e]
Co/Mo atomic ratio (XRF)	-	-	0.44
Co/Mo atomic ratio (ICP)	-	-	0.31

[a] Calculated by applying the Brunauer–Emmett–Teller (BET) method.

[b] Adsorption average pore diameter (4V/A by BET).

[c] Pore volume was calculated from single point adsorption total pore volume of pores less than 266 nm width at P/P0 = 0.99.

[d] For activated carbon, pore volume was calculated from single point adsorption total pore volume of pores less than 331 nm width at $P/P_0 = 0.99$.

[e] Average value (0.4+0.4+0.9)/3= 0.566…≈ 0.57.

4.1.2 Characterization results of (Co)-MoS_2 by emulsion method

Fluorescence microscopy with magnification up to 40x was used for analyzing the droplet size of the emulsions. The droplet size of the emulsions prepared with Span 80 was determined to be ca. 1-5 µm, based on the images in Figures 19-20, which was also later confirmed by laser diffraction (LD) analysis. The droplet size distribution is quite uniform with relatively small droplets present. No noticeable difference in the microscopy images can be seen between the non-promoted and Co-promoted emulsions prepared with Span 80.

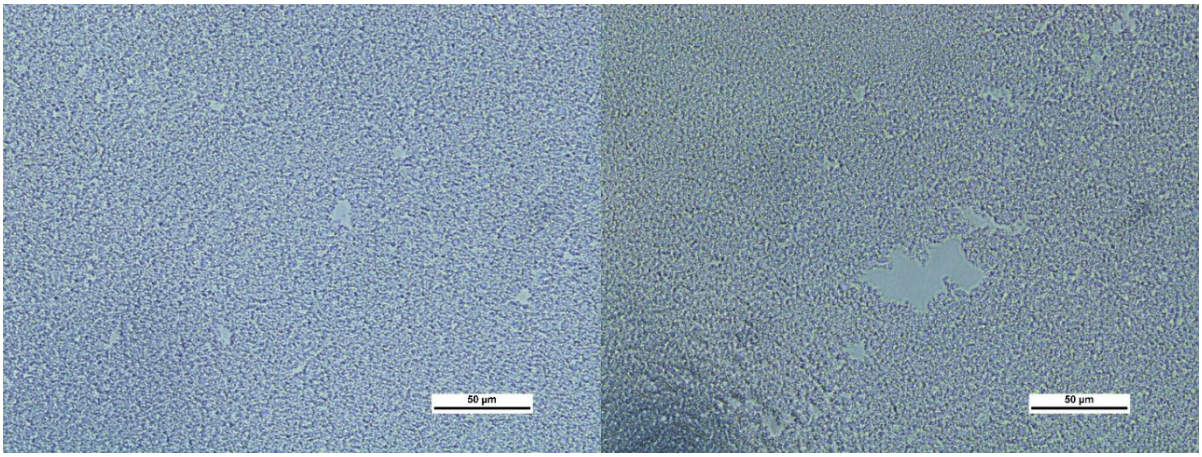

Figure 19. Fluorescence microscopy images of MoS_2 (left) and Co-MoS_2 (right) catalyst emulsions using Span 80 surfactant.

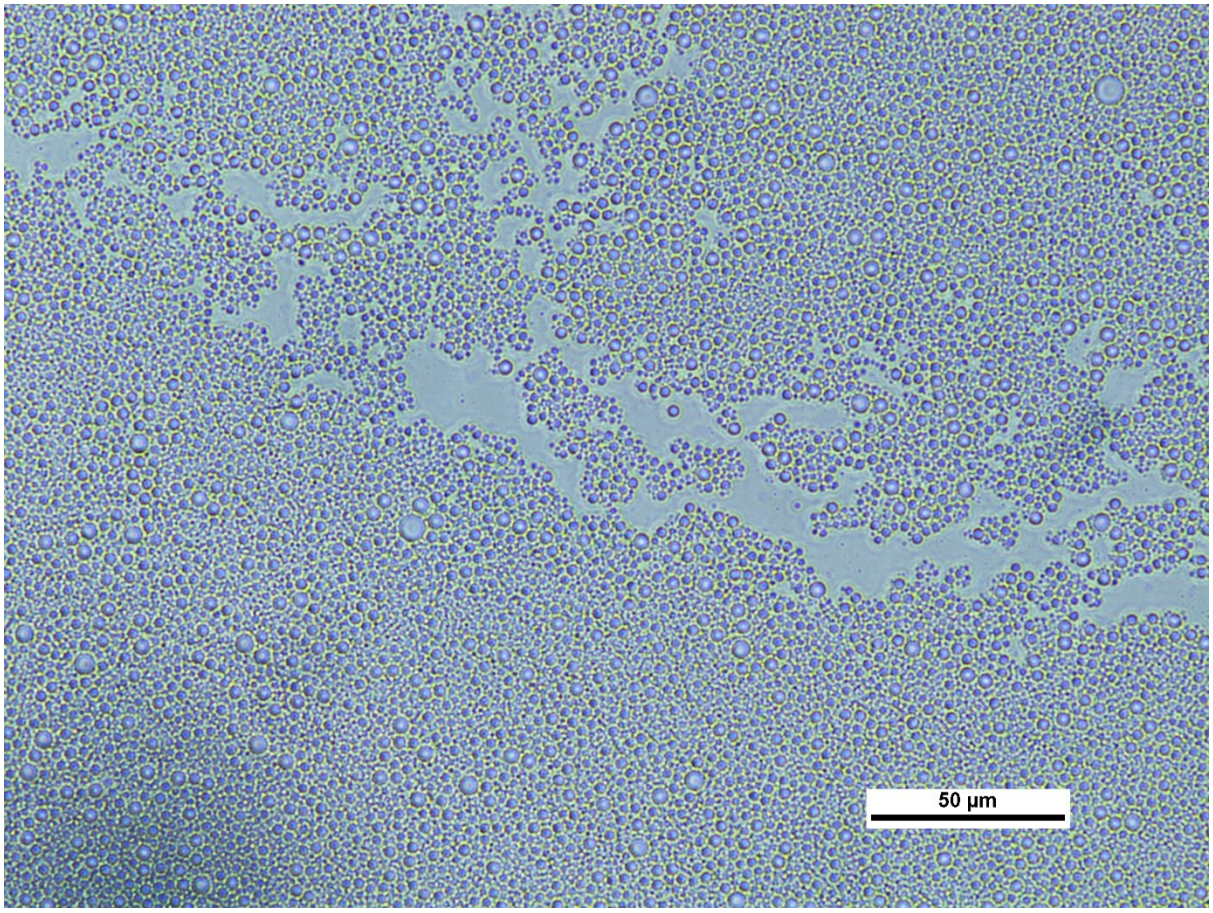

Figure 20. Fluorescence microscopy image of Co-MoS_2 catalyst emulsion using Span 80 surfactant. The emulsion was sulfided prior to HDO run using DMDS.

Fluorescence microscopy images of emulsions prepared with HDK H18 silica nanoparticles are given in Figure 21. As can be seen, the droplet sizes are much larger while the droplet size distribution is also much less uniform than emulsions prepared with Span 80 surfactant. Unlike

the MoS_2 catalyst emulsion, square-shaped particles were observed in the Co-MoS_2 catalyst emulsion, which are possibly undissolved cobalt particles. The large droplets in the Co-promoted MoS_2 as well as the square pieces, which have started to flocculate, are likely the reasons for the emulsion becoming unstable and subsequently failing. In general, emulsions with Span 80 surfactant were more stable than emulsions stabilized by HDK H18 silica nanoparticles. The stability of surfactant stabilized emulsions could be further improved by finding the optimal HLB ratio, by e.g., mixing Tween 80 and Span 80 in different proportions (Kassem et al., 2019). The pH of the aqueous phase also affects the stability of the emulsion and should therefore be investigated (Daaou and Bendedouch, 2012).

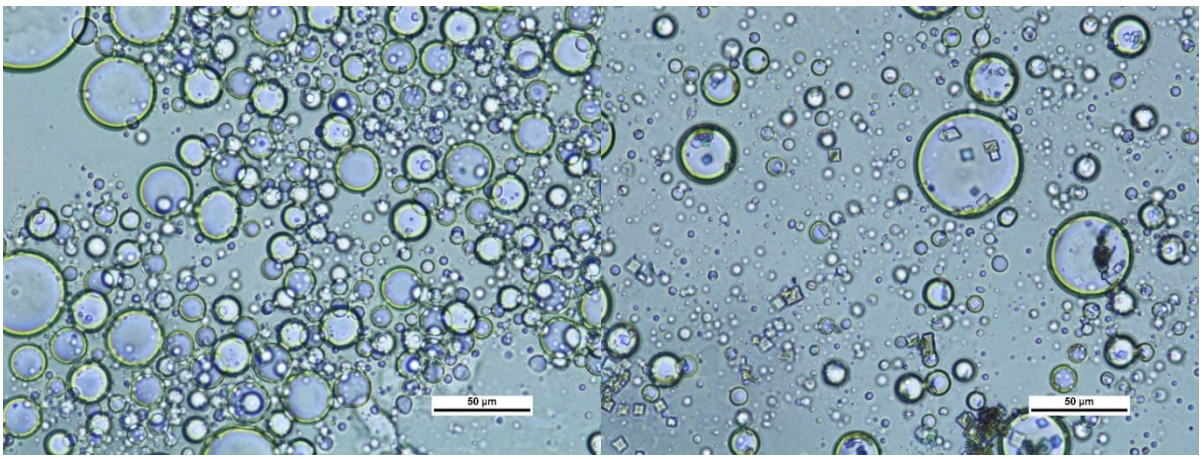

Figure 21. Fluorescence microscopy images of MoS_2 (left) and Co-MoS_2 (right) catalyst emulsions stabilized using HDK H18 silica nanoparticles.

Laser diffraction (LD) results of emulsions can be seen in Table 10. The results confirm the large droplet size of the emulsion prepared with HDK H18 silica nanoparticles compared to emulsions prepared with Span 80 surfactant.

Table 10. Results from laser diffraction of the prepared emulsions.

Emulsion	Mean size (µm)	Median size (µm)	Dv(90) (µm)[a]
MoS_2-E-Span 80	3.2	1.9	7.3
Co-MoS_2-E-Span 80	2.6	2.1	4.5
Co-MoS_2-E-Span 80 DMDS	2.5	2.5	3.7
MoS_2-E-HDK H18	18.3	15.7	38.3

[a] 90 % of the particles are smaller than reported diameter.

The particle size distribution (PSD) of the emulsions is displayed in Figure 22. As discussed previously, the relatively narrow droplet size distribution of the emulsions prepared with Span 80 and the broad size distribution of the HDK H18 emulsion are both confirmed by the laser diffraction results. Peaks in MoS_2-E-Span 80 and Co-MoS_2-E-Span 80 between 5-10 µm as well as 15-20 µm in the latter are likely due to coalescence, i.e., the fusion of two or more droplets to form a larger droplet (Viana et al., 2014). Since the Co-MoS_2-E-Span 80 DMDS emulsion was prepared later than the other emulsions, the time between preparation and PSD measurements was shorter. For this reason, it is likely that less emulsion degradation has taken place and the coalescence phenomenon has not affected it in the same way. A narrow size distribution is beneficial for the formation of uniform catalyst particles with similar surface-to-mass ratios. A more uniform particle size would also make the catalyst recovery easier, since processes such as filtration, sedimentation, and cyclonic separation are very dependent on the particle size. Agitation of the emulsion plays a significant role in the size of the droplets in the emulsion, with a higher energy input during the emulsification process reported to yield smaller droplets (Iqbal et al., 2011). Other parameters affecting the droplet size in w/o emulsions are the w/o ratio and the nature of the components used in the emulsions, including the aqueous phase, the organic phase, and the surfactant (Lindenstruth and Müller, 2004). Parameters affecting the droplet size should be further investigated and tested to improve emulsion compositions.

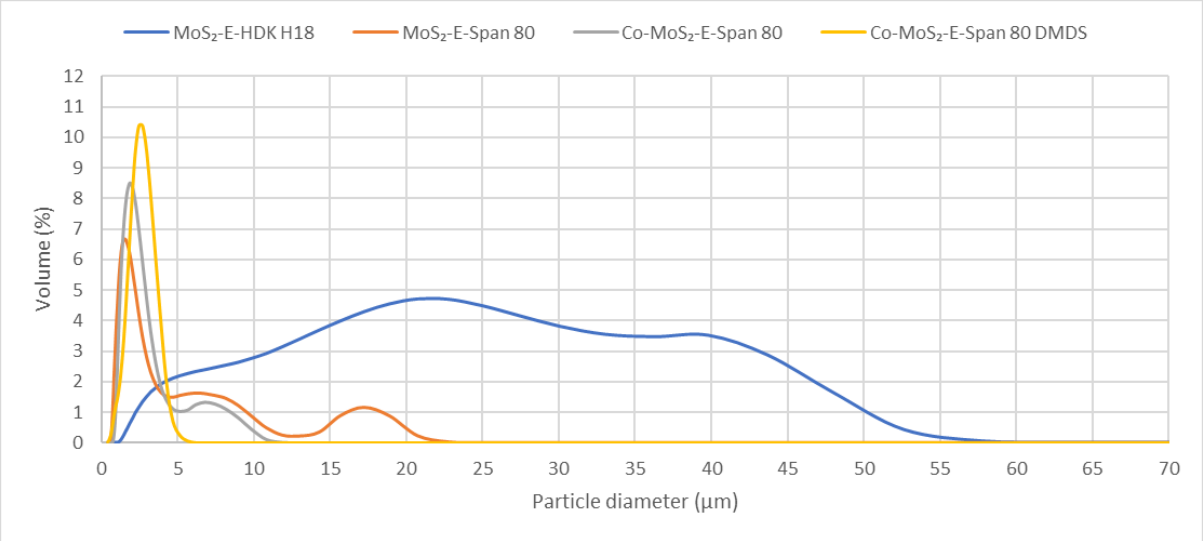

Figure 22. Particle size distribution (PSD) of the prepared emulsions determined by laser diffraction.

The metal content of the prepared emulsion catalyst precursors is given in Table 11. The planned amount of Mo in all Span 80 stabilized emulsions was 27 mg Mo per ml of the emulsion. The amount of planned Co in Co-promoted emulsions was 8 mg per ml of the emulsion. In the emulsion stabilized using HDK H18 silica nanoparticles, the amount of planned Mo was half of this amount due to its w/o ratio being 25/75 vol-% instead of 50/50 vol-%. Assuming that the density of emulsions is ca. 1 g/ml, double the amount of planned Mo is present in all emulsions while the amount of Co is close to the nominal amount. Deviation from the nominal metal concentrations is possibly caused by emulsion degradation and uneven distribution of metals in the emulsions. The measured higher concentration of Mo also means that the Co/Mo atomic ratio in Co-promoted emulsions is lower than the nominal ratio of 0.5. The small sample size of 100 mg used in ICP analysis along with the dilute nature of the emulsions also means that there is risk for error in measurements. As no control samples were analyzed during ICP analysis, the accuracy of ICP results is not confirmed and should be viewed with caution.

Table 11. Metal content of emulsion catalyst precursors determined by ICP analysis.

	MoS_2-E-Span 80	**Co-MoS_2-E-Span 80**	**Co-MoS_2-E-Span 80 DMDS**	**MoS_2-E-HDK H18**
Mo (mg/g)	61	59	58	34
Co (mg/g)	<0.1	9.3	9.1	<0.1
Co/Mo atomic ratio	-	0.26	0.26	-

4.1.3 Characterization results of (Co)-MoS_2 by hydrothermal method

XRD measurements of MoS_2 and Co-MoS_2 were conducted, with commercially available MoS_2 from Fluka used as a reference. XRD spectrums of commercial MoS_2 as well as hydrothermally synthesized MoS_2 and Co-MoS_2 can be seen in Figures 23-25. Commercially available MoS_2 showed intense, sharp peaks at 14°, 32°, 33°, 36°, 39°, 49°, 58°, and 60° with less intense, smaller peaks also present. Hydrothermally synthesized MoS_2 displayed peaks at 33°, 39°, and 58°, which correspond to the (100), (103), and (110) basal planes of MoS_2 (Guo et al., 2019). In addition to these peaks, Co-MoS_2 also exhibited peaks at 28°, 36°, 46°, and 55°, corresponding to (111), (210), (220), and (311) CoS_2 planes (Huirache-Acuña et al., 2006; Liu et al., 2016). The sharp peaks in the commercial MoS_2 sample can be explained by the high crystallinity of the material, while the hydrothermally synthesized MoS_2 and Co-MoS_2 are of amorphous nature, leading to broader and weaker peaks. Sharper peaks in Co-MoS_2 than in MoS_2 could be explained by a higher synthesizing temperature, due to the uneven and unpredictable heating of the heating element as well as the formation of different CoS phases, leading to a higher crystallinity in the formed catalyst (Wang et al., 2014a). The amorphous form of MoS_2 has been reported to exhibit higher hydrogenation activity than the crystalline form, and thus a high crystallinity is not desired (Rezaei et al., 2012; Yoosuk et al., 2012).

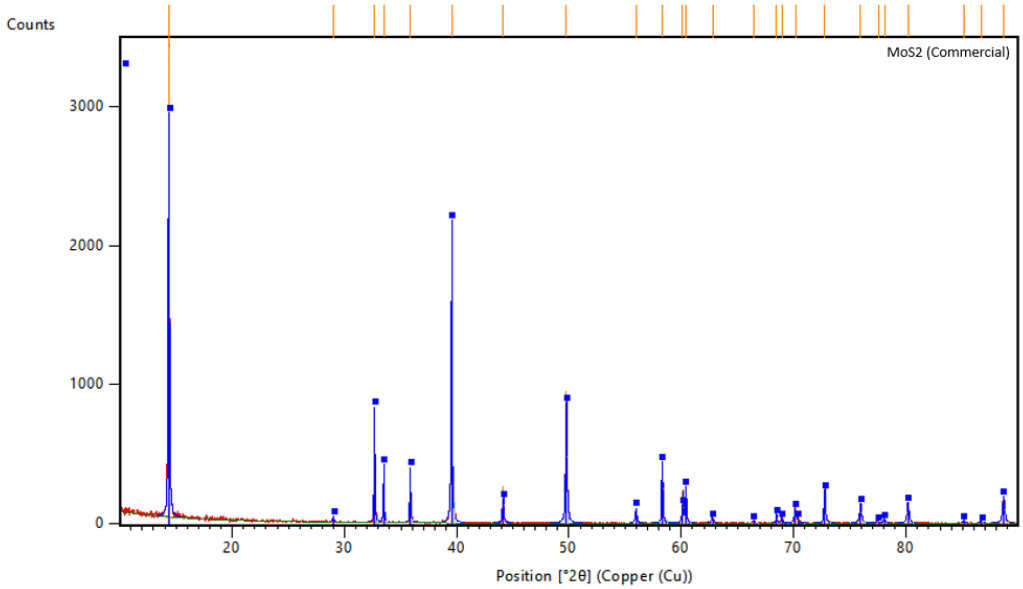

Figure 23. XRD pattern of commercial MoS_2.

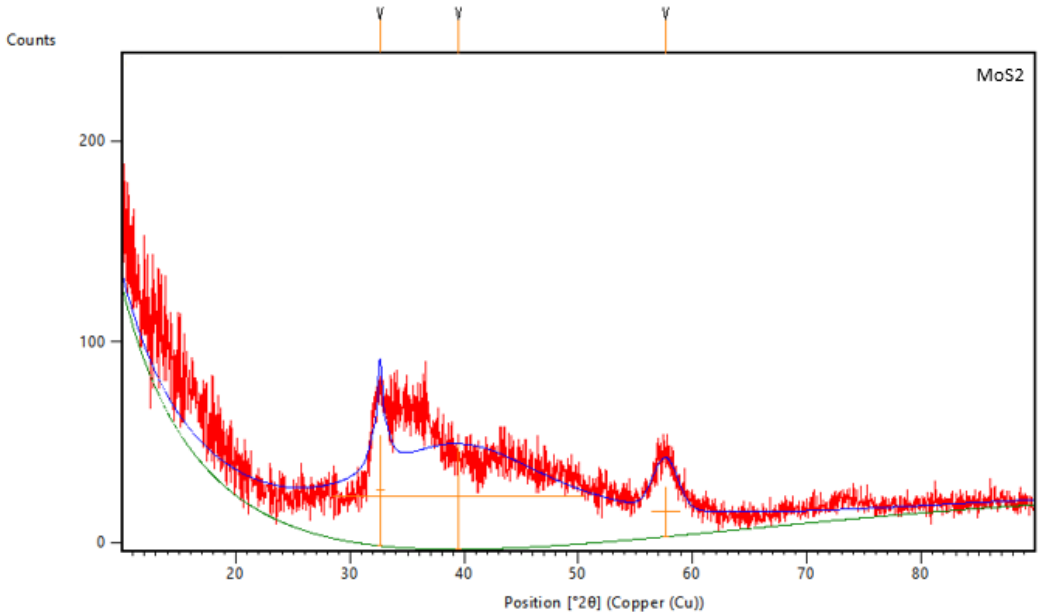

Figure 24. XRD pattern of hydrothermally synthesized MoS_2.

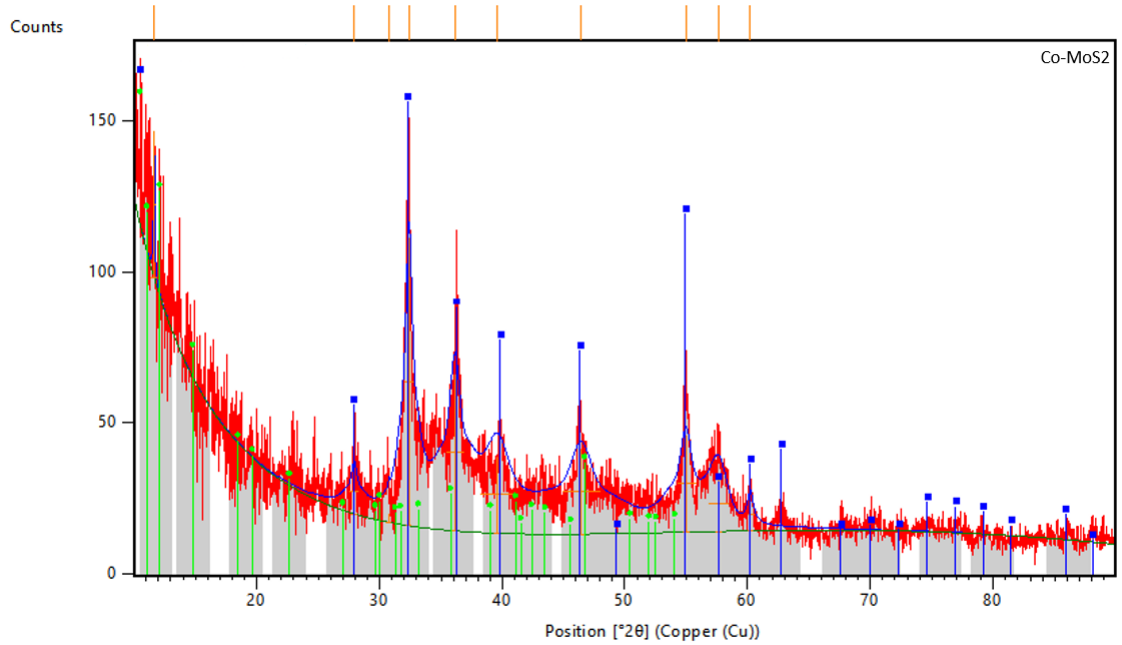

Figure 25. XRD pattern of hydrothermally synthesized Co-MoS_2.

SEM-EDS images of MoS_2 and Co-MoS_2 can be seen in Figures 26 and 27 and show the small size of the crystallites. Both MoS_2 and Co-MoS_2 consist of nanostructures with flower-like morphology. In both catalysts, nanostructures forming clusters can be observed; however, the size of the individual nanostructures appear to be smaller in the Co-MoS_2 catalyst, which also contributes to a rougher catalyst surface. One potential explanation for the formation of smaller crystallites in the Co-MoS_2 catalyst, is the higher precursor concentration in the solution due to addition of cobalt nitrate. A higher precursor concentration has shown to affect the size of the individual crystallites (Waskito et al., 2019). The bulk particle size, however, seems to be larger for the Co-MoS_2 catalyst compared to the MoS_2 catalyst, with the size of aggregates approximated to be ca. 10 µm and 3-5 µm for Co-MoS_2 and MoS_2 catalysts, respectively (see Appendix B).

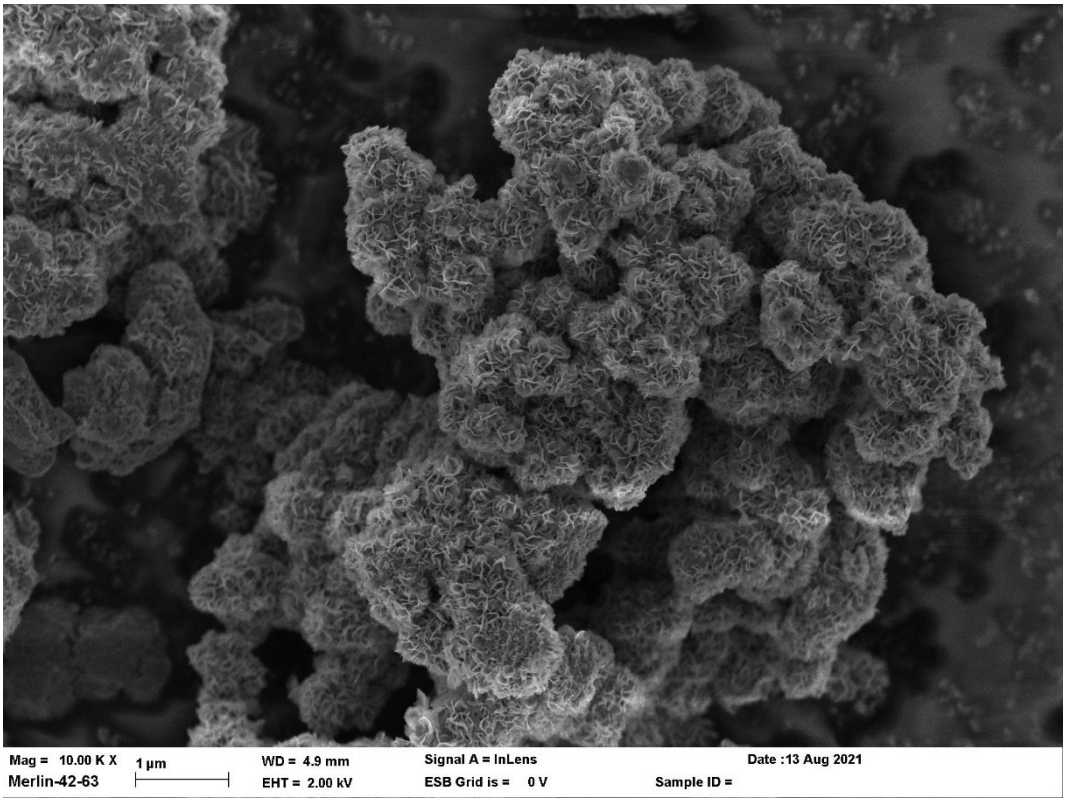

Figure 26. SEM-EDS image of hydrothermally synthesized MoS_2.

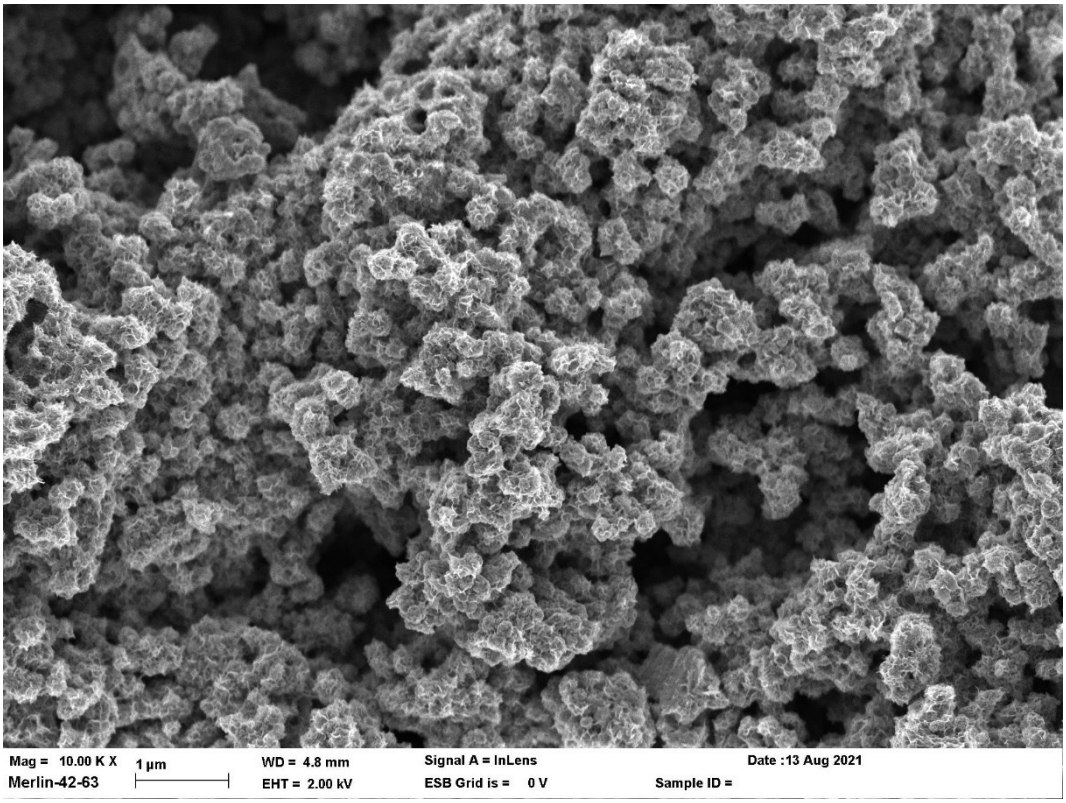

Figure 27. SEM-EDS image of hydrothermally synthesized Co-MoS_2.

Nitrogen physisorption results of hydrothermal catalysts can be seen in Table 12. A similar specific surface area was reported by Wang et al. (2014a); however, with the difference that the specific surface area (SSA) of Co-MoS_2 was higher in this case than the SSA of non-promoted MoS_2. In the literature, it has been reported that the surface area usually decreases by introducing a promoter (Cao et al., 2021; Wang et al., 2014a). The current result could be at least partially explained by the varying temperature during synthesis but also a higher precursor concentration. During synthesis of Co-MoS_2, the temperature stayed quite close to 205 °C, while the synthesizing temperature for MoS_2 was closer to 195 °C. It has been reported that an increase in synthesis temperature correlates with an increase in the specific surface area of the formed catalyst (Luo et al., 2019), while an increase in the solution precursor concentration (due to addition of Co) can increase the surface area due to a decrease of the nanosheet thickness (Waskito et al., 2019). The Co/Mo atomic ratio of the Co-MoS_2 catalyst determined by ICP-OES given in Table 12 is quite consistent with the nominal ratio of 0.5.

Table 12. Nitrogen physisorption and ICP-OES results of hydrothermally synthesized MoS_2 and Co-MoS_2.

	MoS_2-HT	**Co-MoS_2-HT**
Specific surface area (m^2/g)[a]	9.6	55
Average pore diameter (Å)[b]	199	151
Pore volume (cm^3/g)	0.05[c]	0.21[d]
Co/Mo atomic ratio (ICP)	-	0.46

[a] Calculated by applying the Brunauer–Emmett–Teller (BET) method.

[b] Adsorption average pore diameter (4V/A by BET).

[c] Single point adsorption total pore volume of pores less than 3 303 Å width at p/p° = 0.99.

[d] Single point adsorption total pore volume of pores less than 2 971 Å width at p/p° = 0.99.

4.2 Hydrodeoxygenation (HDO) of isoeugenol

Ten different catalysts were tested in HDO of isoeugenol, including two commercial catalysts, namely NiMo/Al_2O_3 and Ru/C. Selectivity in HDO of isoeugenol has been calculated by omitting compounds which were not considered to be originating from isoeugenol. Conversion of isoeugenol and selectivity for tested catalysts are summarized in Table 13. Not surprisingly, almost all catalysts reached close to full conversion of isoeugenol. This is because the double bond in isoeugenol is easily hydrogenated; thus, dihydroeugenol is formed (Tieuli et al., 2019).

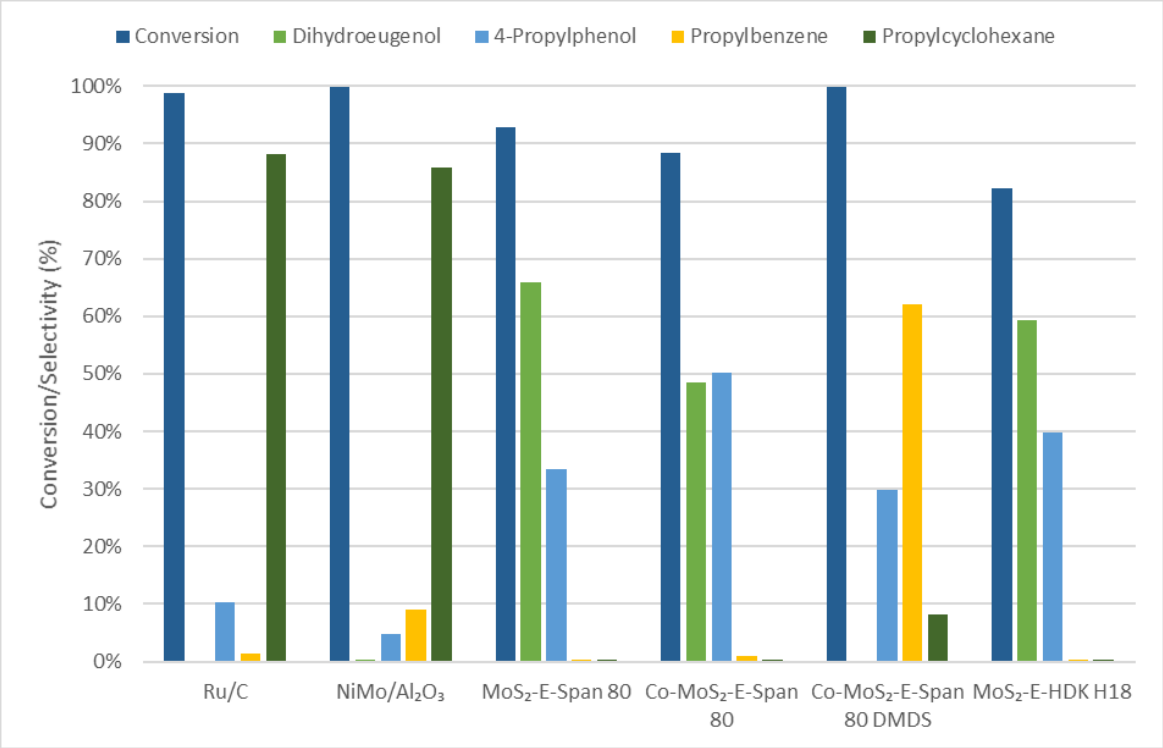

Figure 28. Conversion and selectivity of commercial reference catalysts and the catalysts prepared from emulsion catalyst precursors in HDO of isoeugenol at 300 °C, 30 bar H_2 and 3 h.

As can be seen in Figure 28, the emulsion catalyst precursors sulfided with DMSO in-situ simultaneously during HDO run exhibit clearly worse performance than the other catalysts, with a lower conversion of isoeugenol and a higher selectivity to dihydroeugenol. On the other hand, the Co-MoS_2-E-Span 80 emulsion catalyst precursor sulfided with DMDS prior to HDO, performed clearly better. The difference in the catalyst performance is likely explained by the difference in the sulfiding procedure of the emulsion catalyst precursors. Due to Co-MoS_2-E-Span 80 DMDS being sulfided ex-situ prior to the HDO run, the metal sulfide catalyst particles have already formed when the HDO experiment is started while this is not necessarily the case

when the emulsion catalyst precursor is thermally synthesized simultaneously during the HDO run, as catalyst particles might not have fully formed due to inadequate time. The switch of sulfiding agent is also likely to have affected the formation of MoS_2. It may be added that DMSO was added to emulsions according to the stoichiometry, while DMDS was added in three-fold excess. The Co-MoS_2-E-Span 80 DMDS catalyst precursor was also sulfided at a higher temperature of 350 °C as opposed to 300 °C which was deployed during isoeugenol HDO. Ex-situ presulfiding allows a more flexible temperature control compared to sulfidation done simultaneously during HDO (Nguyen et al., 2016). A higher degree of sulfurization achieved with ex-situ presulfidation is also associated with higher utilization of the metal component, leading to higher catalytic activity (Gao et al., 2010). A further investigation of the optimal sulfidation procedure and conditions is worthwhile considering. Concentration of isoeugenol and products vs reaction time over the catalyst synthesized from the MoS_2-E-Span 80 emulsion precursor are given in Figure 29 while Figure 30 displays the corresponding data for the Co-MoS_2-E-Span 80 emulsion precursor sulfided ex-situ with DMDS. The first sample was taken once the reactor had reached reaction conditions and for this reason a majority of isoeugenol has already reacted to dihydroeugenol during heating. As can be seen when comparing the charts, in the beginning of the experiment dihydroeugenol is being formed in the case of the in-situ formed catalyst while in the case of the presulfided precursor with DMDS, dihydroeugenol is constantly being converted to 4-propylphenol. A low initial activity with the in-situ sulfided catalyst precursor is likely due to formation of particles happening simultaneously and was the case both for the non-promoted and Co-promoted emulsion precursor. The non-promoted emulsion catalyst precursor is displayed here due to inconsistency in the first sample of the in-situ synthesized Co-promoted catalyst. The catalyst formed from ex-situ synthesis of emulsion precursor with DMDS has already converted a majority of isoeugenol to dihydroeugenol and 4-propylphenol during heating to reaction conditions.

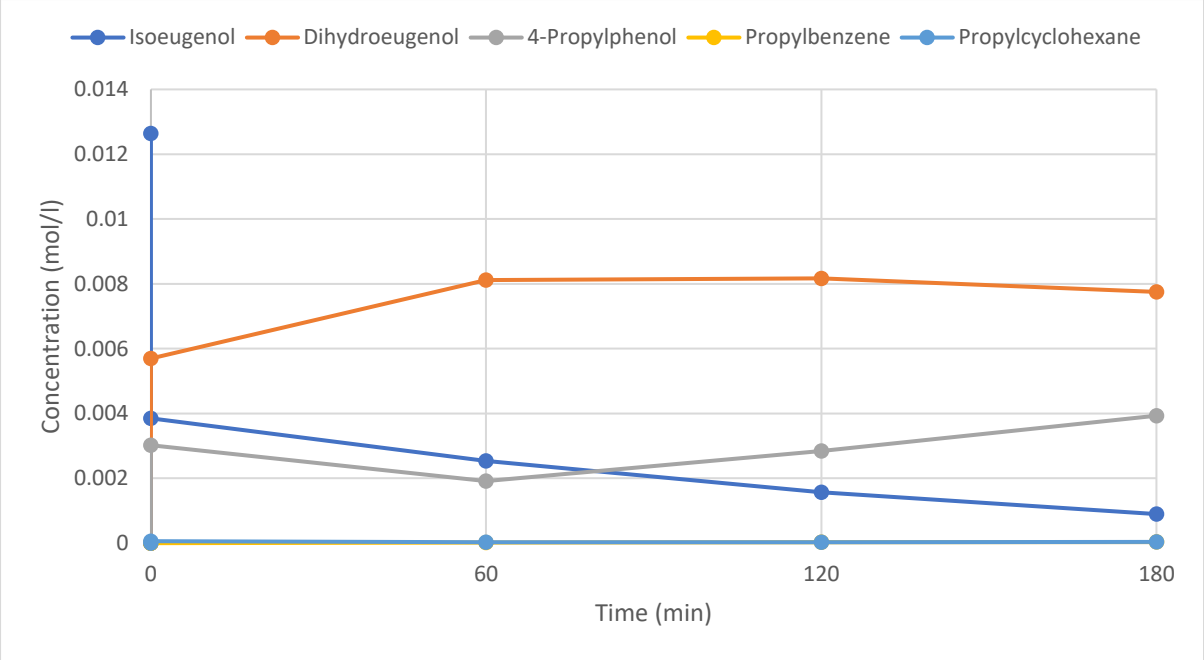

Figure 29. Concentration of isoeugenol and products vs reaction time over the catalyst synthesized in-situ from MoS_2-E-Span 80 emulsion precursor in isoeugenol HDO at 300 °C, 30 bar H_2 and 3 h of reaction time.

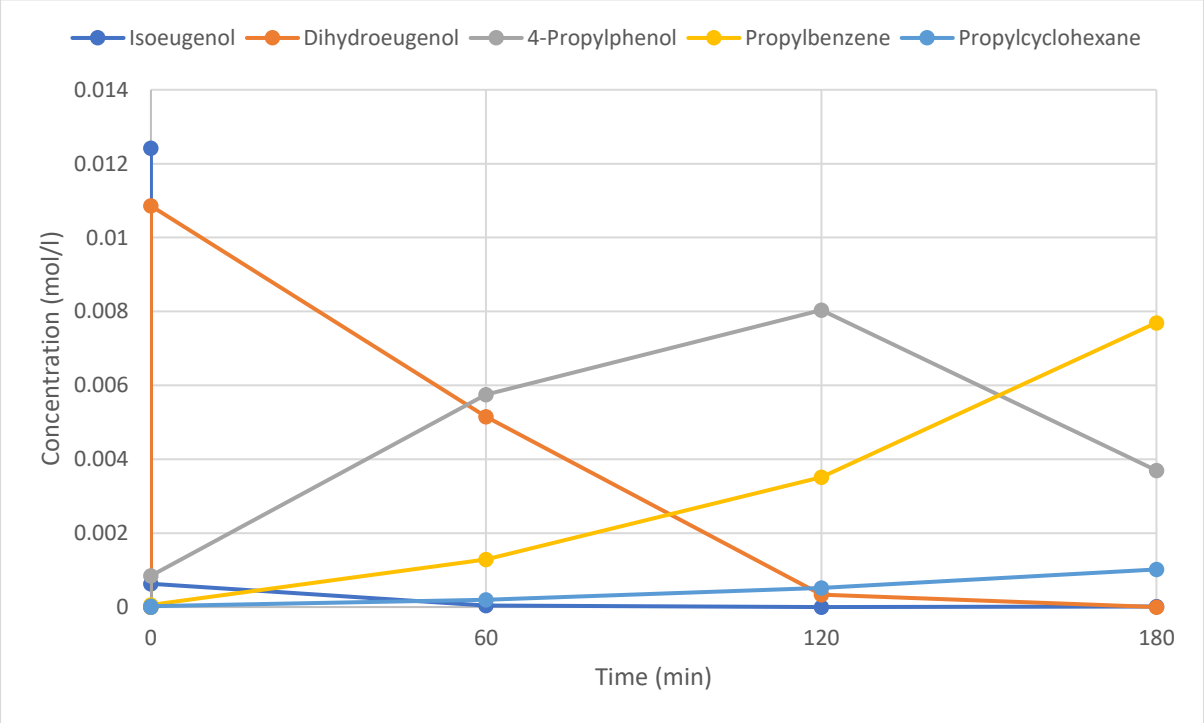

Figure 30. Concentration of isoeugenol and products vs reaction time over the catalyst synthesized ex-situ from Co-MoS_2-E-Span 80 DMDS emulsion precursor in isoeugenol HDO at 300 °C, 30 bar H_2 and 3 h of reaction time.

The selectivity of hydrothermally synthesized MoS_2 and Co-MoS_2 catalysts in isoeugenol HDO can be seen in Figure 31, with all solid catalysts giving close to full conversion. The Co-promoted MoS_2 yielded a lower amount of 4-propylphenol and thus naturally higher selectivity to propylbenzene than the non-promoted MoS_2, demonstrating higher deoxygenation and improved catalytic performance with the addition of Co as a promoter. A similar trend is seen for the AC supported catalysts. For the CoMo/AC catalyst almost no oxygenated compounds were present at the end of the experiment after 3 hours. Regarding the commercial Ru/C and NiMo/Al_2O_3 catalysts, a high selectivity to the fully saturated propylcyclohexane was achieved with both catalysts. A low metal loading in the Ru/C catalyst should be considered when analyzing the results confirming the excellent hydrogenation activity of noble metal catalysts such as Ru/C. A higher catalyst loading or a longer reaction time would most likely have led to the conversion of all dihydroeugenol and 4-propylphenol to either propylbenzene or propylcyclohexane. Similarly, the NiMo/Al_2O_3 catalyst also exhibited high selectivity to propylcyclohexane while a higher selectivity to propylbenzene was also achieved with this catalyst compared to Ru/C. A commercial CoMo/Al_2O_3 would have been a more suitable benchmark, as there would likely have been a selectivity bias towards propylbenzene instead of the fully saturated propylcyclohexane as was the case with the NiMo catalyst.

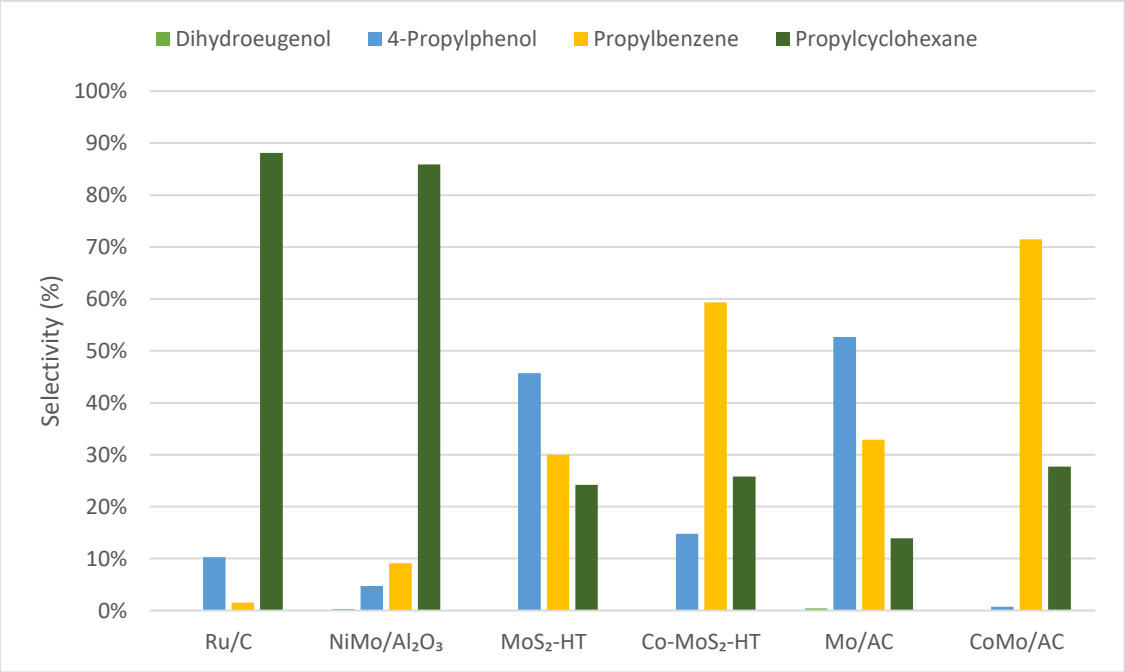

Figure 31. Selectivity of commercial reference catalysts, hydrothermal (Co)-MoS_2, and activated carbon supported (Co)Mo catalysts in HDO of isoeugenol at 300 °C, 30 bar H_2 and 3 h.

Table 13. Conversion of isoeugenol and selectivity using different catalysts after 3 hours of HDO at 300 °C and 30 bar H_2.

Catalyst	Conversion (%)	Selectivity (%)			
		DHE	4-PP	PRB	PCHA
Ru/C	98.8	0.1	10.3	1.5	88.1
$NiMo/Al_2O_3$	99.9	0.3	4.7	9.1	85.9
Mo/AC	99.9	0.4	52.7	32.9	13.9
CoMo/AC	100		0.7	71.5	27.7
MoS_2-HT	100		45.7	30	24.2
Co-MoS_2-HT	99.9		14.8	59.3	25.8
MoS_2-E-Span 80	92.9	66	33.5	0.3	0.3
Co-MoS_2-E-Span 80	88.4	48.5	50.3	1	0.3
Co-MoS_2-E-Span 80 DMDS	99.9		29.8	62	8.2
MoS_2-E-HDK H18	82.2	59.4	39.8	0.4	0.3

Product abbreviations:
DHE = Dihydroeugenol
4-PP = 4-Propylphenol
PRB = Propylbenzene
PCHA = Propylcyclohexane

4.3 Improvement suggestions and future research recommendations

The procedures for synthesizing unsupported catalysts can be improved by applying a few changes. The emulsions acting as liquid catalyst precursors could be improved by refining the compositions. Properties such as stability and droplet size could be improved by varying parameters such as the surfactant used, agitation applied, w/o ratio, and the pH of the aqueous phase. To compare in-situ versus ex-situ sulfidation of the emulsion catalyst precursors, the same sulfiding agent should be used in both cases, to ensure a fair comparison. Regarding the hydrothermally synthesized MoS_2, the effect of different parameters, such as the promoter used and its amount, the hydrothermal synthesizing temperature, as well as the concentration and the pH of the precursor solution, on the formed catalyst and its subsequent HDO performance should be studied. Improving the heating setup to ensure that the synthesizing temperature stays constant for the duration of the synthesis is critical. The influence of catalyst properties such as morphology, particle size, stack layers, and surface area on catalyst performance should be investigated further. Different characterization methods for unsupported MoS_2 should also be explored, with e.g., HRTEM typically used to study morphology and stack layers in MoS_2.

The experimental conditions used in HDO of isoeugenol could be improved by implementing some changes. By increasing the concentration of reactant in relation to the solvent, analytics could be made easier, as a small amount of reactant leads to small amounts of products, making them difficult to identify in GC. A higher reactant concentration would also allow for more flexibility in terms of catalyst loading, since it would be possible to lower it to a more realistic value while the amount of catalyst would still be easily measurable. In terms of the solvent, analytics of the liquid samples would be easier if the solvent peaks in gas chromatograms were easily distinguished from the peaks of some products. Unfortunately, this is not the case with n-dodecane, and it was also observed that the solvent undergoes some reactions during HDO experiments. For this reason, a catalyzed run with the solvent only would be useful to perform and analyze. A similar investigation was conducted within the CaSH project with only the solvent and without catalyst (Gauli, 2021). Regarding liquid samples, taking a liquid sample prior to heating the autoclave is also recommended, as reactions already take place during heating of the reaction mixture. Quantifying gas formation with a gas sampler during or after HDO runs would allow for analysis of gases formed and the amount of catalytic cracking with different catalysts. Finally, HDO runs with real bio-oil feeds are recommended to better investigate and understand the performance and feasibility of unsupported catalysts in bio-oil HDO processes. Studying deactivation of the catalysts due to coking in HDO of real

bio-oil feeds could provide valuable information about the suitability of unsupported catalysts in HDO processes.

5 Conclusions

Climate change and increased environmental awareness has increased the need for chemicals and fuels from renewable sources. Lignocellulosic bio-oil is a promising source of hydrocarbons but comes with its fair share of challenges. The main challenges are related to the upgrading of these bio-oils, with their high oxygen content and chemical instability contributing to rapid catalyst deactivation in the hydrodeoxygenation (HDO) process. A solution to this problem could be to use a slurry reactor, allowing for a fast removal and replacement of deactivated catalyst. In addition, by using a non-acidic unsupported MoS_2 catalyst, coke formation could be mitigated. To study the feasibility of utilizing this kind of catalyst for bio-oil HDO, unsupported MoS_2 and Co-promoted MoS_2 were synthesized by different methods and compared to commercial $NiMo/Al_2O_3$ and Ru/C hydrotreating catalysts in HDO of isoeugenol at 300 °C and 30 bar H_2 for 3 h.

Commercial $NiMo/Al_2O_3$ and Ru/C expectedly yielded close to full conversion of isoeugenol (99.9 % and 98.8 %) and high selectivity to propylcyclohexane (85.9 % and 88.1 %). In contrast, hydrothermally synthesized MoS_2 and Co-MoS_2 exhibited lower selectivity to propylcyclohexane (24.2 % and 25.8 %). Co-promoted MoS_2 afforded higher conversion of 4-propylphenol and subsequently significantly higher selectivity to propylbenzene than the non-promoted MoS_2 (59.3 % vs. 30 %). The same trend was seen for the supported activated carbon catalysts, with Mo/AC yielding 4-propylphenol as the dominating product while CoMo/AC gave almost exclusively fully deoxygenated compounds, primarily propylbenzene. The incorporation of cobalt as a promoter clearly enhanced the deoxygenation performance of mentioned catalysts. As expected, the cobalt promoted catalysts yielded a high degree of unsaturated products, which can be explained by the preferred direct deoxygenation (DDO) reaction pathway.

HDO of isoeugenol using MoS_2 and Co-MoS_2 catalysts synthesized from liquid emulsion precursors produced varying results. The catalysts synthesized prior to isoeugenol HDO using DMDS performed better than the catalysts synthesized in-situ with DMSO simultaneously during isoeugenol HDO. As the particles are already in the active sulfide form when the emulsion is sulfided prior to the HDO experiment, naturally higher initial catalyst activity can be expected. Similarly to the Co-promoted hydrothermal and activated carbon catalysts, the Co-MoS_2 formed from ex-situ synthesis of the catalyst precursor with DMDS resulted in propylbenzene as the main product (62 %). With the catalysts synthesized in-situ simultaneously during the HDO experiment, dihydroeugenol and 4-propylphenol were

obtained as the main products, indicating a relatively low catalytic activity in comparison to other tested catalysts. This is likely explained by the in-situ formation of particles, leading to lower catalytic activity initially while another possible reason is the use of DMSO as a sulfiding agent instead of DMDS.

The activity of unsupported MoS_2 catalysts in HDO of bio-oil model compound isoeugenol has been demonstrated with varying but promising results on which to build upon. Improvements to synthesizing procedures and parameters of both hydrothermally synthesized catalysts and catalysts synthesized from emulsion catalyst precursors have been suggested and should be investigated further. The effect of the catalyst properties such as morphology and the particle size of unsupported MoS_2 on HDO performance and selectivity should be studied and optimized while methods for characterizing such properties in unsupported MoS_2 catalysts should be explored and implemented. HDO runs with real bio-oil feeds and lower catalyst loadings should be conducted to evaluate catalyst performance. Coke formation should be quantified to compare the difference in catalyst deactivation of unsupported and supported catalysts.

6 Svensk sammanfattning – Swedish summary

Slurrykatalysatorer för vätebehandling av bioolja

Den globala övergången från fossila till förnybara källor av bränslen, kemikalier och energi, betyder att framtagandet av nya och innovativa teknologier är centralt. Lignocellulosabaserad biomassa har identifierats som en potentiell ersättare för fossil råolja i bränsle- och kemikalieproduktion. Denna biomassa kan förvätskas genom olika metoder för att erhålla lignocellulosabaserad bioolja. Den erhållna råbiooljan skiljer sig dock markant från fossil råolja i och med att råbiooljan har oönskade egenskaper som hög surhet och hög syrehalt (10–50 massaprocent), vilket leder till kemisk ostabilitet, lågt värmevärde och polaritet. Som sådan kan råbiooljan användas som eldningsolja, men för att kunna användas som transportbränsle bör syrehalten minskas avsevärt. Detta kan åstadkommas genom en process som kallas hydrodeoxygenering (HDO), där råbiooljan utsätts för vätebehandling vid hög temperatur. HDO har visat sig vara problematiskt på grund av råbiooljans kemiska ostabilitet och föroreningar, vilket leder till en snabb deaktivering av traditionella vätebehandlingskatalysatorer. En potentiell lösning är att använda en så kallad slurryreaktor, som möjliggör avlägsnande och ersättning av deaktiverad katalysator. Slurryreaktorer har främst använts för vätebehandling av bottenoljor i fossil råolja, ofta med höga halter föroreningar såsom svavel och kväve men även metaller. Vanligtvis används metallsulfider såsom exempelvis MoS_2, som katalysatorer i slurryreaktorer. Dessa metallsulfider är katalysatorer som saknar bärarmaterial till skillnad från traditionella vätebehandlingskatalysatorer, som NiMo och CoMo på bärarmaterialet Al_2O_3. Användningen av sura bärarmaterial som Al_2O_3 i katalytisk HDO har visat sig bidra till större mängd koks, som sedan fäster sig på katalysatorytan och därmed leder till minskad katalysatoraktivitet. Genom att använda sig av katalysatorer utan bärarmaterial kunde detta problem eventuellt undvikas.

I diplomarbetets litteraturdel har främst katalysatorer utan bärarmaterial såväl som egenskaper och prestanda hos dessa i HDO av råbiooilja och dess modellföreningar studerats. Även andra påverkande faktorer såsom processförhållanden, lösningsmedel och ytaktiva ämnen har studerats. Katalysatorer utan bärarmaterial kan klassificeras enligt typ och framställningsmetod. De tre huvudkategorierna är katalysatorbildande lösningar, katalysatorbildande emulsioner och finfördelade partiklar. Vidare kan de katalysatorbildande lösningarna delas in i olje- och vattenlösliga lösningar medan de finfördelade partiklarna kan delas in i syntetiserade partiklar och naturliga malmer.

Aktiva faser som kan användas i HDO har studerats. Exempel på aktiva faser som använts i forskningen är övergångsmetaller som ädelmetaller (Ru, Pt och Pd) och icke-ädelmetaller (Ni, Co, Fe) och deras olika former inklusive fosfider, oxider, sulfider och även dessa i reducerad form. Metallsulfider utan bärarmaterial identifierades i litteraturdelen som lovande katalysatorer vid HDO av lignocellulosabaserad råbioolja, tack vare deras höga aktivitet i hydrogeneringsreaktioner, förmånlighet, relativt höga stabilitet och låga surhet. Den låga surheten har visat sig främja låg koksbildning. Metallsulfidernas låga surhet leder till obetydlig katalytisk krackning jämfört med katalysatorer på sura bärarmaterial såsom Al_2O_3. Olika promotormetaller på metallsulfider (med och utan bärarmaterial) studerades, varav kobolt, nickel och järn är bland de vanligaste. Katalysatorer med kobolt som promotor sägs föredra så kallad direkt deoxygenering (DDO) varvid syre tas bort direkt utan saturering av aromatringen, medan syreborttagning med nickel som promotor sker genom saturering av aromatringen. Detta påverkar förstås i sin tur vilka typer av produkter som erhålls.

Processförhållanden såsom temperatur, tryck och katalysatormängd och deras inverkan på HDO-prestanda undersöktes. I fråga om temperatur kan nämnas att en högre temperatur leder till högre grad av syreborttagning till en viss gräns. Högre temperaturer leder även till mer krackning, vilket i sin tur innebär högre gasbildning och ett sämre utbyte av vätskefasprodukterna. En för hög temperatur kan även leda till att vissa reaktionsvägar förhindras, och ett exempel på detta är saturering av den aromatiska ringen. En lägre temperatur är positivt ur katalysatorstabilitetens synvinkel men ofta på bekostnad av HDO-prestanda. Vid HDO är ett högre vätgastryck ofta fördelaktigt för stabilisering av radikaler och för att säkerställa god vätgaslöslighet i vätskefasen. Mängden katalysator spelar en viktig roll i HDO av bioolja eftersom en otillräcklig mängd katalysator kan leda till otillräcklig katalytisk hydrogeneringsaktivitet. Andra faktorer som undersöktes i litteraturdelen var bland annat lösningsmedlets roll vid HDO av råbioolja och inverkan av katalysatorstrukturen på katalytisk aktivitet och produktselektivitet.

I den experimentella delen framställdes MoS_2 och Co-MoS_2 utan bärarmaterial med två olika metoder. Den första metoden var en hydrotermisk metod där katalysatorpartiklarna framställdes från en saltlösning som innehöll metallerna (Mo eller Mo och Co) och tiourea som sulfideringsmedel. Ammoniumheptamolybdat tetrahydrat och kobolt (II) nitrat hexahydrat användes som prekursorer för Mo och Co i alla metoder. I den andra metoden framställdes vatten–olja-emulsioner som innehöll metallerna och i vissa fall även dimetylsulfoxid (DMSO) som sulfideringsmedel i vattenfasen. En emulsion sulfiderades skilt med DMDS istället för DMSO. Emulsionerna stabiliserades med antingen det ytaktiva ämnet Span 80 eller Wacker

HDK H18 silica-nanopartiklar som blandades i den organiska fasen, vilket i detta fall var n-dodekan Vattenfasen och den organiska fasen blandades med en homogenisator genom långsam tillsats av vattenfasen i den organiska fasen. Dessa emulsioner fungerade som prekursorer för katalysatorerna och syntetiserades termiskt antingen under själva HDO-experimenten eller skilt före experimentet för att erhålla de fasta katalysatorpartiklarna. Mo och CoMo på aktivt kol framställdes genom torr impregnering. Dessa katalysatorer sulfiderades med dimetyldisulfid (DMDS) före HDO-experiment. Även kommersiellt tillgängliga Ru/C- och $NiMo/Al_2O_3$-katalysatorer användes i HDO. Ru/C användes som sådan medan $NiMo/Al_2O_3$-katalysatorn sulfiderades med DMDS före HDO-experimentet.

HDO av isoeugenol, som användes som modellämne för råbioolja, utfördes i en satsreaktor vid temperaturen 300 °C och vätetrycket 30 bar i 3 timmar. Som lösningsmedel för isoeugenol användes n-dodekan. Resultaten påvisade de kommersiella katalysatorernas ($NiMo/Al_2O_3$ och Ru/C) höga hydrogeneringsaktivitet och därmed höga selektivitet till fullständigt saturerade propylcyklohexan. Tydliga skillnader i resultaten mellan katalysatorerna syntetiserade från emulsionerna observerades. Co-MoS_2-katalysatorn syntetiserad före experimentet med DMDS som sulfideringsmedel uppvisade klart bättre prestanda både i fråga om isoeugenol konversion och produktselektivitet, än övriga katalysatorer syntetiserade från emulsionerna. De senare nämnda katalysatorerna syntetiserades samtidigt under HDO-experimentet med DMSO som sulfideringsmedel. Av de hydrotermiskt syntetiserade MoS_2- och Co-MoS_2-katalysatorerna uppvisade katalysatorn med kobolt som promotormetall bättre syreborttagning i och med högre selektivitet till syrefria produkter som propylbensen och propylcyklohexan. Mo och CoMo på aktivt kol uppvisade liknande resultat och trender som de hydrotermiska MoS_2 och Co-MoS_2. Med Mo/AC-katalysatorn var den största produkten 4-propylfenol följt av propylbensen och propylcyklohexan. CoMo/AC-katalysatorn ledde till hög selektivitet av propylbensen och även en del propylcyklohexan. Mängden 4-propylfenol var minimal i fallet med CoMo/AC-katalysatorn, vilket påvisar katalysatorns goda HDO-aktivitet.

Aktiviteten hos MoS_2-katalysatorer utan bärarmaterial i isoeugenol HDO har påvisats med varierande men lovande resultat. Mer forskning gällande denna katalysatortyp bör utföras. Förbättringsförslag för både katalysatorsyntes och själva HDO-experimenten har föreslagits i diplomarbetet. Emulsionsegenskaper som droppstorleken och emulsionsstabiliteten kunde förbättras genom att testa olika ytaktiva ämnen, vatten-till-olja-förhållanden, pH av vattenfasen och omrörningstid samt hastighet. I framtida forskning gällande den hydrotermiska metoden bör effekten av parametrar som syntetiseringstemperatur, saltlösningens koncentration och pH

samt promotormetall undersökas. För att få en bättre helhetsbild av katalysatorprestandan hos denna typ av katalysator, bör experiment med högre koncentration av isoeugenol och mindre mängd katalysator i förhållande till reaktanten utföras, medan även experiment med råbioolja rekommenderas.

7 References

Al-Attas, T.A., Ali, S.A., Zahir, M.H., Xiong, Q., Al-Bogami, S.A., Malaibari, Z.O., Razzak, S.A., Hossain, M.M., 2019a. Recent advances in heavy oil upgrading using dispersed catalysts. Energy & Fuels 33, 7917–7949.

Al-Attas, T.A., Zahir, M.H., Ali, S.A., Al-Bogami, S.A., Malaibari, Z., Razzak, S.A., Hossain, M.M., 2019b. Novel (Co-,Ni)-p-tert-butylcalix[4]arenes as dispersed catalysts for heavy oil upgrading: Synthesis, characterization, and performance evaluation. Energy & Fuels 33, 561–573.

Al-Attas, T.A., Zahir, M.H., Ali, S.A., Al-Bogami, S.A., Malaibari, Z., Razzak, S.A., Hossain, M.M., 2019c. Kinetics of the synergy effects in heavy oil upgrading using novel Ni-p-tert-butylcalix[4]arene as a dispersed catalyst with a supported catalyst. Fuel Processing Technology 185, 158–168.

Alkhaldi, S., Husein, M.M., 2014. Hydrocracking of heavy oil by means of in situ prepared ultradispersed nickel nanocatalyst. Energy & Fuels 28, 643–649.

Al-Marshed, A., Hart, A., Leeke, G., Greaves, M., Wood, J., 2015. Effectiveness of different transition metal dispersed catalysts for in situ heavy oil upgrading. Industrial & Engineering Chemistry Research 54, 10645–10655.

Al-Rashidy, A.H., Al-Attas, T.A., Ali, S.A., Al-Bogami, S.A., Razzak, S.A., Hossain, M.M., 2019. Hydrocracking of LVGO using dispersed catalysts derived from soluble precursors: Performance evaluation and kinetics. Industrial & Engineering Chemistry Research 58, 14709–14718.

Ambursa, M.M., Juan, J.C., Yahaya, Y., Taufiq-Yap, Y.H., Lin, Y.-C., Lee, H.V., 2021. A review on catalytic hydrodeoxygenation of lignin to transportation fuels by using nickel-based catalysts. Renewable & Sustainable Energy Reviews 138, 110667.

Ancheyta, J., 2013. Modeling of processes and reactors for upgrading of heavy petroleum. CRC Press, Baton Rouge.

Badawi, M., Paul, J.F., Cristol, S., Payen, E., Romero, Y., Richard, F., Brunet, S., Lambert, D., Portier, X., Popov, A., Kondratieva, E., Goupil, J.M., el Fallah, J., Gilson, J.P., Mariey, L., Travert, A., Maugé, F., 2011. Effect of water on the stability of Mo and CoMo hydrodeoxygenation catalysts: A combined experimental and DFT study. Journal of Catalysis 282, 155–164.

Bellussi, G., Rispoli, G., Landoni, A., Millini, R., Molinari, D., Montanari, E., Moscotti, D., Pollesel, P., 2013. Hydroconversion of heavy residues in slurry reactors: Developments and perspectives. Journal of Catalysis 308, 189–200.

Bergvall, N., Molinder, R., Johansson, A.-C., Sandström, L., 2021. Continuous slurry hydrocracking of biobased fast pyrolysis oil. Energy & Fuels 35, 2303–2312.

Boldingh, E., Bauer, L., 2010. Use of supported mixed metal sulfides for hydrotreating biorenewable feeds.

Burimsitthigul, T., Yoosuk, B., Ngamcharussrivichai, C., Prasassarakich, P., 2021. Hydrocarbon biofuel from hydrotreating of palm oil over unsupported Ni–Mo sulfide catalysts. Renewable Energy 163, 1648–1659.

Cao, J., Li, A., Zhang, Y., Mu, L., Huang, X., Li, Y., Yang, T., Zhang, C., Zhou, C., 2021. Highly efficient unsupported Co-doped nano-MoS_2 catalysts for p-cresol hydrodeoxygenation. Molecular Catalysis 505, 111507.

Castañeda, L.C., Muñoz, J.A.D., Ancheyta, J., 2012. Combined process schemes for upgrading of heavy petroleum. Fuel 100, 110–127.

Čelič, T.B., Grilc, M., Likozar, B., Tušar, N.N., 2015. In situ generation of Ni nanoparticles from metal–organic framework precursors and their use for biomass hydrodeoxygenation. ChemSusChem 8, 1703–1710.

Cheng, S., Wei, L., Julson, J., Rabnawaz, M., 2017. Upgrading pyrolysis bio-oil through hydrodeoxygenation (HDO) using non-sulfided Fe-Co/SiO_2 catalyst. Energy Conversion and Management 150, 331–342.

Chenguang, S., Guohe, Q., Ruihua, S., 1998. Hydrocracking of Liaohe vacuum residue on bimetallic oil soluble catalysts. In: ACS Division of Fuel Chemistry, Preprints. pp. 481–483.

Chevron Lummus Global, 2007. Neste Oil inaugurates new diesel line at Porvoo refinery using Chevron Lummus Global's integrated LC-Fining and Isocracking technologies [Press release].

Chianelli, R.R., Siadati, M.H., de la Rosa, M.P., Berhault, G., Wilcoxon, J.P., Bearden Jr, R., Abrams, B.L., 2006. Catalytic properties of single layers of transition metal sulfide catalytic materials. Catalysis Reviews - Science and Engineering 48, 1–41.

Daaou, M., Bendedouch, D., 2012. Water pH and surfactant addition effects on the stability of an Algerian crude oil emulsion. Journal of Saudi Chemical Society 16, 333–337.

Dabros, T., Gaur, A., Pintos, D.G., Sprenger, P., Høj, M., Hansen, T., Studt, F., Gabrielsen, J., Grunwaldt, J.-D., Jensen, A.D., 2018a. Influence of H_2O and H_2S on the composition,

activity, and stability of sulfided Mo, CoMo, and NiMo supported on $MgAl_2O_4$ for hydrodeoxygenation of ethylene glycol. Applied Catalysis A: General 551, 106–121.

Dabros, T., Stummann, M., Høj, M., Jensen, P., Grunwaldt, J.-D., Gabrielsen, J., Mortensen, P., Jensen, A., 2018b. Transportation fuels from biomass fast pyrolysis, catalytic hydrodeoxygenation, and catalytic fast hydropyrolysis. Progress in Energy and Combustion Science 68, 268–309.

Dang, Q., Luo, Z., Zhang, J., Wang, J., Chen, W., Yang, Y., 2013. Experimental study on bio-oil upgrading over $Pt/SO_4^{2-}/ZrO_2$/SBA-15 catalyst in supercritical ethanol. Fuel 103, 683–692.

Deepa, A.K., Dhepe, P.L., 2014. Function of metals and supports on the hydrodeoxygenation of phenolic compounds. ChemPlusChem 79, 1573–1583.

Du, H., Du, H., Li, M., Li, M., Liu, D., Liu, D., Ren, Y., Ren, Y., Duan, Y., Duan, Y., 2015. Slurry-phase hydrocracking of heavy oil and model reactant: Effect of dispersed Mo catalyst. Applied Petrochemical Research 5, 89–98.

Echeandia, S., Arias, P.L., Barrio, V.L., Pawelec, B., Fierro, J.L.G., 2010. Synergy effect in the HDO of phenol over Ni–W catalysts supported on active carbon: Effect of tungsten precursors. Applied Catalysis B: Environmental 101, 1–12.

Eijsbouts, S., Mayo, S.W., Fujita, K., 2007. Unsupported transition metal sulfide catalysts: From fundamentals to industrial application. Applied Catalysis A: General 322, 58–66.

Elliott, D.C., Hart, T.R., Neuenschwander, G.G., Rotness, L.J., Zacher, A.H., 2009. Catalytic hydroprocessing of biomass fast pyrolysis bio-oil to produce hydrocarbon products. Environmental Progress & Sustainable Energy 28, 441–449.

Engelhardt, J., Lyu, P., Nachtigall, P., Schüth, F., García, Á.M., 2017. The influence of water on the performance of molybdenum carbide catalysts in hydrodeoxygenation reactions: A combined theoretical and experimental study. ChemCatChem 9, 1985–1991.

Furimsky, E., 2000. Catalytic hydrodeoxygenation. Applied Catalysis A: General 199, 147–190.

Furimsky, E., 2007. Catalysts for upgrading heavy petroleum feeds, 1st ed, Studies in surface science and catalysis. Elsevier Science & Technology, Oxford.

Galarraga, C.E., Pereira-Almao, P., 2010. Hydrocracking of Athabasca bitumen using submicronic multimetallic catalysts at near in-reservoir conditions. Energy & Fuels 24, 2383–2389.

Gao, D., Xiao, Y., Varma, A., 2015. Guaiacol hydrodeoxygenation over platinum catalyst: Reaction pathways and kinetics. Industrial & Engineering Chemistry Research 54, 10638–10644.

Gao, Y., Fang, X., Cheng, Z., 2010. A comparative study on the ex situ and in situ presulfurization of hydrotreating catalysts. Catalysis Today 158, 496–503.

Gauli, B., 2021. HDO over iron catalysts. MSc thesis. Åbo Akademi University, Turku.

Gillis, D., VanWees, M., Zimmerman, P., Houde, E., 2010. Upgrading residues to maximize distillate yields with UOP Uniflex^{TM} process. Journal of the Japan Petroleum Institute 53, 33–41.

Gochi, Y., Ornelas, C., Paraguay, F., Fuentes, S., Alvarez, L., Rico, J.L., Alonso-Núñez, G., 2005. Effect of sulfidation on Mo-W-Ni trimetallic catalysts in the HDS of DBT. Catalysis Today 107–108, 531–536.

Grilc, M., Veryasov, G., Likozar, B., Jesih, A., Levec, J., 2015. Hydrodeoxygenation of solvolysed lignocellulosic biomass by unsupported MoS_2, MoO_2, Mo_2C and WS_2 catalysts. Applied Catalysis B: Environmental 163, 467–477.

Guo, C., Rao, K.T.V., Yuan, Z., He, S., Rohani, S., Xu, C., 2018. Hydrodeoxygenation of fast pyrolysis oil with novel activated carbon-supported NiP and CoP catalysts. Chemical Engineering Science 178, 248–259.

Guo, X., Wang, W., Wu, K., Huang, Y., Shi, Q., Yang, Y., 2019. Preparation of Fe promoted MoS_2 catalysts for the hydrodeoxygenation of p-cresol as a model compound of lignin-derived bio-oil. Biomass & Bioenergy 125, 34–40.

Hohl, L., Röhl, S., Stehl, D., von Klitzing, R., Kraume, M., 2016. Influence of nanoparticles and drop size distributions on the rheology of w/o pickering emulsions. Chemie Ingenieur Technik 88, 1815–1826.

Horáček, J., Kubička, D., 2017. Bio-oil hydrotreating over conventional CoMo & NiMo catalysts: The role of reaction conditions and additives. Fuel 198, 49–57.

Huber, G.W., Iborra, S., Corma, A., 2006. Synthesis of transportation fuels from biomass: Chemistry, catalysts, and engineering. Chemical Reviews 106, 4044–4098.

Huirache-Acuña, R., Albiter, M.A., Ornelas, C., Paraguay-Delgado, F., Martínez-Sánchez, R., Alonso-Nuñez, G., 2006. Ni(Co)-Mo-W sulphide unsupported HDS catalysts by ex situ decomposition of alkylthiomolybdotungstates. Applied Catalysis A: General 308, 134–142.

Iqbal, J., Petersen, S., Ulrich, J., 2011. Emulsion solidification: Influence of the droplet size of the water-in-oil emulsion on the generated particle size. Chemical Engineering & Technology 34, 530–534.

Kapustin, V., Chernysheva, E., Khakimov, R., 2021. Comparison of moving-bed catalytic tar hydrocracking processes. Processes 9, 500.

Kassem, M.G.A., Ahmed, A.-M.M., Abdel-Rahman, H.H., Moustafa, A.H.E., 2019. Use of Span 80 and Tween 80 for blending gasoline and alcohol in spark ignition engines. Energy Reports 5, 221–230.

Khromova, S.A., Smirnov, A.A., Bulavchenko, O.A., Saraev, A.A., Kaichev, V. v, Reshetnikov, S.I., Yakovlev, V.A., 2014. Anisole hydrodeoxygenation over Ni–Cu bimetallic catalysts: The effect of Ni/Cu ratio on selectivity. Applied Catalysis A: General 470, 261–270.

Kim, S.-H., Kim, K.-D., Lee, H., Lee, Y.-K., 2017. Beneficial roles of H-donors as diluent and H-shuttle for asphaltenes in catalytic upgrading of vacuum residue. Chemical Engineering Journal 314, 1–10.

Kunnas, J., Smith, L., 2011. Improving residue hydrocracking performance. Petroleum Technology Quarterly Q3 49–57.

Kwon, K.C., Mayfield, H., Marolla, T., Nichols, B., Mashburn, M., 2011. Catalytic deoxygenation of liquid biomass for hydrocarbon fuels. Renewable Energy 36, 907–915.

Laurent, E., Delmon, B., 1994. Influence of water in the deactivation of a sulfided NiMo/γ-Al_2O_3 catalyst during hydrodeoxygenation. Journal of Catalysis 146, 281–291.

Lee, H., Kim, Y.-M., Lee, I.-G., Jeon, J.-K., Jung, S.-C., Chung, J. do, Choi, W.G., Park, Y.-K., 2016. Recent advances in the catalytic hydrodeoxygenation of bio-oil. The Korean Journal of Chemical Engineering 33, 3299–3315.

Li, K., Wang, R., Chen, J., 2011. Hydrodeoxygenation of anisole over silica-supported Ni_2P, MoP, and NiMoP catalysts. Energy & Fuels 25, 854–863.

Lindenstruth, K., Müller, B.W., 2004. Parameters with influence on the droplet size of w/o emulsions. Pharmazie 59, 187–190.

Liu, C., Wang, H., Karim, A.M., Sun, J., Wang, Y., 2014. Catalytic fast pyrolysis of lignocellulosic biomass. Chemical Society Reviews 43, 7594–7623.

Liu, F., Zhao, H., Jia, H., Zhu, C., Li, J., Zheng, Z., 2016. Hydrothermal synthesis and electrochemical performance of walnut-like CoS_2 hierarchical structures. Micro & Nano Letters 11, 281–283.

Liu, G., Robertson, A.W., Li, M.M.-J., Kuo, W.C.H., Darby, M.T., Muhieddine, M.H., Lin, Y.-C., Suenaga, K., Stamatakis, M., Warner, J.H., Tsang, S.C.E., 2017. MoS_2 monolayer catalyst doped with isolated Co atoms for the hydrodeoxygenation reaction. Nature Chemistry 9, 810–816.

Liu, J., Fan, K., Tian, W., Liu, C., Rong, L., 2012. Hydroprocessing of Jatropha oil over $NiMoCe/Al_2O_3$ catalyst. International Journal of Hydrogen Energy 37, 17731–17737.

Liu, K., 2016. Catalytic hydrodeoxygenation of bio-oil and model compounds. PhD thesis. Imperial College London, London.

Luo, L., Shi, M., Zhao, S., Tan, W., Lin, X., Wang, H., Jiang, F., 2019. Hydrothermal synthesis of MoS_2 with controllable morphologies and its adsorption properties for bisphenol A. Journal of Saudi Chemical Society 23, 762–773.

Matsumura, A., Kondo, T., Sato, S., Saito, I., de Souza, W.F., 2005. Hydrocracking Brazilian Marlim vacuum residue with natural limonite. Part 1: Catalytic activity of natural limonite. Fuel 84, 411–416.

Montanari, L., Bonoldi, L., Alessi, A., Flego, C., Salvalaggio, M., Carati, C., Bazzano, F., Landoni, A., 2017. Molecular evolution of asphaltenes from petroleum residues after different severity hydroconversion by EST process. Energy & Fuels 31, 3729–3737.

Moon, J.-S., Kim, E.-G., Lee, Y.-K., 2014. Active sites of Ni_2P/SiO_2 catalyst for hydrodeoxygenation of guaiacol: A joint XAFS and DFT study. Journal of Catalysis 311, 144–152.

Mortensen, P., de Carvalho, H., Grunwaldt, J.-D., Jensen, P., Jensen, A., 2015. Activity and stability of Mo_2C/ZrO_2 as catalyst for hydrodeoxygenation of mixtures of phenol and 1-octanol. Journal of Catalysis 328, 208–215.

Mortensen, P., Gardini, D., Damsgaard, C., Grunwaldt, J.-D., Jensen, P., Wagner, J., Jensen, A., 2016. Deactivation of Ni-MoS_2 by bio-oil impurities during hydrodeoxygenation of phenol and octanol. Applied Catalysis A: General 523, 159–170.

Mortensen, P., Grunwaldt, J.-D., Jensen, P., Knudsen, K., Jensen, A., 2011. A review of catalytic upgrading of bio-oil to engine fuels. Applied Catalysis A: General 407, 1–19.

Nguyen, M.T., Nguyen, N.T., Cho, J., Park, C., Park, S., Jung, J., Lee, C.W., 2016. A review on the oil-soluble dispersed catalyst for slurry-phase hydrocracking of heavy oil. Journal of Industrial and Engineering Chemistry 43, 1–12.

Nguyen-Huy, C., Kweon, H., Kim, H., Kim, D.K., Kim, D.-W., Oh, S.H., Shin, E.W., 2012. Slurry-phase hydrocracking of vacuum residue with a disposable red mud catalyst. Applied Catalysis A: General 447–448, 186–192.

Nimmanwudipong, T., Runnebaum, R.C., Block, D.E., Gates, B.C., 2011. Catalytic conversion of guaiacol catalyzed by platinum supported on alumina: Reaction network including hydrodeoxygenation reactions. Energy & Fuels 25, 3417–3427.

Oh, S., Choi, H.S., Choi, I.-G., Choi, J.W., 2017. Evaluation of hydrodeoxygenation reactivity of pyrolysis bio-oil with various Ni-based catalysts for improvement of fuel properties. RSC Advances 7, 15116–15126.

Oh, S., Lee, J.H., Choi, I.-G., Choi, J.W., 2020. Enhancement of bio-oil hydrodeoxygenation activity over Ni-based bimetallic catalysts supported on SBA-15. Renewable Energy 149, 1–10.

Olcese, R.N., Bettahar, M., Petitjean, D., Malaman, B., Giovanella, F., Dufour, A., 2012. Gas-phase hydrodeoxygenation of guaiacol over Fe/SiO_2 catalyst. Applied Catalysis B: Environmental 115–116, 63–73.

Phan, B.M.Q., Phan, B.M.Q., Ha, Q.L.M., Ha, Q.L.M., Le, N.P., Le, N.P., Ngo, P.T., Ngo, P.T., Nguyen, T.H., Nguyen, T.H., Dang, T.T., Dang, T.T., Nguyen, L.H., Nguyen, L.H., Nguyen, D.A., Nguyen, D.A., Luu, L.C., Luu, L.C., 2015. Influences of various supports, γ-Al_2O_3, CeO_2, and SBA-15 on HDO performance of NiMo catalyst. Catalysis Letters 145, 662–667.

Plantenga, F.L., Leliveld, R.G., 2003. Sulfur in fuels: More stringent sulfur specifications for fuels are driving innovation. Applied Catalysis A: General 248, 1–7.

Popov, A., Kondratieva, E., Goupil, J.M., Mariey, L., Bazin, P., Gilson, J.-P., Travert, A., Maugé, F., 2010. Bio-oils hydrodeoxygenation: Adsorption of phenolic molecules on oxidic catalyst supports. Journal of Physical Chemistry C 114, 15661–15670.

Prajapati, R., Kohli, K., Maity, S.K., 2017. Slurry-phase hydrocracking of residue with ultradispersed MoS_2 catalysts prepared by microemulsion methods. Energy & Fuels 31, 3905–3912.

Prasomsri, T., Nimmanwudipong, T., Román-Leshkov, Y., 2013. Effective hydrodeoxygenation of biomass-derived oxygenates into unsaturated hydrocarbons by MoO_3 using low H_2 pressures. Energy & Environmental Science 6, 1732–1738.

Quitian, A., Ancheyta, J., 2016. Experimental methods for developing kinetic models for hydrocracking reactions with slurry-phase catalyst using batch reactors. Energy & Fuels 30, 4419–4437.

Rana, M.S., Ancheyta, J., Rayo, P., Maity, S.K., 2007. Heavy oil hydroprocessing over supported NiMo sulfided catalyst: An inhibition effect by added H_2S. Fuel 86, 1263–1269.

Rezaei, H., Ardakani, S.J., Smith, K.J., 2012. Study of MoS_2 catalyst recycle in slurry-phase residue hydroconversion. Energy & Fuels 26, 6540–6550.

Rodriguez, J.A., Hrbek, J., 1999. Interaction of sulfur with well-defined metal and oxide surfaces: Unraveling the mysteries behind catalyst poisoning and desulfurization. Accounts of Chemical Research 32, 719–728.

Ruinart de Brimont, M., Dupont, C., Daudin, A., Geantet, C., Raybaud, P., 2012. Deoxygenation mechanisms on Ni-promoted MoS_2 bulk catalysts: A combined experimental and theoretical study. Journal of Catalysis 286, 153–164.

Sahebdelfar, S., 2017. Steam reforming of propionic acid: Thermodynamic analysis of a model compound for hydrogen production from bio-oil. International Journal of Hydrogen Energy 42, 16386–16395.

Sahu, R., Song, B.J., Im, J.S., Jeon, Y.-P., Lee, C.W., 2015. A review of recent advances in catalytic hydrocracking of heavy residues. Journal of Industrial and Engineering Chemistry 27, 12–24.

Saidi, M., Samimi, F., Karimipourfard, D., Nimmanwudipong, T., Gates, B.C., Rahimpour, M.R., 2014. Upgrading of lignin-derived bio-oils by catalytic hydrodeoxygenation. Energy & Environmental Science 7, 103–129.

Sangnikul, P., Phanpa, C., Xiao, R., Zhang, H., Reubroycharoen, P., Kuchonthara, P., Vitidsant, T., Pattiya, A., Hinchiranan, N., 2019. Role of copper- or cerium-promoters on NiMo/γ-Al_2O_3 catalysts in hydrodeoxygenation of guaiacol and bio-oil. Applied Catalysis A: General 574, 151–160.

Şenol, O.İ., Viljava, T.-R., Krause, A.O.I., 2007. Effect of sulphiding agents on the hydrodeoxygenation of aliphatic esters on sulphided catalysts. Applied Catalysis A: General 326, 236–244.

Sharma, B.K., Kohli, K., 2020. Slurry phase catalysts for bio-oil upgradation. Champaign, IL: Illinois Sustainable Technology Center.

Shi, B., Que, G., 2003. Hydrocracking of Liaohe vacuum residue with oil-soluble Co-Ni bimetallic catalysts and hydrogen donor. In: ACS Division of Fuel Chemistry, Preprints. pp. 722–724.

Son, J.H., Kim, S.W., Bae, D.S., Han, K.S., Lee, J.K., Kim, C.Y., Kim, B.I., Adair, J.H., 2008. Synthesis and characterization of CeO_2-doped SiO_2 nanoparticles by a reverse micelle and sol–gel processing. Materials Science and Engineering: A 498, 2–4.

Song, W., Nie, T., Lai, W., Yang, W., Jiang, X., 2018. Tailoring the morphology of Co-doped MoS_2 for enhanced hydrodeoxygenation performance of p-cresol. CrystEngComm 20, 4069–4074.

Stanciulescu, M., Kelly, J., Ikura, M., 1996. Production of highly dispersed hydrogenation catalysts. US005283217A.

Ternan, M., Furimsky, E., Parsons, B.I., 1979. Coke formation on hydrodesulphurization catalysts. Fuel Processing Technology 2, 45–55.

Tieuli, S., Mäki-Arvela, P., Peurla, M., Eränen, K., Wärnå, J., Cruciani, G., Menegazzo, F., Murzin, D.Yu., Signoretto, M., 2019. Hydrodeoxygenation of isoeugenol over Ni-SBA-15: Kinetics and modelling. Applied Catalysis A: General 580, 1–10.

Venderbosch, R., Prins, W., 2010. Fast pyrolysis technology development. Biofuels, Bioproducts and Biorefining 4, 178–208.

Venderbosch, R.H., Ardiyanti, A.R., Wildschut, J., Oasmaa, A., Heeres, H.J., 2010. Stabilization of biomass-derived pyrolysis oils. Journal of Chemical Technology & Biotechnology 85, 674–686.

Veses, A., Puértolas, B., López, J.M., Callén, M.S., Solsona, B., García, T., 2016. Promoting deoxygenation of bio-oil by metal-loaded hierarchical ZSM-5 zeolites. ACS Sustainable Chemistry & Engineering 4, 1653–1660.

Viana, C., Bohrer, D., de Carvalho, L.M., do Nascimento, P.C., da Rosa, M.B., 2014. Emulsified systems for metal determination by spectrometric methods. TrAC Trends in Analytical Chemistry 53, 49–59.

Viljava, T.-R., Komulainen, R.S., Krause, A.O.I., 2000. Effect of H_2S on the stability of $CoMo/Al_2O_3$ catalysts during hydrodeoxygenation. Catalysis Today 60, 83–92.

Vroman, H., Soled, S.L., Miseo, S., Riley, K.L., Ho, T.C., Krycak, R., 2001. Nickel molybodtungstate hydrotreating catalysts.

Wang, W., Li, L., Tan, S., Wu, K., Zhu, G., Liu, Y., Xu, Y., Yang, Y., 2016. Preparation of $NiS_2//MoS_2$ catalysts by two-step hydrothermal method and their enhanced activity for hydrodeoxygenation of p-cresol. Fuel 179, 1–9.

Wang, W., Li, L., Wu, K., Zhang, K., Jie, J., Yang, Y., 2015. Preparation of Ni–Mo–S catalysts by hydrothermal method and their hydrodeoxygenation properties. Applied Catalysis A: General 495, 8–16.

Wang, W., Wu, K., Tan, S., Yang, Y., 2017. Hydrothermal synthesis of carbon-coated CoS_2–MoS_2 catalysts with enhanced hydrophobicity and hydrodeoxygenation activity. ACS Sustainable Chemistry & Engineering 5, 8602–8609.

Wang, W., Zhang, K., Li, L., Wu, K., Liu, P., Yang, Y., 2014a. Synthesis of highly active Co–Mo–S unsupported catalysts by a one-step hydrothermal method for p-cresol hydrodeoxygenation. Industrial & Engineering Chemistry Research 53, 19001–19009.

Wang, W., Zhang, K., Qiao, Z., Li, L., Liu, P., Yang, Y., 2014b. Influence of surfactants on the synthesis of MoS_2 catalysts and their activities in the hydrodeoxygenation of 4-methylphenol. Industrial & Engineering Chemistry Research 53, 10301–10309.

Waskito, I.S., Kurniawan, B., Amal, M.I., Hanifuddin, M., 2019. The effect of precursors concentration on the structural properties of MoS_2 nanosheet-microsphere synthesized via hydrothermal route. IOP Conference Series: Materials Science and Engineering 546.

Watanabe, I., Otake, M., Yoshimoto, M., Sakanishi, K., Korai, Y., Mochida, I., 2002. Behaviors of oil-soluble molybdenum complexes to form very fine MoS_2 particles in vacuum residue. Fuel 81, 1515–1520.

Whiffen, V.M.L., Smith, K.J., 2010. Hydrodeoxygenation of 4-methylphenol over unsupported MoP, MoS_2, and MoO_x Catalysts. Energy & Fuels 24, 4728–4737.

Wildschut, J., Mahfud, F., Venderbosch, R., Heeres, H., 2009. Hydrotreatment of fast pyrolysis oil using heterogeneous noble-metal catalysts. Industrial & Engineering Chemistry Research 48, 10324–10334.

Xu, X., Zhang, C., Zhai, Y., Liu, Y., Zhang, R., Tang, X., 2014. Upgrading of bio-oil using supercritical 1-butanol over a Ru/C heterogeneous catalyst: Role of the solvent. Energy & Fuels 28, 4611–4621.

Yang, T., Jie, Y., Li, B., Kai, X., Yan, Z., Li, R., 2016. Catalytic hydrodeoxygenation of crude bio-oil over an unsupported bimetallic dispersed catalyst in supercritical ethanol. Fuel Processing Technology 148, 19–27.

Yang, Y., Luo, H., Tong, G., Smith, K.J., Tye, C.T., 2008. Hydrodeoxygenation of phenolic model compounds over MoS_2 catalysts with different structures. Chinese Journal of Chemical Engineering 16, 733–739.

Yoosuk, B., Tumnantong, D., Prasassarakich, P., 2012. Unsupported MoS_2 and $CoMoS_2$ catalysts for hydrodeoxygenation of phenol. Chemical Engineering Science 79, 1–7.

Zhang, C., Li, P., Liu, X., Liu, T., Jiang, Z., Li, C., 2018. Morphology-performance relation of (Co)MoS_2 catalysts in the hydrodesulfurization of FCC gasoline. Applied Catalysis A: General 556, 20–28.

Zhang, H., Lin, H., Zheng, Y., 2020. Deactivation study of unsupported nano MoS_2 catalyst. Carbon Resources Conversion 3, 60–66.

Zhang, S., Liu, D., Deng, W., Que, G., 2007. A review of slurry-phase hydrocracking heavy oil technology. Energy & Fuels 21, 3057–3062.

Zhang, Y., Monnier, J., Ikura, M., 2020. Bio-oil upgrading using dispersed unsupported MoS_2 catalyst. Fuel Processing Technology 206, 106403.

Zhu, Y., Ramasse, Q.M., Brorson, M., Moses, P.G., Hansen, L.P., Topsøe, H., Kisielowski, C.F., Helveg, S., 2016. Location of Co and Ni promoter atoms in multi-layer MoS_2 nanocrystals for hydrotreating catalysis. Catalysis Today 261, 75–81.

Ziegelaar, P., Schleiffer, A., 2016. Process and apparatus for hydroconversion of hydrocarbons. WO2016071776A3.

8 Appendices

8.1 Appendix A

Catalyst screening with Span 80

The first emulsions were prepared using Span 80 (sorbitane monooleate) as the surfactant. Span 80 is a non-ionic surfactant with a hydrophilic-lipophilic balance (HLB) value of 4.3 (Kassem et al., 2019). The surfactant was mixed with the organic phase, which was kerosene during the tests. The aqueous phase consisting of Mo-precursor ammonium heptamolybdate (AHM) and sulfur donor dimethyl sulfoxide (DMSO) was mixed with the oil-phase. DMSO was added according to the stoichiometry to form MoS_2. Aqueous and organic phases were initially mixed using a Vortexer test tube shaker, but it was quite apparent that agitation with this method was not sufficient and therefore an IKA T18 Ultra-Turrax Homogenizer was used for high shear mixing of the two phases. With the homogenizer, agitation was performed by mixing at 6500 rpm and 9500 rpm for 5 minutes at each mixing speed. Parameters such as w/o ratio and vol-% surfactant in the organic phase were varied during screening. Tested compositions can be seen in Table A.1. The most stable emulsion was number 12, which comprised 5 vol-% surfactant in the organic phase and a w/o ratio of 50:50 vol-%. The emulsion stability was tested with vials and the phase separation over time was observed. The formula used to calculate emulsion stability was:

$$Emulsion\ stability\ (\%) = \frac{V}{V_{initial}} \times 100\% \qquad (A.1)$$

where $V_{initial}$ is the initial volume of emulsion added to a vial and V is the volume of the heavy phase after a certain time. A graph showing the emulsion stability over time can be seen in Figure A.1.

Table A.1. Emulsion compositions during screening using Span 80 surfactant.

No.	Surfactant (vol-%)	w/o ratio (%)
1	15.00 %	20 %
2	10.00 %	20 %
3	10.00 %	10 %
4	10.00 %	5 %
5	10.00 %	40 %
6	10.00 %	40 %
7	7.50 %	40 %
8	12.50 %	40 %
9	10.00 %	30 %
10	10.00 %	50 %
11	10.00 %	50 %
12	5.00 %	50 %

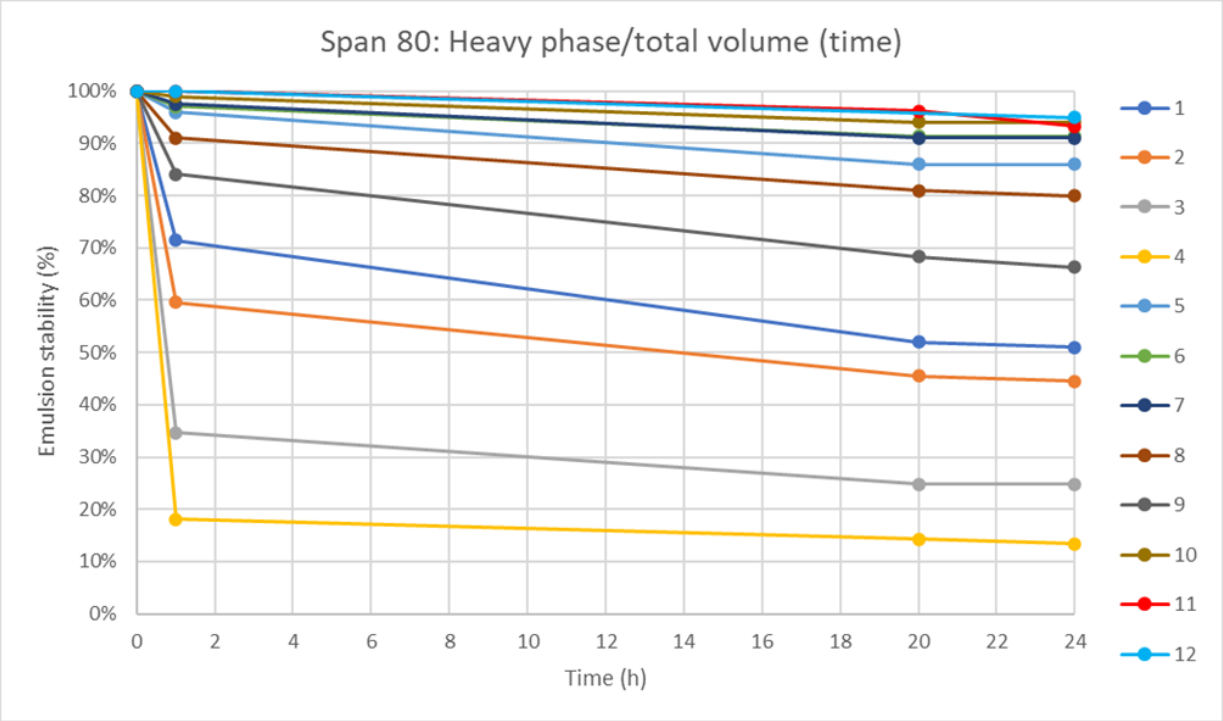

Figure A.1. Emulsion stability measured as phase separation in vials as a function of time using Span 80 as a surfactant.

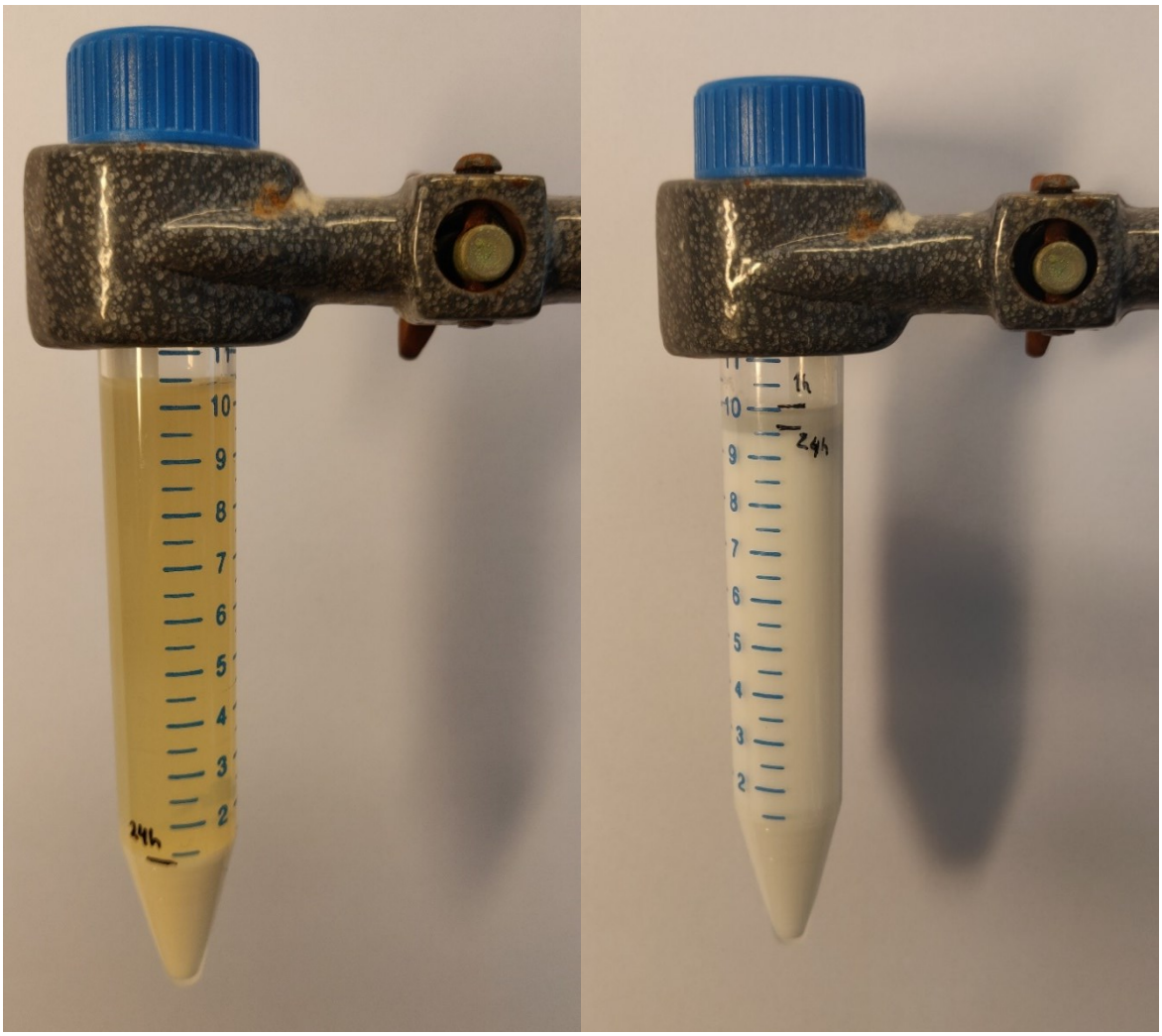

Figure A.2. Side-by-side comparison of the emulsions number 4 and number 12 after 24 h.

Emulsion screening with HDK silica nanoparticles

Emulsions were also prepared using Wacker HDK H18 and HDK H20 pyrogenic silica nanoparticles. The organic phase was prepared by adding silica nanoparticles to stirred kerosene in different amounts. The aqueous phase consisted of distilled water, Mo-precursor AHM and sulfur donor DMSO. The aqueous phase was added dropwise to the organic phase during agitation with a homogenizer. Emulsions were once again agitated at 6500 rpm and 9500 rpm for 5 minutes at each mixing speed. Tested compositions are summarized in Table A.2. Emulsions 1 and 2 were the most stable, both containing 5 w/v-% HDK H18 silica nanoparticles. The w/o ratio in number 1 was 50:50 vol-% while number 2 had a w/o ratio of 25:75 vol-%. Emulsions 3, 4, and 6 turned into viscous slurries and were for this reason not included in Figure A.3.

Table A.2. Emulsion compositions during screening using HDK H18 and H20 silica nanoparticles as emulsion stabilizing particles.

No.	Silica	Conc. HDK (w/v-%)	w/o ratio (%)
1	HDK H18	5.00 %	50 %
2	HDK H18	5.00 %	25 %
3	HDK H18	7.50 %	50 %
4	HDK H18	7.50 %	25 %
5	HDK H20	2.00 %	50 %
6	HDK H20	2.00 %	25 %
7	HDK H20	1.50 %	50 %
8	HDK H20	1.50 %	25 %
9	HDK H18	2.50 %	25 %
10	HDK H20	0.50 %	25 %

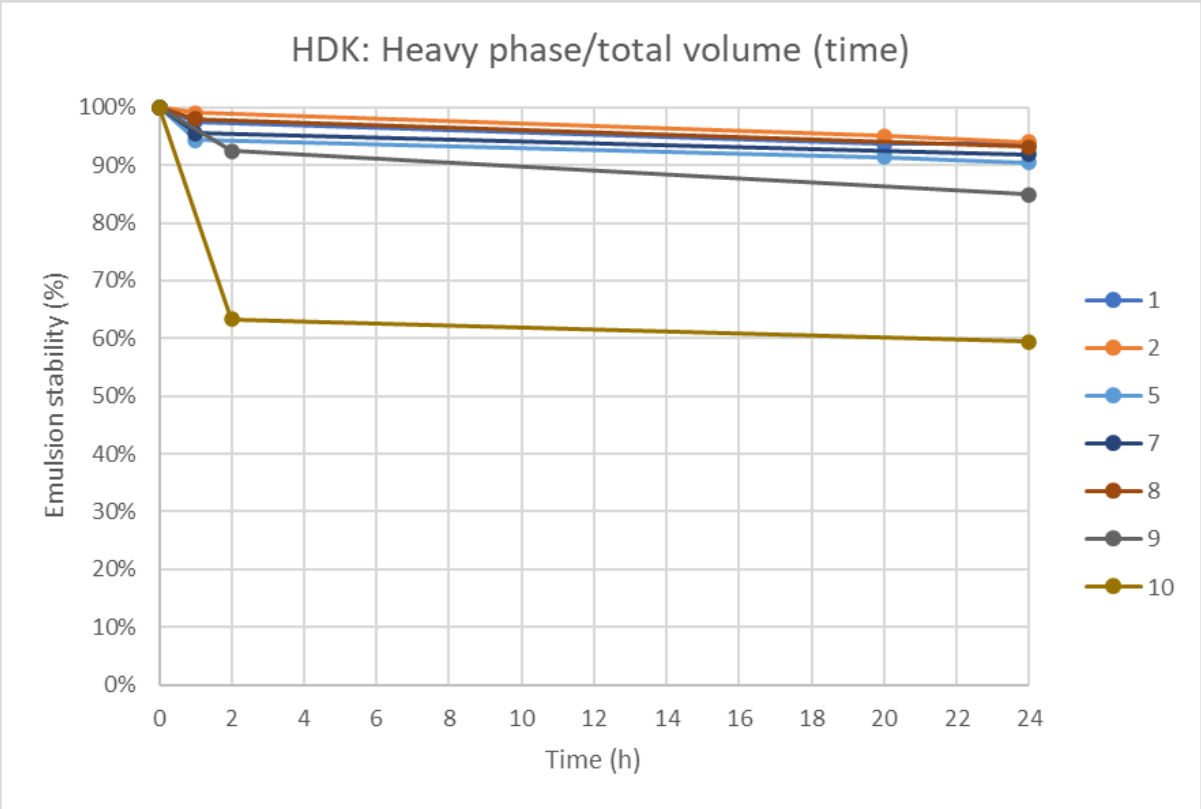

Figure A.3. Emulsion stability measured as phase separation in vials as a function of time using HDK H18 silica nanoparticles as a surfactant.

As can be seen in Figure A.3, compositions 9 and 10 were the least stable compositions, which can be explained by the low concentration of silica nanoparticles in the organic phase. A side-by-side comparison after 24 hours of the least and most stable silica nanoparticle emulsions can be seen in Figure A.4.

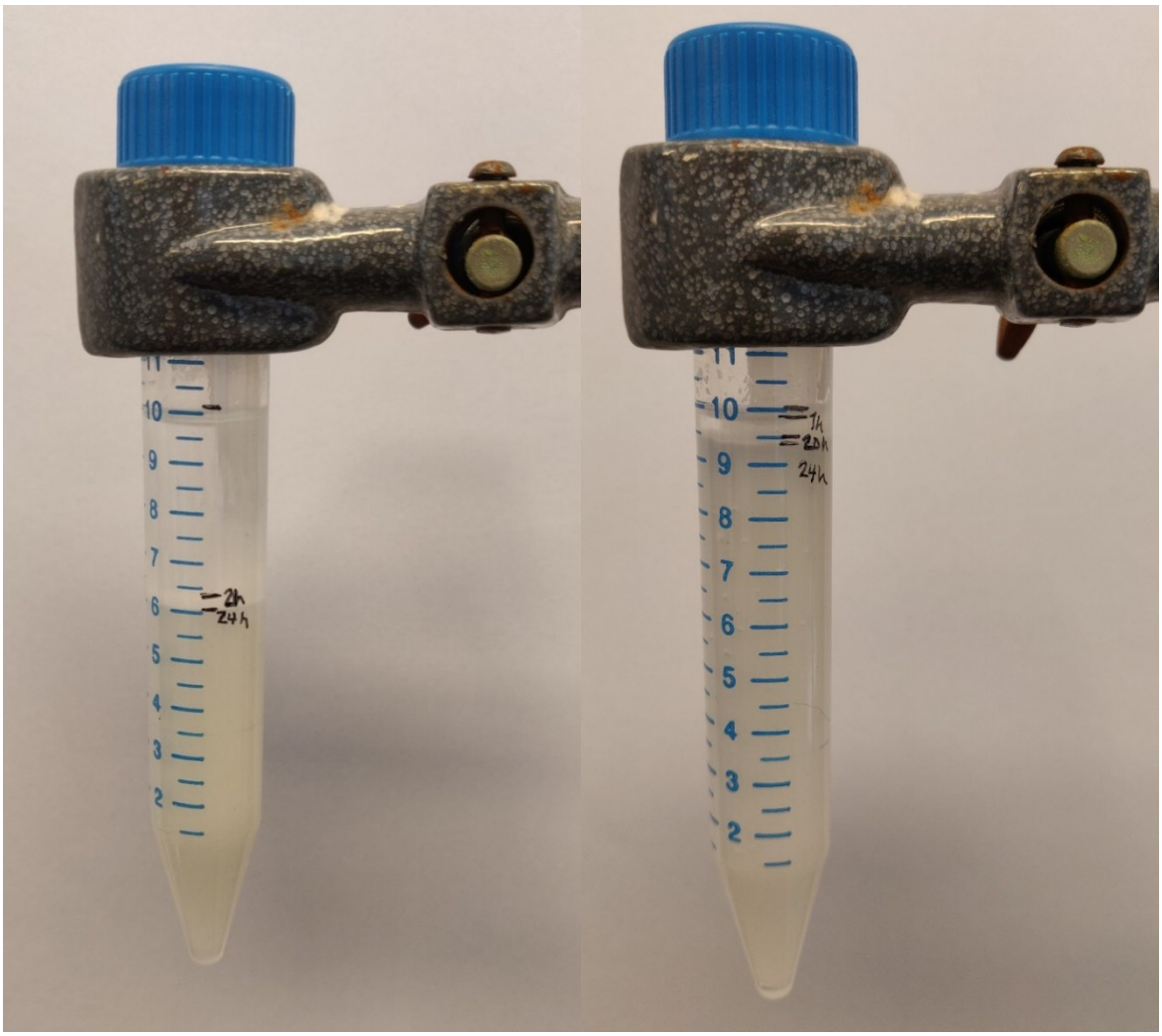

Figure A.4. Side-by-side comparison of the emulsions number 10 and number 2 after 24 h.

8.2 Appendix B

SEM-EDS images of hydrothermal MoS_2 and Co-MoS_2

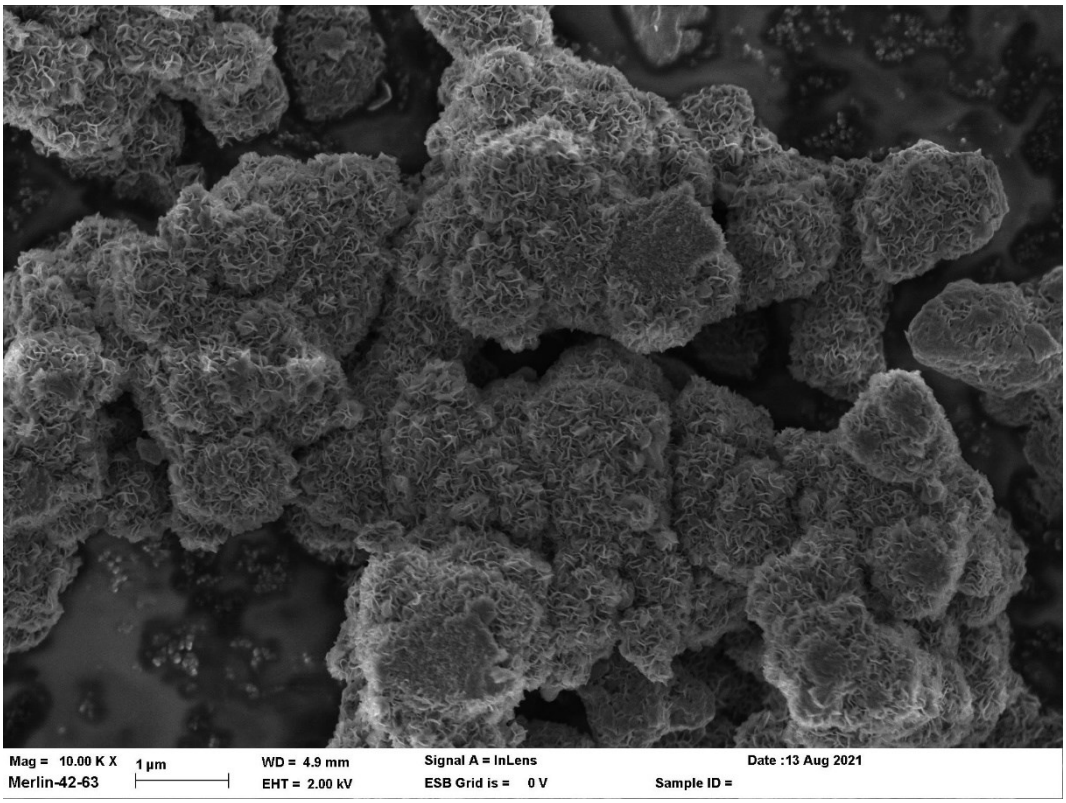

Figure B.1. SEM-EDS image of MoS_2-HT with 10,000x magnification.

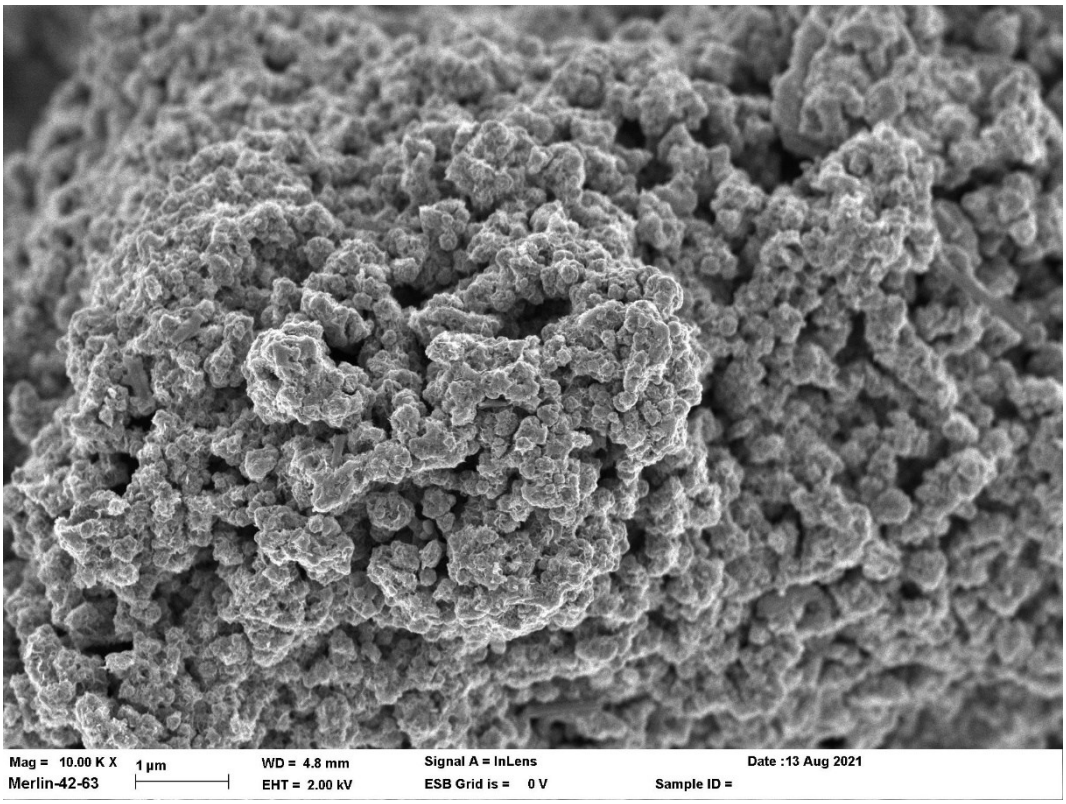

Figure B.2. SEM-EDS image of Co-MoS_2-HT with 10,000x magnification.

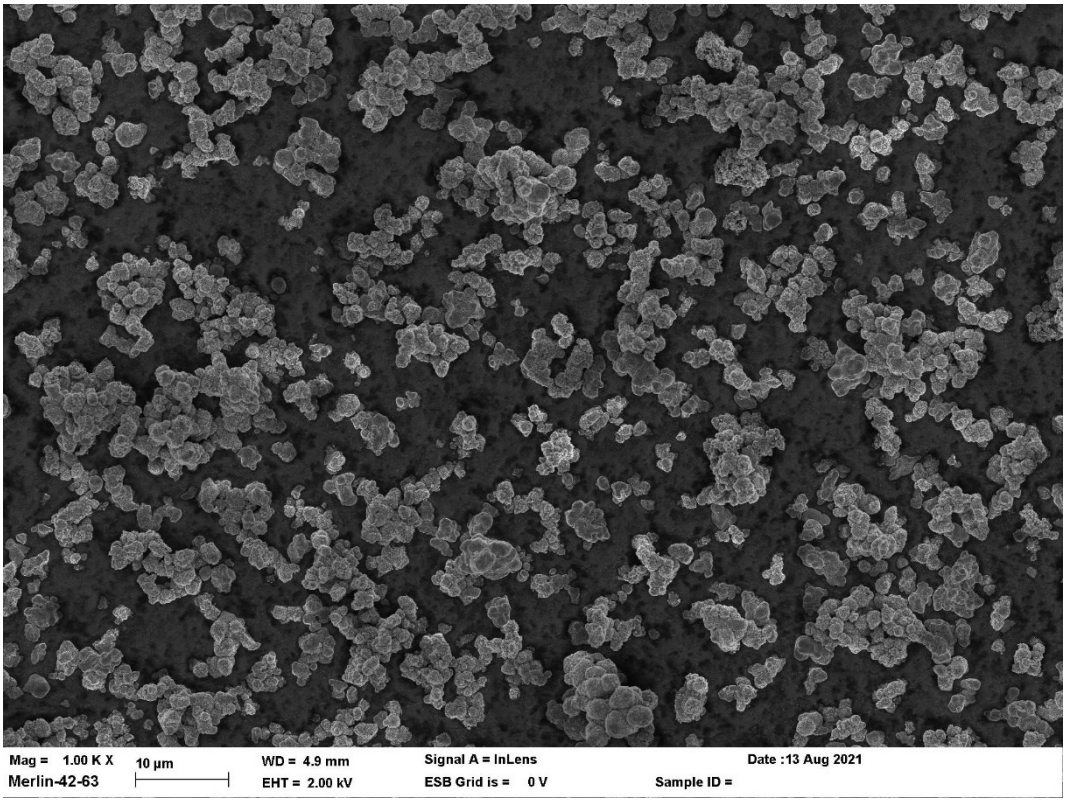

Figure B.3. SEM-EDS image of MoS_2-HT with 1,000x magnification.

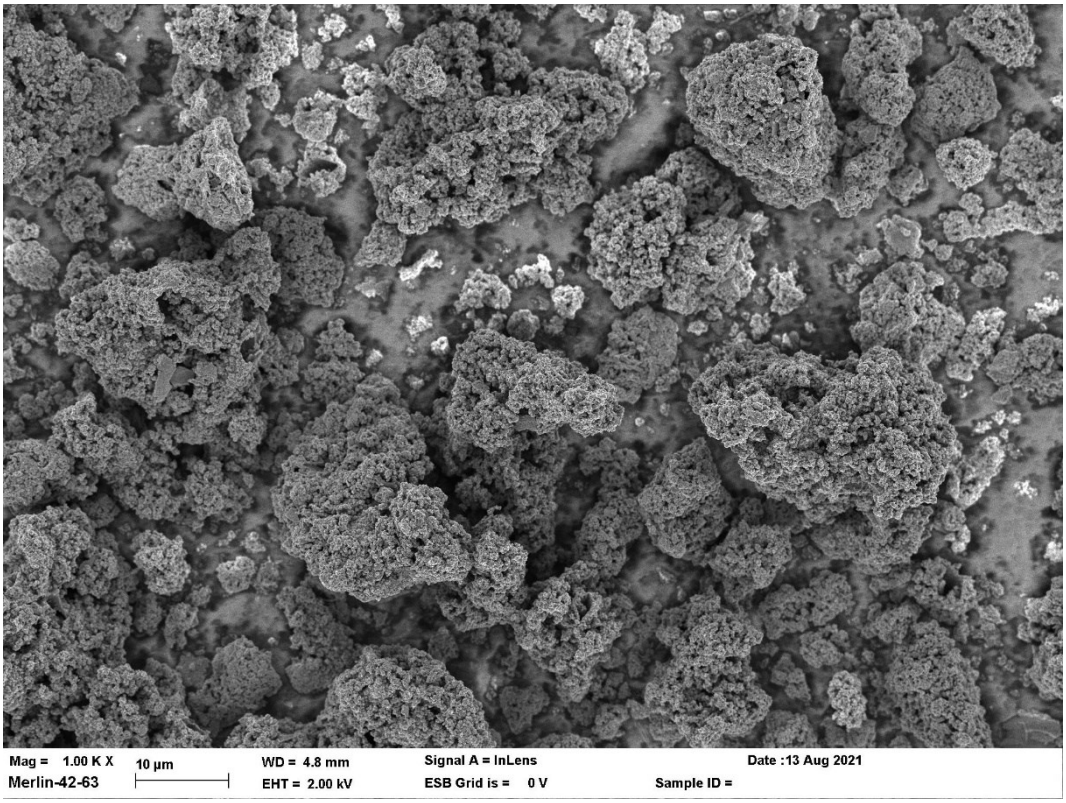

Figure B.3. SEM-EDS image of Co-MoS_2-HT with 1,000x magnification

8.3 Appendix C

Piping and instrumentation diagram (P&ID) of Buchi autoclave

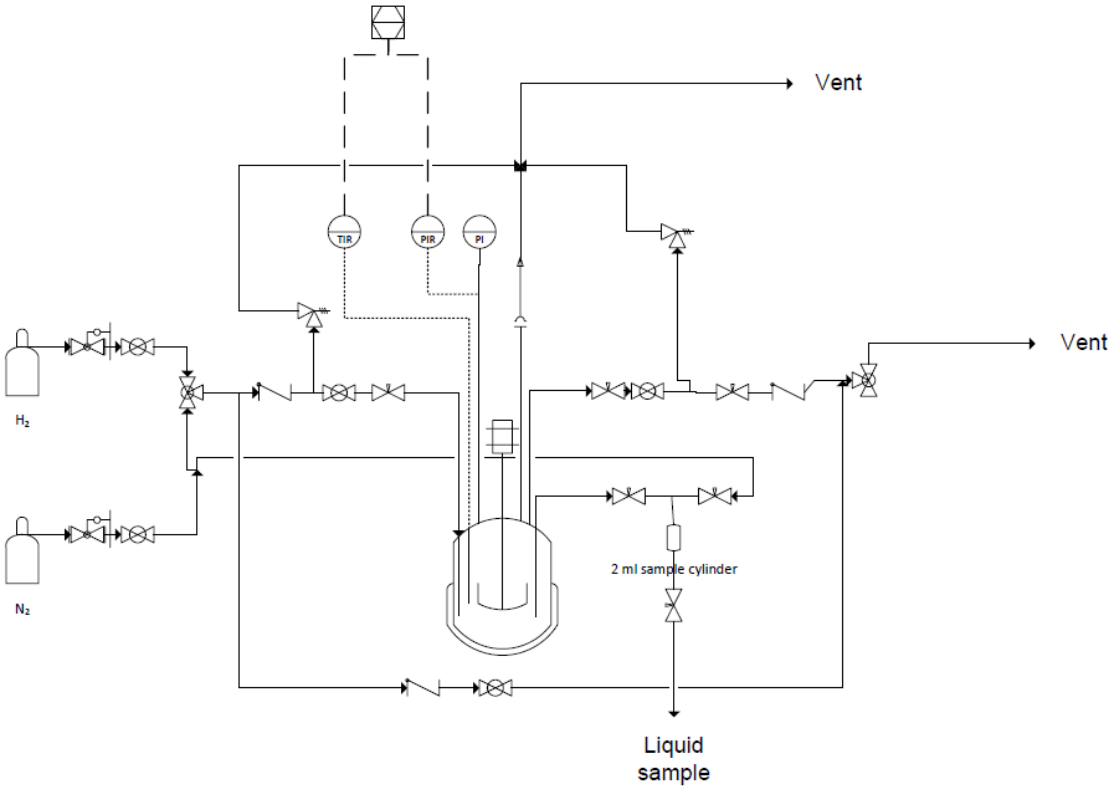

Figure C.1. P&ID of Buchi autoclave used in HDO of isoeugenol.

8.4 Appendix D

Operating procedure for ICP analysis of samples

ICP analysis was carried out using the following procedure:

1. Sample was added to digestion tube.
2. 9 ml of concentrated HNO_3 and 1 ml of H_2O_2 was added to digestion tube.
3. The tube was closed and placed in a Milestone Ethos Up microwave digestion system.
4. The digestion program used comprised of:
    i. Temperature increase to 210 °C in 20 minutes.
    ii. Temperature hold at 210 °C for 15 minutes.
5. After the samples had cooled down, they were diluted to 50 ml with distilled water.
6. Prior to analysis with ICP-OES, the samples were further diluted to 1/10 or 1/100 with 1% HNO_3. Concentrations were measured with both the sample diluted to 50 ml as well as the sample diluted to either 1/10 or 1/100.
7. Calibration was conducted using Merck IV and Labdig-19 ICP standard solutions.